N78-20077

NASA CR-145323

AN IMPROVED VERSION OF THE NASA-LOCKHEED MULTIELEMENT AIRFOIL ANALYSIS COMPUTER PROGRAM

G. W. Brune and J. W. Manke

March 1978

Prepared under contract NAS1-14522 by

Boeing Commercial Airplane Company
P.O. Box 3707
Seattle, Washington 98124

for
Langley Research Center
NATIONAL AERONAUTICS AND SPACE ADMINISTRATION

1. Report No.	2. Government Accession No.	3. Recipient's Catalog No.
NASA CR-145323		

4. Title and Subtitle	5. Report Date
An Improved Version of the NASA-Lockheed Multielement Airfoil Analysis Computer Program	March 1978
	6. Performing Organization Code

7. Author(s)	8. Performing Organization Report No.
G. W. Brune and J. W. Manke	D6-45099
	10. Work Unit No.

9. Performing Organization Name and Address	11. Contract or Grant No.
Boeing Commercial Airplane Company P.O. Box 3707 Seattle, Washington 98124	NAS1-14522
	13. Type of Report and Period Covered
12. Sponsoring Agency Name and Address	Final
Langley Research Center National Aeronautics and Space Administration Washington, D. C. 20546	14. Sponsoring Agency Code

15. Supplementary Notes

Technical Monitor. Dr. R.W. Barnwell.
NASA Langley Research Center
Hampton, VA 23669

16. Abstract

An improved version of the NASA-Lockheed computer program for the analysis of multielement airfoils is described. The predictions of the program are evaluated by comparison with recent experimental high lift data including lift, pitching moment, profile drag, and detailed distributions of surface pressures and boundary layer parameters. The results of the evaluation show that the contract objectives of improving program reliability and accuracy have been met.

17. Key Words (Suggested by Author(s))		18. Distribution Statement
Two-dimensional airfoil theory	High lift	Unclassified – Unlimited
Multielement airfoils	Viscous flow	
Potential flow	Iteration	
Confluent boundary layer	Subsonic	

19. Security Classif. (of this report)	20. Security Classif. (of this page)	21. No. of Pages	22. Price*
Unclassified	Unclassified	196	

*For sale by the National Technical Information Service, Springfield, Virginia 22151

CONTENTS

CONTENTS (Continued)

Page

CONTENTS (Continued)

CONTENTS (Concluded)

TABLES

FIGURES

FIGURES (Concluded)

AN IMPROVED VERSION OF THE NASA-LOCKHEED MULTIELEMENT AIRFOIL ANALYSIS COMPUTER PROGRAM

G. W. Brune and J. W. Manke
Boeing Commercial Airplane Company

SUMMARY

This document contains a description of an improved version of the NASA-Lockheed computer program for the performance prediction of high lift airfoils. Modifications of the aerodynamic model and the computer program include:

- Boundary layer and wake displacement effects are represented by an equivalent distribution of sources along the airfoil surface and along the wake centerlines.
- Wake parameters are predicted using the lag-entrainment method of Green.
- Profile drag is calculated by the Squire and Young formula.
- Parameters of ordinary turbulent boundary layers are calculated by the method of Nash and Hicks.
- Onset of the separation of confluent turbulent boundary layers is determined by a modification of Goradia's confluent boundary layer method.
- High lift airfoils with up to 10 components can be analyzed.
- The Boeing version of the computer code is well structured featuring new control routines and new subroutines for geometry and potential flow calculations. Old subroutines are thoroughly commented and documented.

The program is evaluated by comparison with recent experimental high lift data, comprising lift, pitching moment, and profile drag, as well as, detailed distributions of surface pressures, boundary layer integral parameters, skin friction coefficients, and velocity profiles. The results of this evaluation show that the contract objectives of improving program reliability and accuracy have been met.

INTRODUCTION

HISTORICAL REMARKS

In the past, high lift design and technology rested in the hands of a few experienced aerodynamicists. Design methodology and criteria were heavily influenced by the analytical inviscid flow methods and the experimental data available. With the advent of high-speed computers and the appearance of improved models for turbulent flows, many of these complex problems, including high lift design and analysis, were attacked theoretically.

One such approach to high lift or multielement airfoil analysis was developed by Goradia and his coworkers (ref. 1) at Lockheed-Georgia under the sponsorship of the NASA-Langley Research Center. This program was among the first attempts at analyzing the complex viscous flow about slotted airfoils and has received worldwide distribution and usage. A unique feature of this multielement airfoil program is the model of the confluent boundary layer flow (ref. 2).

Over the years, the original version of the program was modified extensively to improve its predictions for different types of high lift airfoils. Many improvements, mainly in the area of the potential flow calculation, were made by researchers at the Langley Research Center (ref. 3). For this reason, the code is generally referred to as the NASA-Lockheed multielement airfoil program. A version for single element airfoils was recently extracted from the multielement airfoil code by researchers at North Carolina State University (ref. 4).

Widespread and steady usage of the computer program clarified its strengths and weaknesses. Both favorable and unfavorable aspects have been brought to the surface by continued attempts at using the program as an engineering tool. The more serious shortcomings were the lack of agreement between the documentation and the available version of the code and the high-failure rate in applying the method for various configurations. However, the program was found to contain sufficient positive features to justify its choice as a starting point for future theoretical work in the high lift area.

In July 1976 work was begun in the high lift research group of The Boeing Company on a joint program with NASA-Langley to evaluate and improve the NASA-Lockheed multielement airfoil code. The work consisted of two phases. The first phase had the objective to document and evaluate the "baseline" version of the code which was supplied to Boeing by NASA-Langley prior to the beginning of the contract work. In addition, certain minor improvements of the aerodynamic methodology were made during the first work phase. In February 1977, the phase one version of the computer code was delivered to the Langley Research Center together with a detailed documentation of its underlying aerodynamic theory (ref. 5).

The second phase of the contract work involved a major revision of the flow model used in the NASA-Lockheed program that in turn required substantial modifications of the computer code. This document contains the results of the second phase of the contract work including the complementary Boeing IR&D work. The evaluation of the predictions of the various versions of the computer code by comparison with recent experimental data of high lift airfoils is described in a separate document (ref. 6). However, this document contains a few of these comparisons to provide the user with a reasonably self-contained guide to the latest version of the computer program.

MULTIELEMENT AIRFOILS

The flow around high lift airfoils is characterized by many different inviscid and viscous flow regions. Their complex physics is illustrated in figure 1. In particular, the existence of confluent boundary layers and the regions of separated flow distinguish the high lift airfoil problem from the aerodynamic problem of airfoils at cruise conditions. The various flow regions, including the outer potential flow, the ordinary laminar and turbulent boundary layers, viscous wakes, and the confluent boundary layer, are analyzed by the code. Furthermore, the prediction of transition from laminar to turbulent boundary layer flow and the prediction of the onset of boundary layer separation are a necessary part of the code. Cove separation and large scale separation phenomena, however, are not modeled.

The computer code described in this document calculates the flow about high lift airfoils assuming that:

- The flow is attached to the airfoil's surface
- The flow is two-dimensional and subcritical
- The high lift airfoil consists of up to 10 components

These are the main assumptions of the multielement airfoil method. Additional assumptions are listed in the pertinent sections of this document.

MODIFICATIONS OF THE AERODYNAMIC MODEL

The described aerodynamic theory differs from the theory of the baseline version of the NASA-Lockheed program in the following areas:

- The method used to represent the effect of the viscous flow on the outer potential flow within the overall iterative solution procedure, that is termed *equivalent airfoil representation* in the baseline version of the program, has been modified. It has been replaced by the surface transpiration method which uses an equivalent distribution of sources along the airfoil surface and the wake centerlines to model the boundary layer and wake displacement effects.

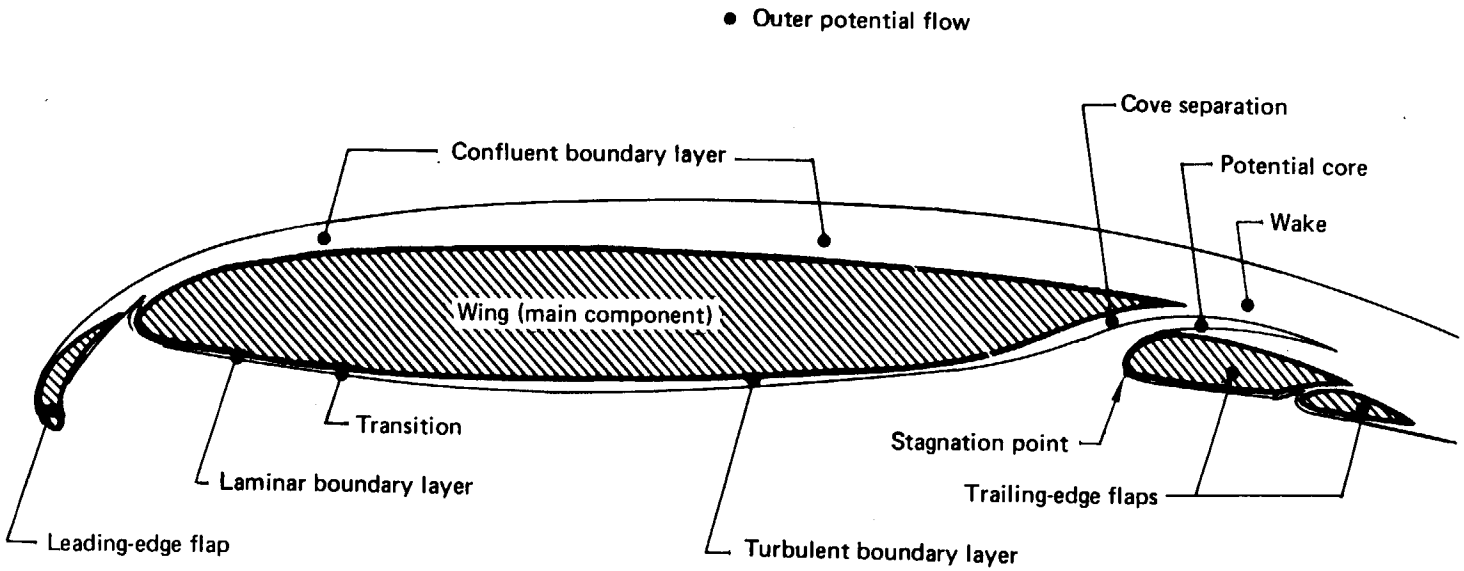

Figure 1. — Flow Regions of Multielement Airfoil

- The flow model of the potential core region has been changed. The new method performs independent boundary layer and wake calculations. These calculations utilize the ordinary laminar and turbulent boundary layer routines of the baseline version of the code, and in addition, the lag-entrainment method of Green (ref. 7) for wake flows. The revised flow model of the core region calculates the location of the wake centerlines.

- An attempt is made to predict the onset of separation of the confluent boundary layer by a modified version of Goradia's confluent boundary layer method. In this method, the power law velocity profile of the wall layer is replaced by Coles' two-parameter velocity profile (ref. 8). The latter is known to be an adequate representation of thin turbulent boundary layers.

- The drag prediction method of Squire and Young (ref. 9) has been incorporated into the program, replacing the previous pressure and skin friction integration scheme.

- The original method used for the prediction of separation for ordinary turbulent boundary layer flow has been replaced by the Boeing version of the method of Nash and Hicks (ref. 10).

- The slot flow calculation has been removed from the program. The flow in the slot between adjacent airfoil components is now calculated as an integral part of the overall computation. This is based on the same potential flow and viscous flow models, including the same account of compressibility effects, that are used in the remainder of the flow field.

- The code has been made operational for negative airfoil overlap.

- Several logical errors in the formulation of the aerodynamic model and its numerical implementation have been corrected.

COMPUTER CODE

The outlined modifications of the aerodynamic theory required a major overhaul of the computer code. Most parts of the code have been rewritten using a systematic approach to computer software design. This work was guided by a functional decomposition of the many aspects of the aerodynamic model and its numerical implementation. In addition, a detailed study was made of the data flow within the program, and the logic of the code was outlined prior to the actual program development using a pseudo code. The most important results of this work, such as the higher levels of the functional decomposition, a brief description of the data structure, and a unified list of symbols, are included in this document.

All control routines, the geometry package, and the potential flow routines of the program have been replaced. Other subroutines performing such functions as tracing streamlines, computing wake flow characteristics, predicting confluent boundary layer separation, etc., have been added to the code. However, several major subroutines of the

old code including LAMNA, TURBL, TURB, CONF7, CONF8, and some mathematical subroutines, had to be retained with only minor modifications. The schedule of the contract did not permit time to restructure these routines. Nevertheless, a considerable amount of time was spent reorganizing the COMMON blocks of these old subroutines, rationalizing conflicts of symbols, and interfacing the data structure with the new code. A list of symbols and comment cards, sufficient to guide an experienced user through the code, were added to each of the old subroutines.

The new routines in the computer program use dynamic data structures that do not limit explicitly the number of surface points representing the airfoil geometry. The input format and the boundary layer routines of the baseline version of the code limited the number of computational surface points to 165 and the number of data points to 65 per upper or lower airfoil surface.

Previous users of the computer program should note that small changes have been made in the input and output formats.

ON THIS DOCUMENT

The document combines the results of contract work and complementary Boeing IR&D work. The Boeing IR&D funds supported the following work and documentation.

- The confluent boundary layer model.
- The top-down design of the computer code including the functional decomposition of the aerodynamic theory, the investigation of the data flow, and the pseudo code.
- The evaluation of the computer program by comparison with experimental data of McGhee and Beasley; Wentz, Seetharam, and Fiscko; Foster; Ljungström; and The Boeing Company. Most of these results are described in a separate document (ref. 6).

The table of contents closely follows the functional decomposition of the code. The letters behind a heading refer to the corresponding function of the functional decomposition. No attempt has been made to document the code on a subroutine by a subroutine basis.

Those sections of the document describing the theory of old subroutines have an individual list of symbols. All other sections share one common list of symbols relating the theory to the computer code. Cross referencing from section to section has been avoided.

ACKNOWLEDGEMENTS

James Mark and Emily White contributed greatly to the documentation and computer programming of the turbulent boundary layer and transition methods.

STRUCTURE OF THE COMPUTER CODE

The described version of the NASA-Lockheed multielement airfoil computer program conforms to the Langley Research Center computer programming standards. It is written in the CDC FORTRAN Extended 4 (FTN4) language and will run under the CDC Network Operating System (NOS). Program I/O is performed only by FTN4 statements using the standard system file names INPUT (TAPE5) for card reading and OUTPUT (TAPE6) for printing.

In the sections below, the design of the computer code is discussed, the overlay structure of the code is described, and a short description of each subroutine is given.

DESIGN OF THE CODE

The programming methodologies used to design and develop the new version of the computer code include:

- Functional decomposition
- Data flow analysis
- Control flow analysis

Each of these interrelated design tasks were performed several times in an iterative manner to produce a final design for the new version of the computer code before any changes or improvements to the baseline code were made. The final design for the new version of the code resulted in major changes in the three following program sections; upper level control routines, geometry preprocessing routines, and the potential flow solution routines. The final design was also used to integrate the major new aerodynamic models into the baseline code; they include the representation of the displacement thickness with sources, Green's wake solution technique, and the modified confluent boundary layer method. Table 1 lists all subroutines in the baseline version of the code and indicates the type changes made to incorporate them in the new version.

The functional decomposition of the code was based on the engineering specification of the aerodynamic models and the numerical techniques necessary for their solution. Figures 2 and 3 show the upper level decomposition charts where the major functions are defined in engineering terms. The complex physics of the flow about multielement airfoils is reflected in these charts, e.g., the potential flow solution, the ordinary laminar and turbulent boundary layer solutions, the confluent boundary layer solution, and the wake layer solution. The charts also demonstrate that the overall iteration of a solution is a high level function; and, the prediction of the transition from laminar to turbulent boundary layer flow and the prediction of the occurence of separation are functions of importance equal to the laminar and turbulent flow solutions. All new subroutines in the code identify which module in the functional decomposition they implement.

Table 1. — Modifications of the Subroutines in the Baseline Version

Subroutine	No change	Minor change	Major change	Delete
MAIN			X	
POINT	X			
SLOPE	X			
TRANS			X	
DISTP	X			
FTLUD				X
DIR	X			
LSQ				X
PROOT	X			
MAIN1			X	
READIT		X		
GEOM			X	
ROTRAN			X	
ASLOT			X	
NORMAL			X	
MAIN 2			X	
CHEN			X	
MATRIX			X	
POTLF			X	
CAMBER				X
SMOOTH	X			
VOVBT				X
THICK				X
COMPR			X	
STAG			X	
MAIN 3			X	
LOAD			X	
LAMNA		X		
BLTRAN		X		
TURBL		X		
TURB		X		
DERIV		X		
START		X		
CONFBL				X
CONF 5				X
CONF 7		X		
CONF 8		X		
DLIM	X			

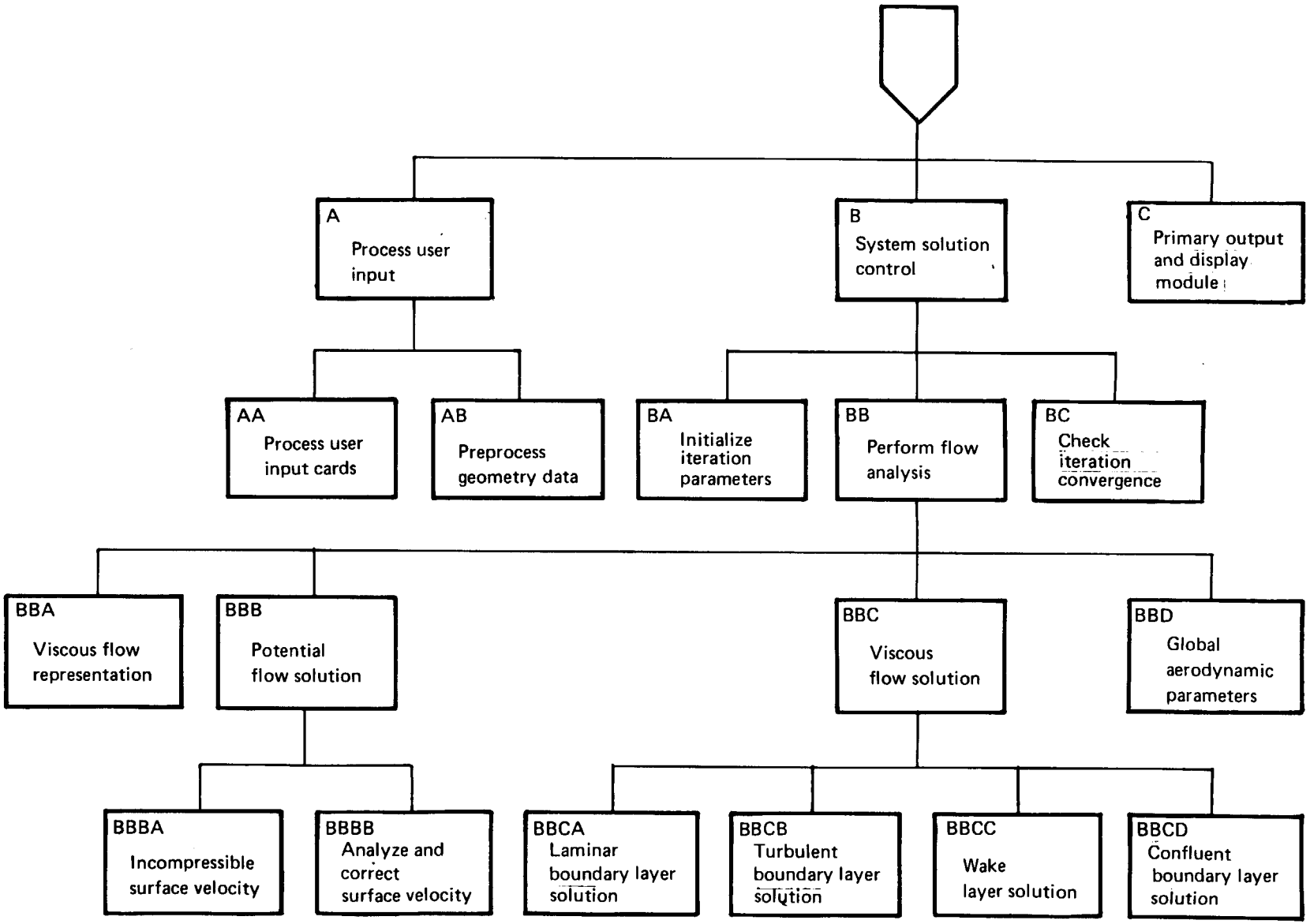

Figure 2. — Functional Decomposition of NASA-Lockheed Program

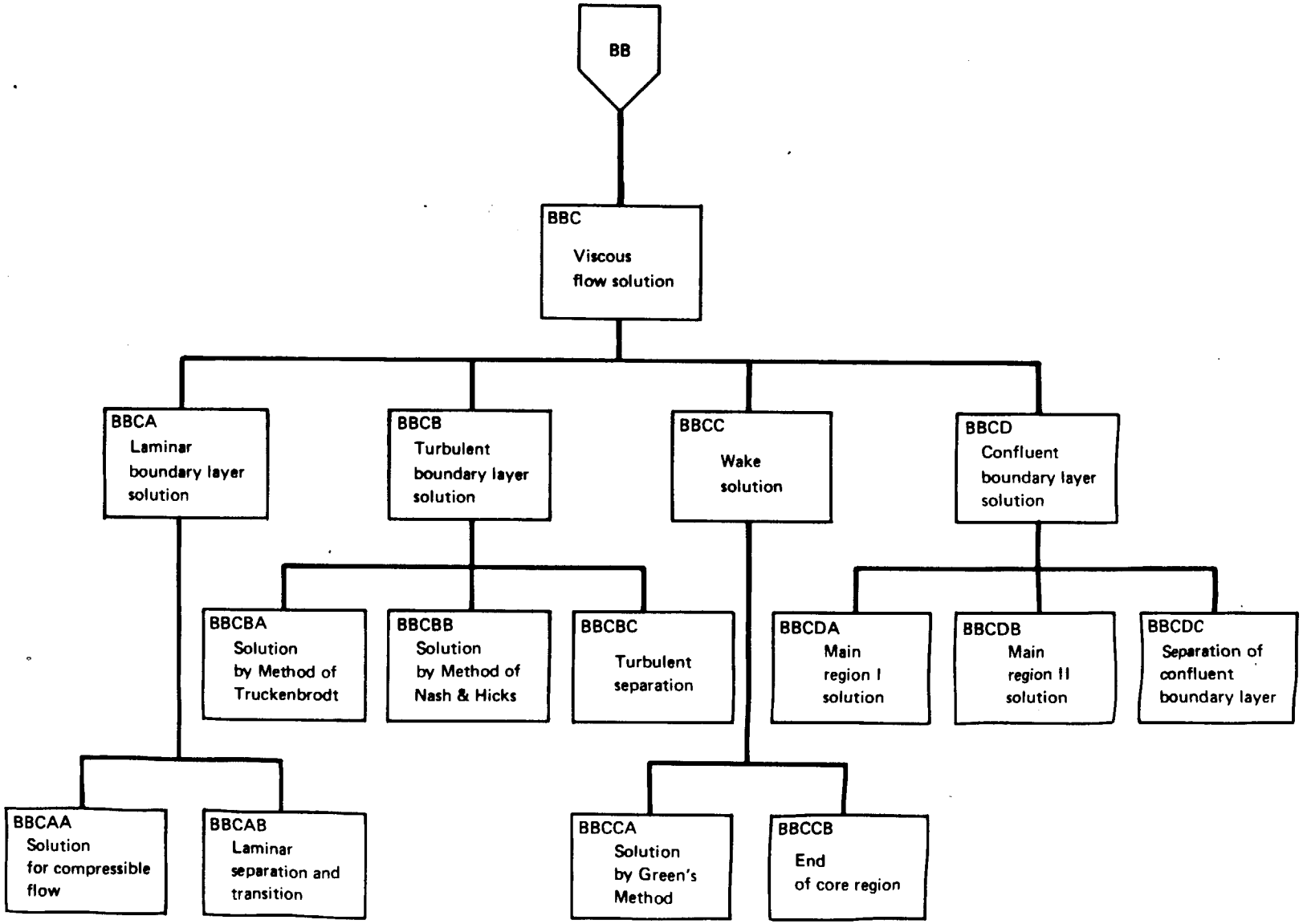

Figure 3. – Functional Decomposition of Viscous Flow Solution

The data flow analysis of the code was done with the aid of HIPO charts: an example of a completed HIPO chart is given in figure 4. For each module identified in the functional decomposition, the input and output data for the module, as well as its decomposition, are specified on the chart. Control of the data flow within a module is maintained by requiring that the input to any of its submodules must be either an input to the module or the output of another of its submodules. Once HIPO charts have been completed for all modules in the functional decomposition, all data groups have been identified, and the data flow specified. The data groups identified for the new version of the code by this process are listed in the section of this document titled Symbols.

The control flow analysis of the new code was done with the aid of pseudo code; an example is given in figure 5. Pseudo code is a small set of simple logic and loop statements which suffice to describe the control within a module of the functional decomposition. Although the submodules of a particular module can be used in any sequence and any number of times to complete the function of the module, it is an aim of the design process to keep the control within a module as simple as possible. All new subroutines in the code include as comment cards the pseudo code for the module which they implement.

OVERLAY STRUCTURE

The CDC overlay system is used to assure that the computer code will execute in a field length less than 100 K (octal). The division of the code into overlay sections follows the decomposition of the solution process: user input processing and geometry data preprocessing, the potential flow solution, and the viscous flow solution. The viscous flow solution divides into the laminar flow solution, turbulent flow solution, wake layer solution, the confluent boundary layer solution of Goradia, and the modified confluent boundary layer method. The overlay structure of the program is described in detail by the table in figure 6.

SUBROUTINE DESCRIPTION

This section contains a description of those subroutines which perform the analysis. The subroutines can be divided into several groups according to their function; major control routines, user input and geometry data processing, potential flow solution, viscous flow solution, and library routines. In the succeeding descriptions the subroutines are divided into these groups.

The execution of the program is directed by the major control routines which are listed below:

MAIN	Provides the primary logic and data flow control for the entire program.
SYSOL	Provides the logic and data flow control for the solution iteration for each requested angle of attack and freestream Mach number.
INITR	Initializes parameters of the solution iteration procedure.

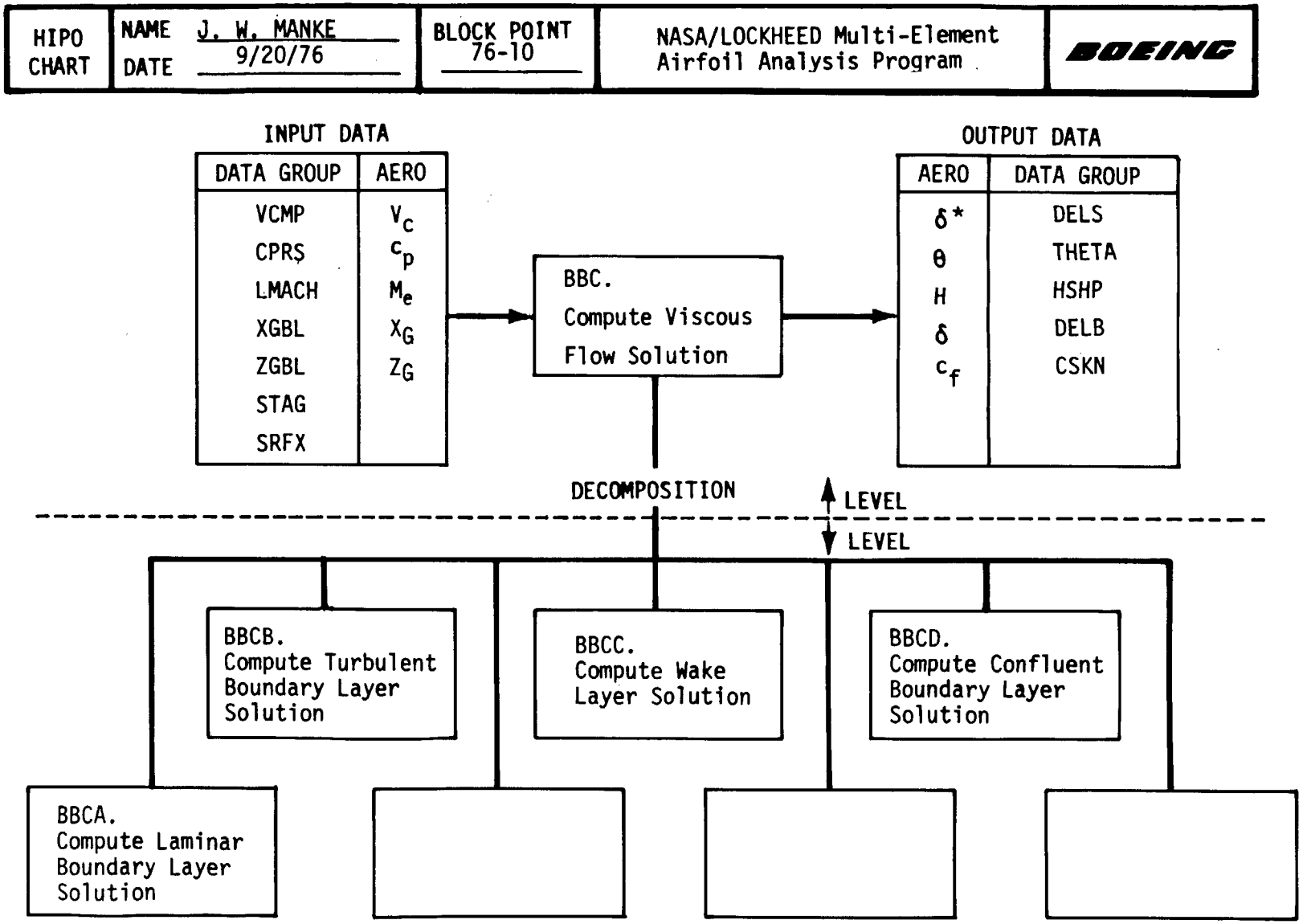

Figure 4. — Sample HIPO Chart

```
BEGIN MODULE BBC

FOR EACH AIRFOIL COMPONENT DO

   FOR EACH AIRFOIL COMPONENT SURFACE DO

      BEGIN MODULE BBCA : COMPUTE LAMINAR BOUNDARY
                          LAYER SOLUTION

      IF TRANSITION TO TURBULENT FLOW THEN

         BEGIN MODULE BBCB : COMPUTE TURBULENT
                             BOUNDARY LAYER SOLUTION

      ENDIF

   ENDDO

ENDDO

FOR EACH AIRFOIL COMPONENT DO

   BEGIN MODULE BBCC : COMPUTE WAKE LAYER SOLUTION

   IF NOT THE LAST AIRFOIL COMPONENT AND CORE REGION
   ENDS BEFORE THE TRAILING EDGE THEN

      BEGIN MODULE BBCD : COMPUTE CONFLUENT BOUNDARY
                          LAYER SOLUTION FOR NEXT AFT
                          COMPONENT

      IF CONFLUENT BOUNDARY LAYER FLOW SOLUTION

      DEGENERATES INTO ORDINARY TURBULENT FLOW THEN

         BEGIN MODULE BBCB : COMPUTE TURBULENT BOUNDARY
                             LAYER SOLUTION

      ENDIF

   ENDIF

ENDDO

END MODULE BBC
```

Figure 5. — Sample Pseudo Code

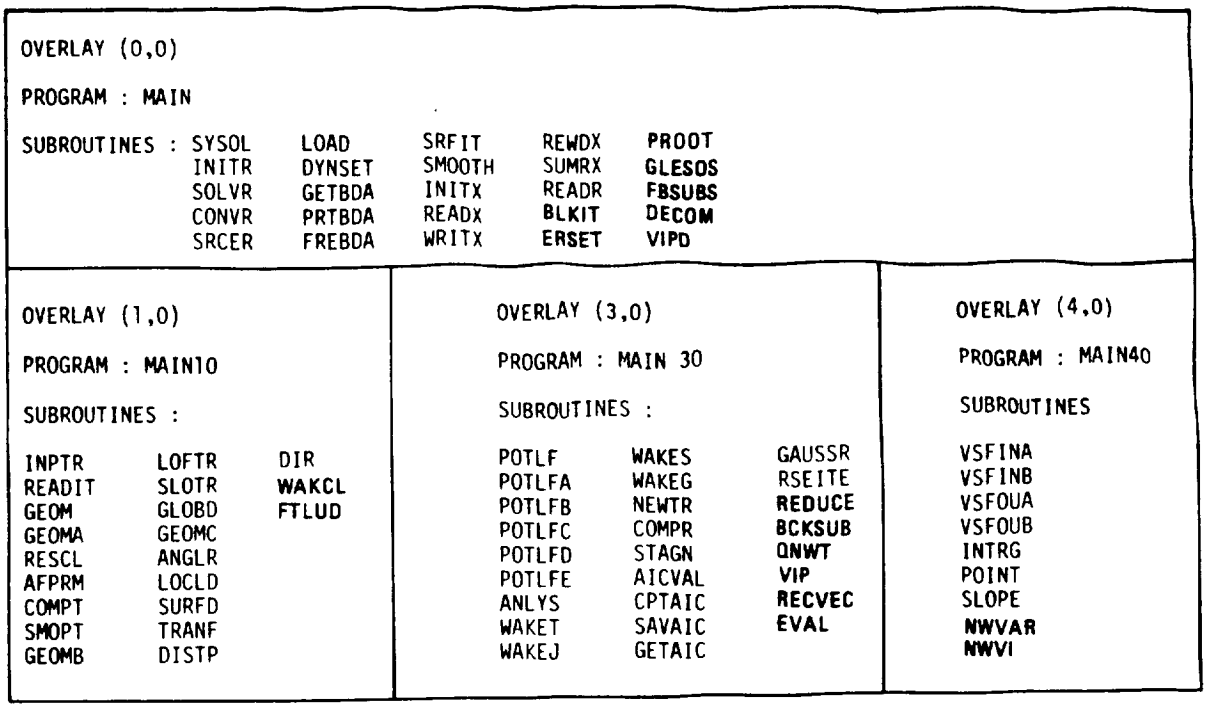

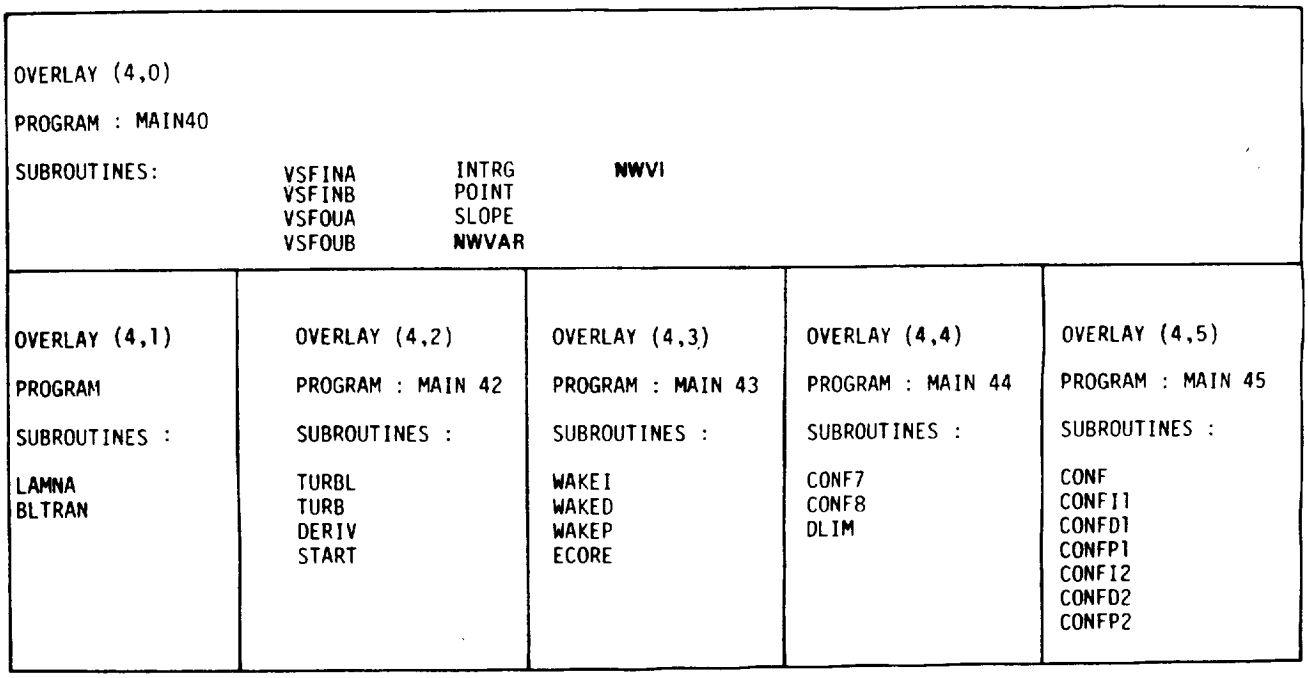

Figure 6. — Overlay Structure of the NASA-Lockheed Multielement Airfoil Computer Program

SOLVR — Provides the logic and data flow control for one step in the solution iteration procedure: this includes representation of the boundary layer, potential flow solution, viscous flow solution, and loads estimate.

CONVR — Checks the convergence criteria to determine when the solution iteration procedure can be terminated.

Listed are the subroutines that read and analyze the user input data and preprocess the geometry.

MAIN10 — Provides the primary logic and data flow control for reading the user input and preprocessing the geometry.

INPTR — Provides the interface between the data structures of the new version of the program and READIT, the input reading routine of the baseline version.

READIT — Reads the user input data cards and stores the problem description. Some format and consistency checking of the input is performed.

GEOM — Provides the primary logic and data flow control for the preprocessing of the geometry data.

GEOMA — Provides the logic and data flow control for the airfoil parameter determination phase of the geometry analysis.

RESCL — Stores the input geometry data in the internal basic data array format, and applies the user specified geometry scaling factor.

AFPRM — Determines the basic airfoil parameters; e.g., number of computational surface points, airfoil chord length.

COMPT — Computes the computational surface points. The input surface points are redistributed by an algorithm based on curvature (DISTP).

SMOPT — Smooths the geometry data computed by COMPT with a simple smoothing algorithm (SMOOTH).

GEOMB — Provides the logic and data flow control for the lofting of the geometry data in the global coordinate system.

LOFTR — Components other than the main component, are rotated and translated into the coordinate system of the main component.

SLOTR — Analyzes the slot geometry of the lofted airfoil.

GLOBD	Computes the initial wake centerline geometry and stores the final lofted airfoil geometry data in the global coordinate data array.
GEOMC	Provides the logic and data flow control for the calculation of the local coordinate geometry data.
ANGLR	Calculates the global-to-local coordinate system transformation data.
LOCLD	All components are rotated and translated into their respective local coordinate system.
SURFD	Computes the surface fitted coordinates (arclength) for each component.
WAKECL	Computes the initial wake centerlines.

The subroutines that calculate and analyze the potential flow solution are listed below:

MAIN30	Provides the primary logic and data flow control for the calculation and analysis of the inviscid flow solution.
POTLF	Provides logic and data flow control for calculation of the incompressible surface velocity by Oeller's potential flow solution technique.
POTLFA	Calculates the solution matrix determined by Oeller's method and the specification of the Kutta condition.
POTLFB	Provides an interface with a linear equation solution package and checks the numerical conditioning of the solution matrix.
POTLFC	Calculates the right hand side determined by the freestream velocity, wake centerline sources, and the Kutta condition.
POTLFD	Provides an interface with a linear equation solution package and computes the vortex strengths determined by the right hand side.
POTLFE	Calculates the incompressible surface velocity from the freestream velocity and the source and vortex strengths.
ANLYS	Provides the logic and data flow control for the analysis and correction of the incompressible surface velocity.
WAKET	Computes the initial values of the wake centerline parameters for the update of the wake centerline geometry.
WAKEJ	Computes the Jacobian matrix for the wake centerline parameters for the update of the wake centerline geometry.
WAKES	Computes the stream function value of the potential flow solution velocity field at the corner points of the wake centerline.

WAKEG Computes the geometry of the updated wake centerline from the values of the wake centerline parameters.

COMPR Applies the compressibility corrections to the incompressible surface velocity and computes the local Mach number and pressure coefficient.

STAGN Estimates the location of the stagnation point of the flow field for each airfoil component.

The subroutines which calculate the boundary layer parameters for the viscous flow solution are:

MAIN40 Provides the primary logic and data flow control for the calculation and analysis of the viscous flow solution.

VSFINA Provides an input interface between the data structures of the new version of the program and the laminar and turbulent boundary layer analysis routines of the baseline version.

VSFINB Provides an input interface between the data structures of the new version of the program and the confluent boundary layer analysis routines of the baseline version.

LAMNA Computes compressible laminar, boundary layer flow solution using an integral method similar to the method of Cohen and Reshotko.

BLTRAN Computes transition of compressible laminar flow to turbulent flow or separation of the laminar boundary layer.

TURBL Computes incompressible, turbulent, boundary layer flow solution using an integral method similar to the method of Truckenbrodt.

TURB Computes incompressible, turbulent boundary layer flow solution using an integral method due to Nash and Hicks. The method can predict separation of the turbulent boundary layer.

DERIV Computes values of partial derivatives of parameters defined in the Nash and Hicks method.

START Computes initial values for the parameters defined in the Nash and Hicks method.

WAKEI Computes the initial values of the parameters for Green's wake layer solution method.

WAKED Computes derivatives of the parameters for Green's wake layer solution method.

WAKEP	Computes the values of the parameters for Green's wake layer solution method at each wake centerline corner point.
ECORE	Estimates the end of the potential flow core region in the flow field behind each slot.
CONF7	Computes and displays the parameters of Main Region I in the analysis of the confluent boundary layer with the method due to Goradia.
CONF8	Computes and displays the parameters of Main Region II in the analysis of the confluent boundary layer with the method due to Goradia.
DLIM	Limits the magnitude of estimates of derivatives used in CONF7, CONF8.
CONF	Provides the logic and data flow control for the analysis of the modified confluent boundary layer method.
CONFI1	Computes the initial values of the parameters of Main Region I in the analysis of the modified confluent boundary layer method.
CONFD1	Computes the derivatives of the parameters of Main Region I in the analysis of the modified confluent boundary layer method.
CONFP1	Computes and displays the parameters of Main Region I in the analysis of the modified confluent boundary layer method.
CONFI2	Computes the initial values of the parameters of Main Region II in the analysis of the modified confluent boundary layer method.
CONFD2	Computes the derivatives of the parameters of Main Region II in the analysis of the modified confluent boundary layer method.
CONFP2	Computes and displays the parameters of Main Region II in the analysis of the modified confluent boundary layer method.
VSFOUA	Provides an output interface between the data structures of the new version of the program and the laminar and turbulent boundary layer analysis routines of the baseline version.
VSFOUB	Provides an output interface between the data structures of the new version of the program and the confluent boundary layer analysis routines of the baseline version.
SRCER	Computes the source strength values to represent the displacement thickness of the viscous layers.

LOAD — Computes the global aerodynamic parameters: lift coefficient, drag coefficient, pitching moment coefficient, axial - and normal force coefficients.

The library routines support the control and analysis routines listed above. Among the functions supported by the library routines are: dynamic storage control, aerodynamic influence coefficients (AIC's) calculation, solution of a system of linear equations, Newton algorithm, and integration of a system of ordinary differential equations. The library routines are:

DYNSET — Initializes and controls the dynamic storage work area.

GETBDA — Reserves storage in the dynamic storage work area for one of the several types of basic data arrays.

FREBDA — Frees the storage in the dynamic storage work area which was assigned to a basic data array by GETBDA.

PRTBDA — Displays the contents of a basic data array which was assigned by GETBDA.

AICVAL — Provides the logic and data flow control for the calculation of the aerodynamic influence coefficients (AIC's) for Oeller's potential flow solution technique.

CPTAIC — Computes the stream function and velocity AIC's for vortex and source distributions on the surface (and wake) segments.

SAVAIC — Saves the AIC's generated by CPTAIC on an I/O unit.

GETAIC — Reads the AIC's stored on an I/O unit by SAVAIC.

GAUSSR — Provides an in core, Gaussian, linear equation solution package with a pivoting capability.

RSEITE — Provides a second solution capability for the algorithm implemented in GAUSSR.

REDUCE — Provides an out of core, Gaussian, linear equation solution package with a pivoting capability which reduces the system to triangular form. An in core equation solver is available upon request.

BCKSUB — Completes the out of core Gaussian solution process in REDUCE by doing the back solution process.

NEWTR — Provides the logic and data flow control for solving a system of nonlinear equations with a Newton algorithm.

INTRG	Provides the logic and data flow control for integrating a system of ordinary differential equations with an integration algorithm.
TRANF	Rotates and translates a coordinate geometry array.
DISTP	Computes a coordinate geometry array such that the corner points are separated by equal increments of curvature of the surface.
DIR	Computes an estimate of the derivative of a tabulated function at one of the tabular points.
POINT	Computes an estimate of the value of a tabulated function at a value of the independent variable with parabolic interpolation.
SLOPE	Computes an estimate of the derivative of a tabulated function at a value of the independent variable with parabolic interpolation.
PROOT	Computes the roots of a cubic polynomial.
SRFIT	Uses a parabolic fit to surface coordinate points to estimate the normal to the surface from a point.
SMOOTH	Provides a smoothing algorithm for a tabulated function.
INITX	Initializes an array to a specified value.
READX	Performs a binary or buffered read from the specified I/O unit into an array.
WRITX	Performs a binary or buffered write of an array onto the specified I/O unit.
REWDX	Rewinds the specified I/O unit.
SUMRX	Computes the sum of all the numbers in an array.
READR	Reads a matrix stored by rows on the specified I/O unit into core, storing it in the standard FORTRAN order.
BLKIT	Reads a specified number of rows of a matrix stored on the specified I/O unit into core, storing it by rows.

SYMBOLS

Aero Symbol	Data Group	Data Item	Explanation
α	ANGL	ANGL	Angle of attack in degrees
		NANGL	Number of angles of attack to process
		IANGL	Index of ANGL of present angle of attack
c_T	CHRD	CTOT	Total airfoil chord length
c		CHRD	Component chord length
		NCRD	Index of point of maximum chord
c_P	CPRS	CPRS	Surface pressure coefficient
		NCPR	Index array for CPRS
c_f	CSKN	CSKN	Skin friction coefficient
		NSKN	Index array for CSKN
δ	DELB	DELB	Boundary layer thickness
		NDLB	Index array for DELB
δ^*	DELS	DELS	Boundary layer displacement thickness
		NDLS	Index array for DELS

Aero Symbol	Data Group	Data Item	Explanation
M_∞	FSMACH	FSMACH	Freestream Mach number
		NMACH	Number of freestream Mach numbers to process
		IMACH	Index of FSMACH of present freestream Mach number
H	HSHP	HSHP	Boundary layer shape factor
			Index array for HSHP
M_e	LMACH	ML	Local Mach number
		NLMH	Index array for ML
	LOFT	MAIN	Index of main component
		INC	Index array of components being lofted
		INR	Index array of reference component
		IPC	Index array of pivot points for lofted component
		IPR	Index array of pivot points for reference component
X_P		XP	X coordinates of pivot points
Z_P		ZP	Z coordinates of pivot points
		IFIN	Flag to indicate lofted components
Δ		DLT	Angle of rotation for lofted component relative to reference component

Aero Symbol	Data Group	Data Item	Explanation
c_d	PARMS	DRAG	Drag coefficient
c_ℓ		LIFT	Total lift coefficient
c_m		PITCH	Pitching moment coefficient
c_a		AXIAL	Axial force coefficient
c_n		NORML	Normal force coefficient
S_F	SCALE	SF	Scale factor to convert input geometry data to feet
c_{ref}		CREF	Reference chord in feet
s	SLOC	SLOC	Arc length (surface fitted coordinate)
		NSLC	Index array for SLOC
x_o, h_{slot}	SLOT	SLOT	Location and height of slot exit for each component
		NSLT	Index of first surface point beyond slot exit
σ	SRC	SRC	Source strength
		NSRC	Index array for SRC
T_o	SRFX	T0	Freestream stagnation temperature in °R
$Re_{ft}10^{-6}$		RN	Reynolds number in million/feet
P_r		PR	Prandtl number
k		KF	Heat transfer factor
p_o		P0	Stagnation pressure

Aero Symbol	Data Group	Data Item	Explanation
	STAG	XSTAG	X coordinate of stagnation point
		ZSTAG	Z coordinate of stagnation point
		ISTAG	Index of stagnation points
		SSTAG	Arc length of stagnation points
θ	THETA	THETA	Boundary layer momentum thickness
		NTHA	Index array for THETA
	TRANS	UGTRN	User to global coordinate transformation data
		GLTRN	Global to local coordinate transformation data
	TRNSIT	XTRAN	X coordinate of transition point
		ZTRAN	Z coordinate of transition point
		LTRAN	Fixed transition flag
		SSTRN	Arc length of transition point
V_c	VCMP	VCMP	Compressible surface velocity
		NVCM	Index array for VCMP
V_i	VSRF	VSRF	Incompressible surface velocity (corner points)
		NSRF	Index array for VSRF
V_T		VSRX	Tangential component of incompressible surface velocity (corner points)
		NSRX	Index array for VSRX

Aero Symbol	Data Group	Data Item	Explanation
V_N		VSRZ	Normal component of incompressible surface velocity (corner points)
		NSRZ	Index array for VSRZ
X_G	XGBL	XGBL	X coordinate, global coordinate system
		NXGB	Index array for XGBL
X_l	XLOC	XLOC	X coordinate, local coordinate system
		NXLC	Index array for XLOC
X_I	XUSR	XUSR	X coordinate, user input coordinate system
		NXUS	Index array for XUSR
Z_G	ZGBL	ZGBL	Z coordinate, global coordinate system
		NZGB	Index array for ZGBL
Z_l	ZLOC	ZLOC	Z coordinate, local coordinate system
		NZLC	Index array for ZLOC
Z_I	ZUSR	ZUSR	Z coordinate, user input coordinate system
		NZUS	Index array for ZUSR

Aero Symbol	Data Group	Data Item	Explanation
K_{ij}^{s}	AIC	ASZ	Source stream function AIC work array
		NASS	Index array for ASS
$\frac{\partial K_{ij}^{s}}{\partial X}$		ASX	Source X velocity AIC work array
		NASX	Index array for ASX
$\frac{\partial K_{ij}^{s}}{\partial Z}$		AVZ	Source Z velocity AIC work array
		NAVZ	Index array for ASS
K_{ij}^{v}		AVS	Vortex stream function AIC work array
		NAVS	Index array for AVS
$\frac{\partial K_{ij}^{v}}{\partial X}$		AVX	Vortex X velocity AIC work array
		NAVX	Index array for AVX
$\frac{\partial K_{ij}^{v}}{\partial Z}$		AVZ	Vortex Z velocity AIC work array
		NAVZ	Index array for AVZ
	AIJ	AIJ	Work array for row of Jacobian matrix for wake centerline update
		NAIJ	Index array for AIJ
C		CJJ	Wake centerline chord lengths
		NCJJ	Index array for CJJ
C_x		CJX	Wake centerline segment length in X direction
		NCJX	Index array for CJX
C_Z		CJZ	Wake centerline segment length in Z direction
		NCJZ	Index array for CJZ

Aero Symbol	Data Group	Data Item	Explanation
	CONV	LCONV	Convergence control flag
θ	CTH	CTH	Wake centerline segment angles
		NCTH	Index array for CTH
		STR	Stream function value array for wake centerline update
		NSTR	Index array for STR
	DYNAM	DYNM	Dynamic storage reference array
		NDYN	Number of words in DYNM available for dynamic storage
		LDYN	First available word in DYNM for dynamic storage
	ERROR	DSPLY	Display area for error message
		LOCERR	Local error flag
		GLBERR	Global error flag
ϵ_m	ETAL	ETAL	Trailing edge angle
	INDVIS	IXGB	Index for XGBL
		IZGB	Index for ZGBL
		ISLC	Index for SLOC
		IVCM	Index for VCMP
		ILMH	Index for ML
		ICPR	Index for CPRS
		IDLB	Index for DELB
		IDLS	Index for DELS
		ISHP	Index for HSHP
		ITHA	Index for THETA
		ICSK	Index for CSKN

Aero Symbol	Data Group	Data Item	Explanation
	IOTAB	IOTAB	Table of available I/O units
		NPRT	Print unit
	ITNUM	ITNUM	Number of current iteration
		ITMAX	Maximum number of iterations
	KEYS	KEYA	Process AVS, AVX, AVZ, ASS, ASX, ASZ type AIC's on unit 1
		KEYB	Process AVS, ASS type AIC's in unit 1
		KEYC	Process ASS, ASX, ASZ type AIC's on unit 1
		KEYD	Process ASS type AIC on unit 1
		KEYE	Process AVX, AVZ, ASX, ASZ type AIC's on unit 2
		KEYF	Process ASX, ASZ type AIC's on unit 3
	LEND	LEND	End of user input flag
N_C	NC	NC	Number of components
	NSP	NSP	Maximum number of surface points
		NSM	Minimum number of points on a surface of a component
		NPN	Number of surface points defined by user for each component
		IDISP	Flag for input points redistribution
	NCMP	NCMP	Number of computational points

Aero Symbol	Data Group	Data Item	Explanation
	RHS	RHS	Right-hand side array for vortex strength calculation
		NRHS	Index array for RHS
	SOL	SOL	Work array for rows of the solution matrix
		NSOL	Index array for SOL
	VARIN	VARIN	Work array for integration variable in wake and modified Goradia solution
	VISC	ICMP	Number of component for which viscous flow solution is being performed
		ISRF	Surface on the component
		ITRN	Transition to turbulent flow flag
		ICORE	End of potential flow core flag
X_A	XWKA	XWKA	X coordinate, work array
		NXWA	Index array for XWKA
X_B	XWKB	XWKB	X coordinate, work array
		NXWB	Index array for XWKB
X_c	XWKC	XWKC	X coordinate, work array
		NXWC	Index array for XWKC

Aero Symbol	Data Group	Data Item	Explanation
Z_A	ZWKA	ZWKA	Z coordinate, work array
		NZWA	Index array for ZWKA
Z_B	ZWKB	ZWKB	Z coordinate, work array
		NZWB	Index array for ZWKB
Z_C	ZWKC	ZWKC	Z coordinate, work array
		NZWC	Index array for ZWKC
x_e	WAKEA	DWAK	Width of wake at the end of the core
		UWAK	Wake velocity at the end of the core
		XWAK	X coordinate of the end of core
		NWAK	Index of surface point on aft component at end of core
		IWAK	Number of wake centerline points before end of core

PROCESSING OF USER INPUT (A)

In this section, the input cards and the preprocessing of the geometry data are described. The computer code is contained in OVERLAY (1,0), subroutines

INPTR	SMOPT	ANGLR	WAKECL
READIT	GEOMB	LOCLD	
GEOM	LOFTR	SURFD	
GEOMA	SLOTR	TRANF	
RESCL	GLOBD	DISTP	
AFPRM	SRFIT	FTLUD	
COMPT	GEOMC	DIR	

INPUT CARDS (AA)

The input cards are read by subroutines INPTR and READIT.

DESCRIPTION OF INPUT CARDS

Card 1 — Format (8A10)

- Title – 80 column title

Card 2 — Format (2F10.0)

- NC – Number of components (1<NC<10)
- NSP – Number of computational surface points, 2*NC ≤ NSP ≤ 200

Cards 3 through 6 are input NC times

Card 3 — Format (2F10.0)

- NPP – Number of pivot points connected to this component (up to 3 pivot points per component)
- NPT – Number of points to be input for this component (sum of NPT for all components≤306)

Card 4 — Format (6F10.0)

- (Xp,Zp) – Coordinates of the pivot point referenced to this coordinate system; if NPP=0, skip this card

Card 5	Format (8A10)
FMT	– The format of the input point coordinates, enclosed in parentheses. Example (6F10.0)
Card 6	Format from Card 5
$(X_I.Z_I)$	– The input point coordinates in (X_I,Z_I) pairs starting at the upper-surface trailing edge and ending at the lower-surface trailing edge Use as many cards as necessary
Card 7	Format (F10.0)
IM	– Index of the main component Card 7 is skipped if NC=1
Card 8	Format (5F10.0)
IC	– Index of this component
IPP	– Index of the pivot point to be used in placing this component
ICR	– Index of the reference component
IPPR	– Index of the pivot point on the reference component to be used in placing this component
DELTA	– Angle of rotation between this coordinate system and the reference coordinate system in degrees
Note:	This card is included for each component other than the main component, i.e., Card 8 is repeated (NC-1) times. Card 8 is skipped if NC=1
Card 9	Format (F10.0)
NA	– Number of angles of attack to be input. ($1 \leq NA \leq 10$)
Card 10	Format (5F10.0)
ALPHA	– Angle of attack in degrees, NA values
Card 11	Format (F10.0)
NM	– Number of freestream Mach numbers. ($1 \leq NM \leq 10$)
Card 12	Format (5F10.0)
FSMCH	– Freestream Mach number, NM values
Card 13	Format (2F10.0)
CREF	– Reference chord in feet. This number is used to nondimensionalize output quantities.
SF	– Scale factor. This factor converts the input geometry to feet.

Card 14	Format (4F10.0)
TO	– Stagnation temperature – °R
RN	– Reynolds number – millions/ft
PR	– Prandtl number (use 0.77)
KF	– Heat transfer factor (use 1.0)
Card 15	Format (3F10.0)
LTRAN	– Fixed transition option, = 0. implies free transition = 1. implies fixed transition
(XTRAN, ZTRAN)$_L$	– location of fixed transition (use (0.0) if free transition)
Note:	Card 15 is repeated (2NC) times. Upper surface, first component; lower surface, first component; upper surface, second component; etc.
Card 16	Format (A10)
THEbENDbbb	– The last data card of last case to be processed

SYMBOLS OF INPUT CARDS

The following list of symbols is included to facilitate cross references to other sections of the computer code.

Theory	Code	Definition
c_{ref}	CREF	Reference chord in feet
	IC	Indices of components in the order that their data are stored
	ICR	Index of reference component for each component
	IM	Index of main component
	IPP	Index of pivot point used in placing each component
	IPPR	Index of pivot point on reference component to be used in placing each component
k	KF	Heat transfer factor
	LTRAN	Transition option: = 0 free transition, = 1 fixed transition
M_∞	FSMACH	Freestream Mach number
	NA	Number of angles of attack
N_C	NC	Number of components
	NM	Number of Mach numbers
	NPP	Number of pivot points for each component
	NPT	Number of input points for each component
	NSP	Total number of computational surface points
Pr	PR	Prandtl number
$Re_{ft}\ 10^{-6}$	RN	Reynolds number in millions per foot
S_F	SF	Scale factor for conversion of input geometry to feet

Theory	Code	Definition
T_0	TO	Freestream stagnation temperature in °R
X_I, Z_I	X, Z	Surface point in input coordinate system
X_p, Z_p	XP, ZP	Pivot point coordinates in input coordinate system
X_{tr}, Z_{tr}	XTRAN, ZTRAN	Location of fixed transition in input coordinates
α	ALPHA	Angle of attack in degrees
Δ	DELTA	Angle of rotation from the component's coordinate system into its reference component coordinate system

PREPROCESSING OF GEOMETRY DATA (AB)

The geometry package of the program is described in this section. The code is contained in the following subroutines.

GEOM	SMOPT	SURFD	TRANF
GEOMA	GEOMB	GEOMC	FTLUD
RESCL	LOFTR	ANGLR	DIR
AFPRM	SLOTR	LOCLD	SRFIT
COMPT	GLOBD	DISTP	WAKECL

GEOMETRY DEFINITION

Examples of multielement airfoil geometries are contained in figure 7. Each of the airfoil geometries shown represents a two-dimensional cut through a high lift wing configuration and may consist of up to 10 airfoil components. The airfoil geometries may be quite general having

- Arbitrary distributions of camber and thickness
- Blunt or pointed trailing edge shape
- Positive, zero, or negative overlap of neighboring airfoil components

Figure 8 illustrates some of these geometric features.

Note: Even though the geometry package of the program can handle quite arbitrary geometries, the user of the program must be warned that severe limitations are imposed on the geometry by the various aerodynamic models of the method. As an example, the assumption of attached flow requires a smooth geometry without abrupt changes of the airfoil's surface. Other limitations are pointed out in the description of the aerodynamic theory.

The input geometry of an airfoil is defined by a set of surface points (X_I, Z_I). The coordinates of these points may be specified in a different coordinate system for each component. They are read into the program beginning at the upper surface trailing edge point. The reading of the data then proceeds along the upper and lower surfaces of the airfoil component and ends at the lower surface trailing edge point. The trailing edge point of airfoils with a sharp trailing edge, appears twice in the data set.

COORDINATE SYSTEMS

The program uses three types of coordinate systems (fig.9). They are defined as follows.

- Input coordinates (X_I,Z_I)

  These are Cartesian coordinate systems selected by the user. The user can either

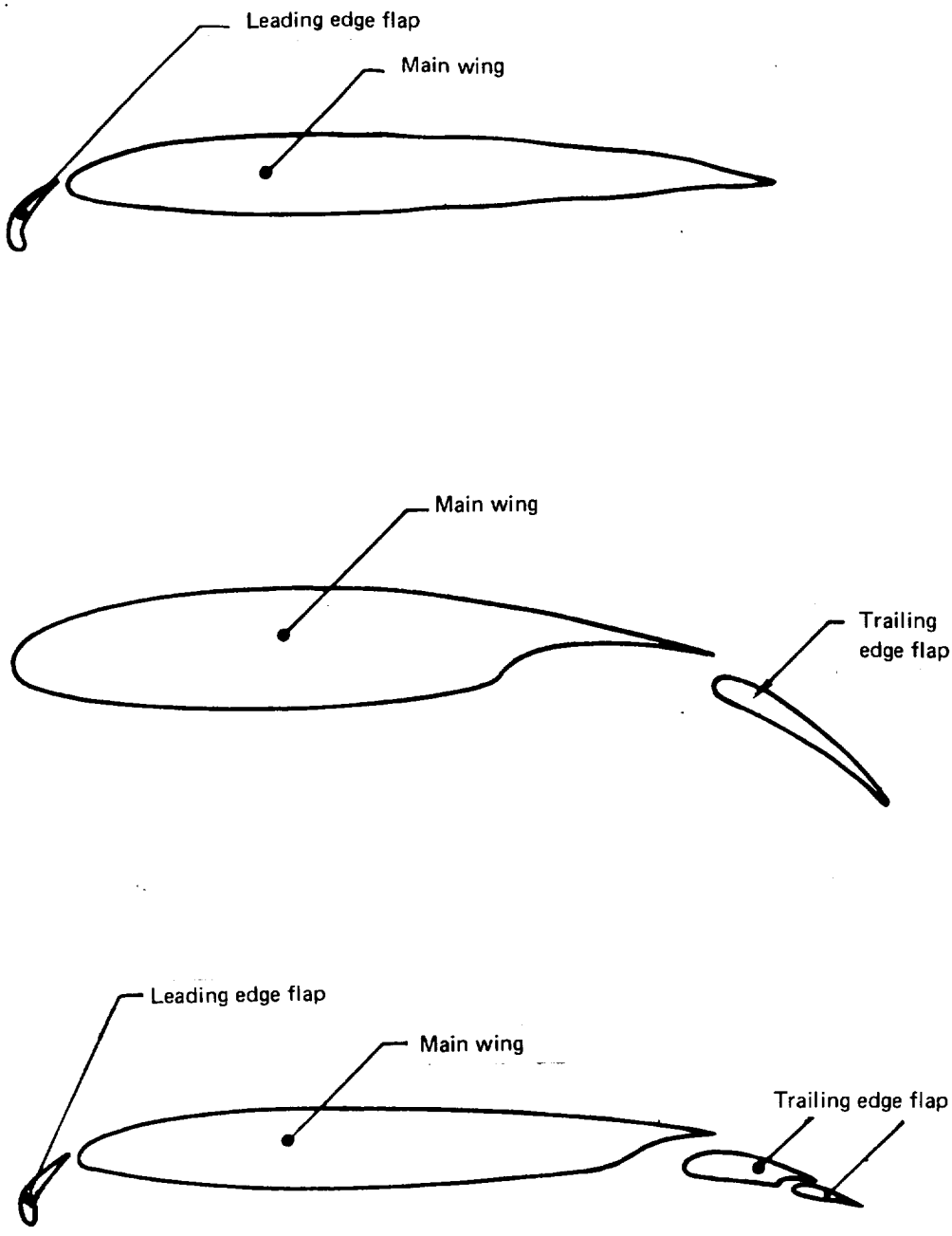

Figure 7. – Examples of Multielement Airfoil Geometries

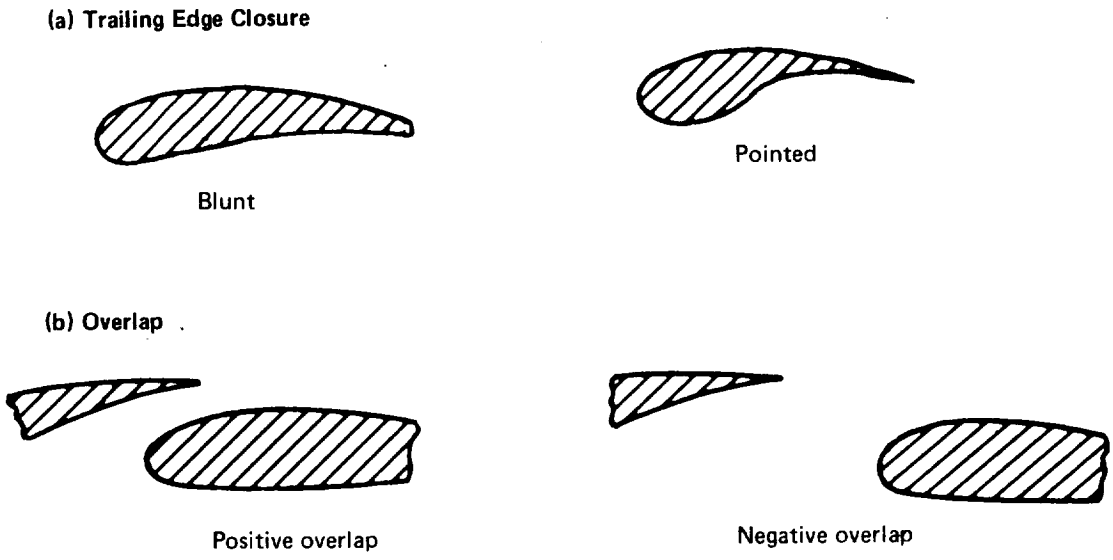

Figure 8. — Geometry Features

specify a different coordinate system for each component or can choose to define all input geometries in one and the same coordinate system.

- Global coordinates (X_G,Z_G)

  This is the input coordinate system of the main component.

- Local coordinates

  There are two types of coordinate systems (fig. 9). One type is the boundary layer coordinate system, and the other is the local Cartesian coordinate system.

  The coordinates (X_l,Z_l) are defined such that their origin is located at the leading edge and the X_l axis passes through the average trailing edge point. The leading edge point is that point of the airfoil which is farthest away from the average trailing edge point. The distance between the two points defines the chord length, c, of the airfoil component.

  The coordinates (x,y) are surface fitted or boundary layer coordinates. The x coordinate is identical with the arc length, s, calculated by summation of the distances between surface points. The calculation of arc length begins at the lower surface trailing edge point.

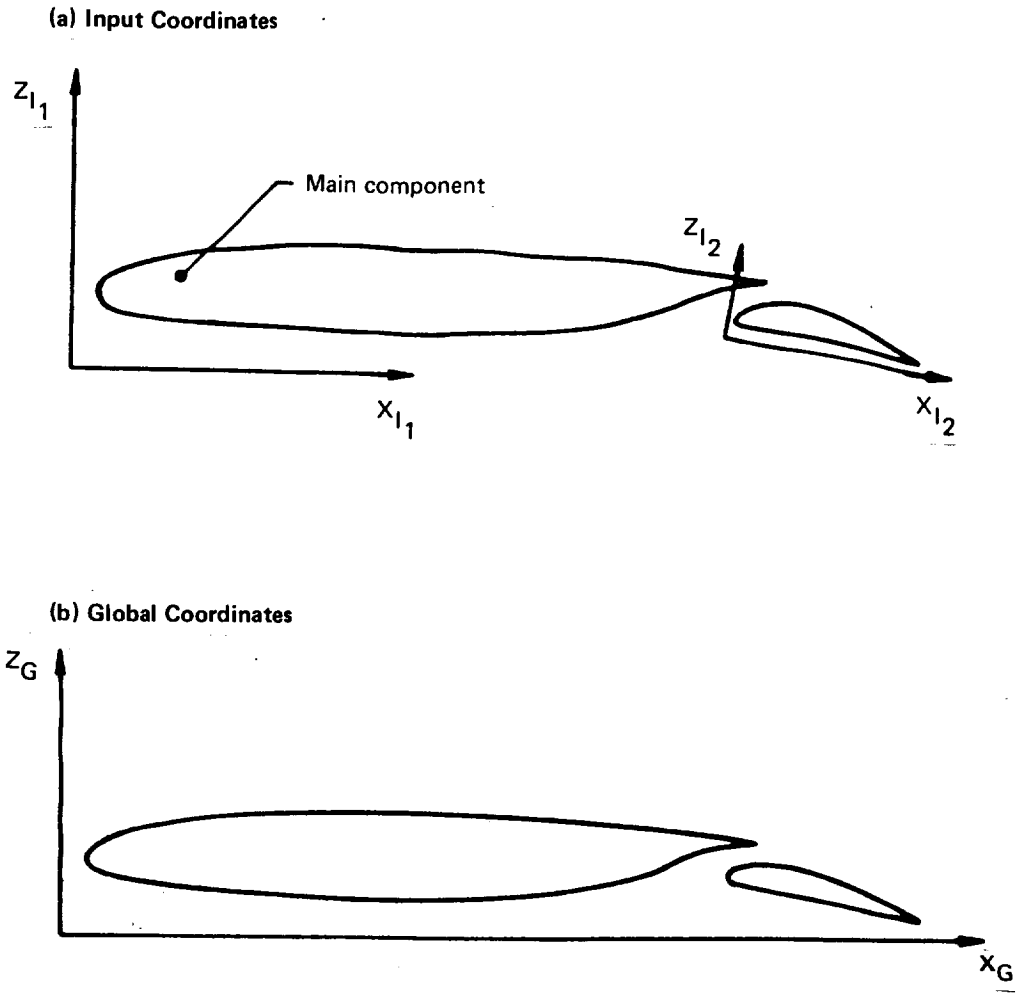

Figure 9. — Coordinate Systems

Computational Surface Points

To obtain accurate potential flow results, computational surface points are chosen which differ from the input surface points in both number and location. The calculations are performed in subroutine COMPT.

The total number of computational surface points NSP is an input variable. The numbers of computational surface points N_i of an airfoil component is calculated using the formula

$$N_i = \left(NSP - 21 \quad N_C\right)\frac{c}{c_T} + 21 \tag{1}$$

where c is the chord length of the considered airfoil component and c_T is the sum of the chord lengths of all components. The symbol N_C denotes the total number of airfoil components. The numerical result of the term

$$\left(NSP - 21 \quad N_C\right)\frac{c}{c_T}$$

is truncated to its integer value. The above formula divides the NSP computational surface points among the N_C airfoil components such that each component has an odd number of points with a minimum of 21.

The location of the computational surface points is determined in subroutine DISTP based on surface curvature. The new surface points cluster in the regions of high curvature. The following sequence of calculations is used for each airfoil surface.

Step 1

The input surface points (X_j, Z_j) $j = 1, 2, \ldots j_{max}$ are used to define the arc length from the trailing edge

$$s_1 = 0$$

$$s_j = \sum_{i=2}^{j_{max}} \left[\left(X_j - X_{j-1}\right)^2 + \left(Z_j - Z_{j-1}\right)^2\right]^{1/2} \tag{2}$$

Step 2

The arc length is considered as a parameterization of the (X,Z)-coordinates of the surface $X + X(s)$; $Z + Z(s)$. The curvature of the point $(X_j, Z_j) = (X(s_j), Z(s_j))$ is

$$K\left(s_j\right) = \frac{\left|\frac{\partial X}{\partial s}\frac{\partial^2 Z}{\partial s^2} - \frac{\partial Z}{\partial s}\frac{\partial^2 X}{\partial s^2}\right|}{\left[\left(\frac{\partial X}{\partial s}\right)^2 + \left(\frac{\partial Z}{\partial s}\right)^2\right]^{\frac{3}{2}}} \tag{3}$$

where the derivatives on the right hand side are evaluated at s_j.

Step 3

A function SUM(K(s)) is computed using the formula

$$SUM(s) = \int_0^s [K(X)]^{1/4}\, dX \tag{4}$$

Step 4

The arc length is considered as a function of SUM. Evaluation points are chosen as follows.

$$SUM_j^* = \frac{SUM(s_{j_{max}})}{j_{max} - 1}(j-1); \quad j = 1, 2, \ldots, j_{max} \tag{5}$$

Interpolation is used to predict the arc length at SUM^*_j,

$$s_j^* = s\left(SUM_j^*\right)$$

Note: If SUM represents the integral of curvature along the surface, then s^*_j are separated by equal increments of curvature.

Step 5

Finally, interpolation is used to compute the values of X,Z corresponding to s^*_j, i.e.,

$$\left.\begin{aligned} X_j^* &= X\left(s_j^*\right) \\ Z_j^* &= Z\left(s_j^*\right) \end{aligned}\right\} j = 1,2, \ldots, j_{max}$$

Lofting

The components other than the main component are rotated and translated from their input coordinate systems into the global coordinate system. This is done in subroutine LOFTR as follows.

For each component a reference component is specified. Translation is performed by moving a specified pivot point in the coordinate system of the translated component to a specified pivot point in the coordinate system of the reference component. Rotation is performed about the pivot point by a specified angle between the reference component coordinate system and the coordinate system of the rotated component.

The transformation is performed according to these equations:

$$X_i' = \left(X_i - X_P\right)\cos\Delta + \left(Z_i - Z_P\right)\sin\Delta + X_P' \tag{6}$$

$$Z_i' = \left(Z_i - Z_P\right)\cos\Delta - \left(X_i - X_P\right)\sin\Delta + Z_P'$$

The symbols have the meaning:

X'_i, Z'_i Surface point in coordinates of reference component

X_i, Z_i Surface point in coordinates of lofted component

Δ Angle of rotation (positive clockwise)

X_P, Z_P Pivot point in coordinates of lofted component

X'_P, Z'_P Pivot point in coordinates of reference component

The program ensures that a component geometry is not rotated and translated into the global coordinate system unless its reference component has been rotated and translated.

As an example, figure 10 shows the lofting of a high lift airfoil with four components. The second component is the main component (wing). Its coordinate system serves as the global coordinate system in which the geometry of the other three components (leading edge flap and trailing edge flaps) has to be defined by the process of lofting. The points A, B, C are the pivot points. The rotation angles are also indicated in the figure. The following table lists the components and their reference components. The sequence of the lofting procedure is the sequence in which the components are shown below.

Component	Reference Component	Δ	Pivot Point
1	2	1-2	A
4	2	4-2	B
3	4	3-4	C

The pivot point, C, is transformed into the global coordinate system during the lofting of component 4.

AIRFOIL PARAMETERS

Slot Height

The slot height at the exit of the slot is defined as illustrated in figure 11 for the two geometric cases of positive and negative overlap of neighboring airfoil components. A straight line defining the slot height is drawn from the lower surface trailing edge point of the upstream component perpendicular to the surface of the downstream component.

The slot height, h_{slot}, and the coordinates of the point, P_N, on the surface of the aft component are determined in subroutine SLOTR as follows:

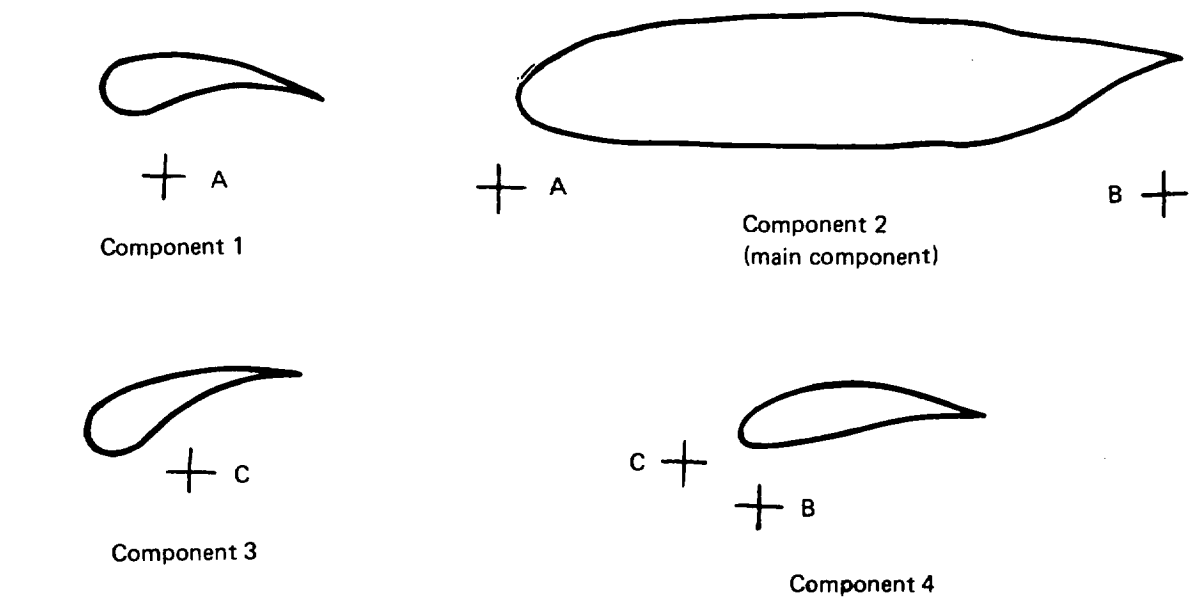

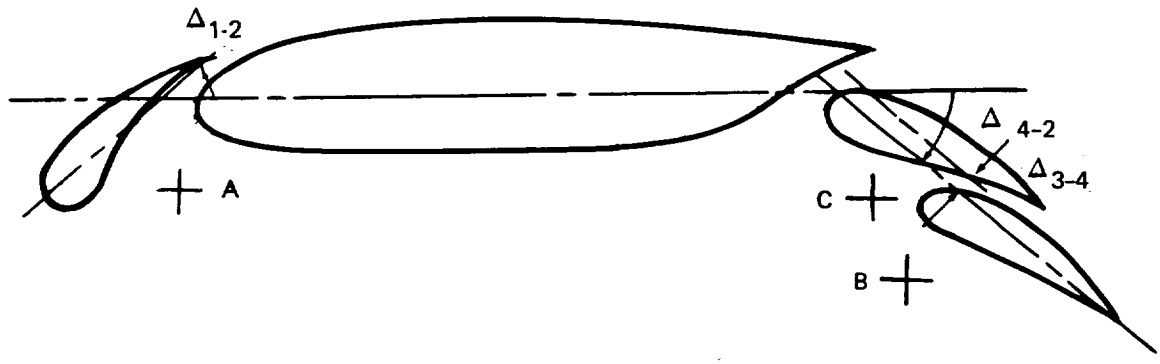

Figure 10. — Example of Lofting a High-Lift Airfoil

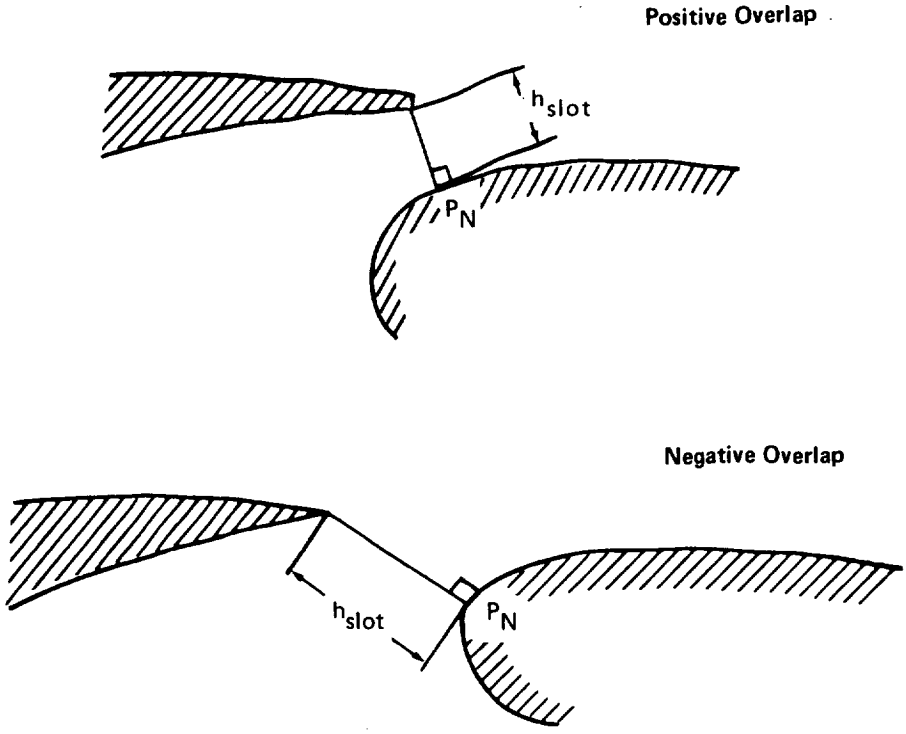

Figure 11. – Definition of Slot Height

Step 1

The minimum distance $\overline{P_{TE}P_i}$ from the trailing edge point, P_{TE}, to the points on the upper surface of the aft component determines the point P_i (fig. 12).

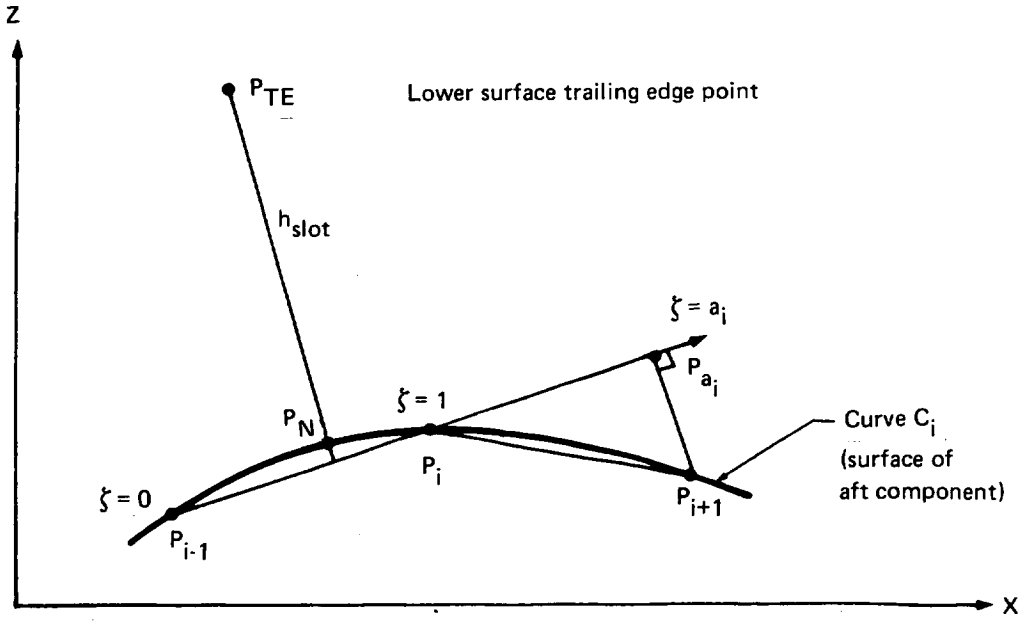

Figure 12. — On the Calculation of Slot Height

Step 2

A curve, C_i, passing through the points P_{i-1}, P_i, P_{i+1} is calculated. The parametric representation of C_i in terms of a nondimensional chord length ζ reads

$$X_i(\zeta) = \zeta X_i + (1-\zeta) X_{i-1} + \zeta(1-\zeta)\alpha_i$$
$$Z_i(\zeta) = \zeta Z_i + (1-\zeta) Z_{i-1} + \zeta(1-\zeta)\beta_i \qquad (7)$$

The values of ζ at the various points are shown in figure 12. The point, P_{a_i}, where $\zeta = a_i$, is the projection of P_{i+1} on the chord length ζ. The variable a_i is obtained from geometric relations as

$$a_i = \frac{(X_{i+1} - X_i)(X_i - X_{i-1}) + (Z_{i+1} - Z_{i-1})(Z_i - Z_{i-1})}{(X_i - X_{i-1})^2 + (Z_i - Z_{i-1})^2} \qquad (8)$$

Since the computational surface points are distinct, one always computes $a_i \neq 1$. The coefficients α_i, β_i of the equations for C_i follow from

$$\alpha_i = \frac{X_{i+1} - a_i X_i - (1 - a_i) X_{i-1}}{a_i (1 - a_i)} \qquad \beta_i = \frac{Z_{i+1} - a_i Z_i - (1 - a_i) Z_{i-1}}{a_i (1 - a_i)} \tag{9}$$

Step 3

The coordinates of the point $P_N = (X_N, Z_N)$ are calculated using

$$\begin{aligned} X_N &= \zeta_N X_i + (1 - \zeta_N) X_{i-1} + \zeta_N (1 - \zeta_N) \alpha_i \\ Z_N &= \zeta_N Z_i + (1 - \zeta_N) Z_{i-1} + \zeta_N (1 - \zeta_N) \beta_i \end{aligned} \tag{10}$$

and the equation of the normal to the surface at P_N that passes through the trailing edge point (X_{TE}, Z_{TE}).

$$(X_{TE} - X_N) \left.\frac{dX_i}{d\zeta}\right|_{\zeta=\zeta_N} + (Z_{TE} - Z_N) \left.\frac{dZ}{d\zeta}\right|_{\zeta=\zeta_N} = 0$$

Combining these equations produces a cubic equation for ζ_N

$$c_o + c_1 \zeta_N + c_2 \zeta_N^2 + c_3 \zeta_N^3 = 0 \tag{11}$$

with the coefficients

$$c_o = (X_i - X_{i-1} + \alpha_i)(X_{TE} - X_{i-1}) + (Z_i - Z_{i-1} + \beta_i)(Z_{TE} - Z_{i-1})$$

$$c_1 = -2\alpha_i (X_{TE} - X_{i-1}) - 2\beta_i (Z_{TE} - Z_{i-1}) - (X_i - X_{i-1} + \alpha_i)^2 - (Z_i - Z_{i-1} + \beta_i)^2$$

$$c_2 = 3\alpha_i (X_i - X_{i-1} + \alpha_i) + 3\beta_i (Z_i - Z_{i-1} + \beta_i)$$

$$c_3 = -2 (\alpha_i^2 + \beta_i^2)$$

The real value of ζ_N in the range $0 \leq \zeta_N \leq a_i$ is chosen. Once ζ_N is known, the coordinates X_N, Z_N can be calculated from equation (10).

Step 4

The slot height follows from

$$h_{slot} = \sqrt{(X_{TE} - X_N)^2 + (Z_{TE} - Z_N)^2} \tag{12}$$

Trailing Edge Closure Angle

Given the coordinates of the computational surface points P_1, P_2, P_N, P_{N+1} in global coordinates, the trailing edge closure angle ϵ_m of the m-th airfoil component is calculated from

$$\epsilon_m = \arctan \frac{\bar{S}_1 - \bar{S}_N}{1 + \bar{S}_1 \bar{S}_N} \tag{13}$$

where $\bar{S}_1$, $\bar{S}_N$ are the slopes of the first and last segments of the airfoil component, i.e.,

$$\bar{S}_1 = \left.\frac{dZ}{dX}\right|_1 = \frac{Z_1 - Z_2}{X_1 - X_2}$$

$$\bar{S}_N = \left.\frac{dZ}{dX}\right|_N = \frac{Z_{N+1} - Z_N}{X_{N+1} - X_N}$$

The notation is illustrated in figure 13.

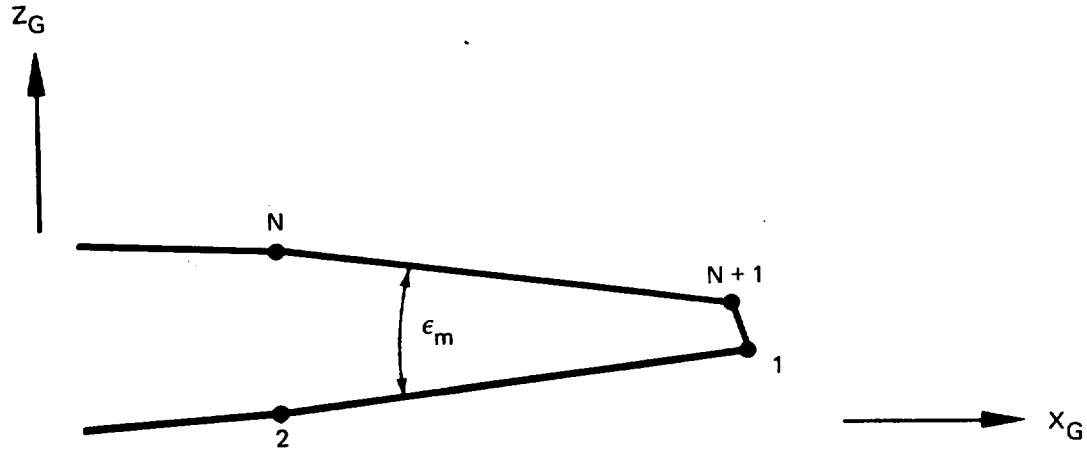

Figure 13. – Airfoil Trailing Edge Geometry

AERODYNAMIC ANALYSIS

The flow field of multielement airfoils can be divided into several flow regions with different physical characteristics. These are:

- Outer potential flow
- Laminar boundary layers
- Transition
- Ordinary turbulent boundary layers
- Wakes
- Confluent boundary layers
- Regions of separated flow.

The last two flow regions distinguish the flow problem of multielement airfoils from the problem of airfoils at cruise conditions.

The following sections of this document contain a detailed description of the mathematical formulation and solution of each flow region. Regions of separated flow are not modeled by the aerodynamic analysis.

ITERATION PROCEDURE (BA, BB, BC)

GENERAL DESCRIPTION

The concept of displacement thickness is used to represent the effect of the various viscous layers on the outer potential flow. Instead of adding the displacement thickness to the airfoil geometry, a distribution of sources along the airfoil surface and along the wake centerlines is utilized for the simulation of the viscous flow displacement effects. This is the so-called surface transpiration method which, within the framework of thin boundary layer theory, is completely equivalent to the method of adding geometrically the displacement thickness to the basic airfoil geometry. Details of the scheme are described in the section titled Viscous Flow Representation.

The mathematical formulations of the inviscid and viscous flow problems are coupled through their respective boundary conditions. A solution of the potential flow problem, such as the distribution of surface velocity, depends on the airfoil geometry and on the boundary layer displacement thickness. The solutions of the boundary layer problems, in turn, which include the displacement thickness, depend on the potential flow velocities.

The objective of the solution procedure, therefore, is to find those particular distributions of surface velocity and boundary layer displacement thickness which simultaneously satisfy both the potential flow problem and the boundary layer problems. The desired solutions of surface velocity and displacement thickness, from which all other flow parameters can be computed, must be arrived at in an iterative procedure since the coupling of the flow problems is mathematically nonlinear. The computer program uses a cyclic iteration procedure described below. The main loop of the iteration procedure is contained in subroutine SYSOL.

CYCLE 0

The computation performed during this iteration cycle consists of the following steps.

1. The first potential flow solution is calculated without any representation of viscous flow effects.

2. The position of the wake centerlines is computed.

3. Solutions of all viscous flow problems including laminar and turbulent boundary layers, confluent boundary layers, and viscous wakes are calculated with the surface velocities and wake centerline location obtained in the previous step as input data. At the end of this computational step, a first estimate of the displacement thicknesses of all boundary layers and wakes is available.

CYCLE 1

The following computational steps are performed.

1. A source distribution representing the displacement effect of all boundary layers and wakes is calculated.

2. A new potential flow solution is calculated for the basic airfoil geometry with a distribution of sources computed in the previous step along the surface and wake centerlines of the multielement airfoil.

3. The position of the wake centerlines is updated using the result of the previous potential flow calculation.

4. All boundary layer and wake properties are recomputed with the last available potential flow velocities and wake centerline geometries as input data.

In subsequent cycles of the iteration procedure, the calculations described under Cycle 1 are repeated. Several refinements of the iteration procedure which are used to assist in the convergence of the scheme are described in the following chapter.

CONVERGENCE ASSISTANCE

The following techniques are used to improve the convergence characteristics of the iteration procedure.

SMOOTHING

The distributions of surface velocity and displacement thickness exhibit rapid changes or discontinuities in certain areas, due to deficiencies of the chosen aerodynamic model, and are physically not realistic. Anomalies of this kind typically occur in the following areas.

- Trailing edges of airfoil components
- Transition points
- End of the potential core region

Consequently, the source distribution, which is computed from the potential flow velocity and the boundary layer displacement thickness, will also exhibit an unrealistic behavior in these areas. To arrive at a physically meaningful converged solution, the computed source distributions are modified as described in detail in the section titled Viscous Flow Representation.

SCALING

To assist the iteration scheme to arrive at a converged solution, the increments of the computed source strength σ are scaled according to the formula

$$\sigma^{(i)} = \sigma^{(i-1)} + \frac{2}{3}\left(\bar{\sigma}^{(i)} - \sigma^{(i-1)}\right) \tag{14}$$

The symbol $\bar{\sigma}^{(i)}$ denotes the computed source strength of the i-th iteration cycle prior to scaling. The scaled source strengths of the i-th and (i-1)-st iteration cycle are denoted by $\sigma^{(i)}$ and $\sigma^{(i-1)}$, respectively.

The formula states that the source strength σ is scaled by adding 2/3 of σ computed in the present iteration cycle to 1/3 of a σ computed in the previous iteration cycle.

CONVERGENCE CHECK

The code does not rely on a convergence criterion. Instead, all solutions are obtained in five iteration cycles whether or not a converged solution is arrived at after the last cycle. The quality of the convergence of the solution must be judged by the user of the code.

A reliable check on the convergence of the iteration procedure does not seem to exist. A convergence check on lift coefficient and/or surface pressures might be useful for some cases but is not always reliable. An automatic check on lift coeffient could terminate the computation before a truly converged solution is obtained. Nevertheless, the computer code contains a dummy subroutine called CONVR which can be used for the addition of a convergence check.

VISCOUS FLOW REPRESENTATION (BBA)

The representation of the displacement effect of boundary layers and wakes in the solution procedure for the inviscid part of the flow field is described in this section. The computer code is contained in OVERLAY (0,0), subroutine SRCER.

EQUIVALENT SOURCES

The method is the so-called surface transpiration method in which a distribution of sources along the airfoil surface and along the wake centerlines simulates the displacement effect of the viscous layers. The strength σ of this equivalent source distribution is calculated from

$$\sigma = \frac{d}{ds}\left(\frac{V_i}{U_\infty}\delta^*\right) \tag{15}$$

In this formula, σ denotes an incompressible source, nondimensionalized by the freestream velocity U_∞. The symbol V_i stands for the incompressible dimensional value of the surface velocity.

The use of the boundary layer displacement thickness in the equation for the computation of σ requires a detailed explanation. In the computer code, the displacement thickness δ^* is calculated using a mixed compressible-incompressible method. This approach is adequate within the theoretical framework of the Karman-Tsien compressibility correction which does not require any geometry scaling and, consequently, does not distinguish between compressible and incompressible values of the displacement thicknesses.

MODIFICATIONS OF SOURCES

The computed distribution of δ^* is discontinuous at certain locations, e.g., at the point of transition from laminar to turbulent boundary layer flow, and at the end of the core region. Furthermore, the distributions of displacement thickness and potential flow velocity exhibit a rapid change near the trailing edge of an airfoil. These discontinuities and rapid changes of δ^* and V_i are caused by deficiencies of the aerodynamic modeling and are not physically realistic. Consequently, the source distribution, which is computed from δ^* and V_i will also exhibit such anomalies in certain areas, and would produce erroneous results or could even lead to catastrophic program failures if left uncorrected. Therefore, the following modifications of the source distribution are made.

- Before the sources are computed, the distribution of δ^* on all airfoil surfaces is smoothed once. Wake displacement thicknesses are not smoothed.

- A negative value of an airfoil source is eliminated by substituting the last positive source strength found upstream, i.e., in the direction of the stagnation point. Negative wake sources (sinks) are not modified.

- Unlimited growth of the source strength, upstream and downstream of a trailing edge, is avoided by overriding the computed values of σ. Airfoil sources are kept constant on the last four segments of each airfoil surface. Similarly, wake sources are constant on the first four segments of the wake centerline. The distributions of airfoil sources and wake sources are continuous, but σ will in general be discontinuous at trailing edges.

- The value of the source strength σ is limited to the range $-.07 \leq \sigma \leq .07$

POTENTIAL FLOW (BBB)

The calculation of the incompressible potential flow solution, the compressibility corrections, and the calculation of the stagnation points are described in this section of the document. The computer code is contained in OVERLAY (3,0) consisting of the following subroutines:

POTLF	POTLFE	AICVAL	WAKET	REDUCE
POTLFA	ANLYS	CPTAIC	WAKEJ	BCKSUB
POTLFB	COMPR	SAVAIC	WAKES	QNEWT
POTLFC	STAGN	GETAIC	WAKEG	NEWTR
POTLFD		GAUSSR	NEWTR	VIP
			RSEITE	RECVEC
				EVAL

METHOD OF OELLER

The potential flow solution uses the stream function method of Oeller (ref. 11). Its main assumptions are that the flow is

- Two-dimensional
- Incompressible
- Irrotational
- Attached to the airfoil surface

The principles of the potential flow method are now introduced using a single airfoil without boundary layer representation as an example. The problem is formulated and solved in global coordinates, (X_G,Z_G), where the subscript G is dropped for convenience. The above assumptions allow the problem to be formulated in terms of the stream function as the dependent variable. The stream function Ψ is governed by Laplace's equation,

$$\nabla^2\Psi = 0 \tag{16}$$

which is linear, so the solution of the flow field can be obtained by superposition. The airfoil is represented by a distribution of vorticity along the surface of strength $\gamma(s)$. Adding the stream function of a uniform freestream, whose velocity $\vec{U}_\infty$ meets the X_G axis under an angle of attack α, to the stream function of this vortex sheet results in the stream function of the whole flow field.

$$\Psi = \underbrace{U_\infty \cos\alpha\, Z - U_\infty \sin\alpha\, X}_{\text{free stream}} + \underbrace{\frac{1}{2\pi}\int_0^{s_{TE}} \gamma(s')\, \ln r(s,s')\, ds'}_{\text{vortex sheet}} \tag{17}$$

The notation is illustrated in figure 14, where, in particular, the radius r is the distance between a point on the airfoil surface and a field point (X,Z). The stream function of the vortex sheet is found by integration of the stream functions of elementary vortices from the lower surface trailing edge point (s=0) to the upper surface trailing edge point ($s= s_{TE}$). The value of the stream function Ψ is constant along a streamline. Hence, Ψ is also constant along the airfoil's contour, which is part of the stagnation streamline. This fact is used in calculating the unknown strength of the vortex sheet, γ, and the unknown value of Ψ at the airfoil surface from equation (17)

To solve this integral equation, the airfoil geometry and the vortex distribution are discretized as follows (fig. 15). The airfoil surface is divided into N segments. The (N+1) corner points of these segments are placed on the airfoil surface and are then connected by straight lines, i.e., the airfoil geometry is represented by a polygon. The vorticity is distributed along this polygon such that its value is constant along each segment. If further N collocation points or control points (X_i,Z_i) are chosen, the integral equation (17) reduces to a set of linear algebraic equations.

$$\Psi_c - \sum_{j=1}^{N} K_{ij}^{V} \gamma_j = U_\infty \cos\alpha\, Z_i - U_\infty \sin\alpha\, X_i \qquad (i=1,2,\ldots N) \qquad (18)$$

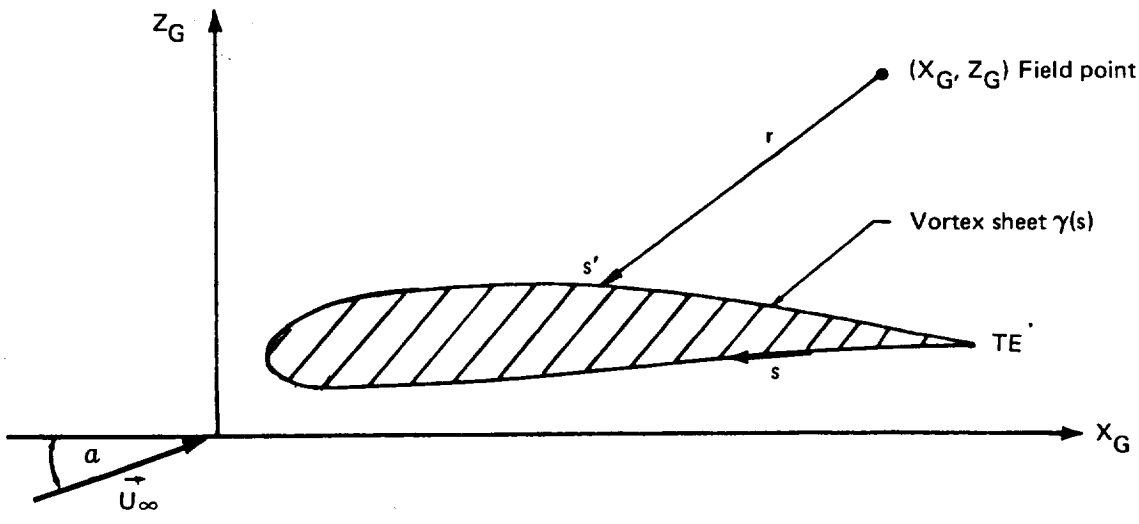

Figure 14. — Notation of Stream Function Method

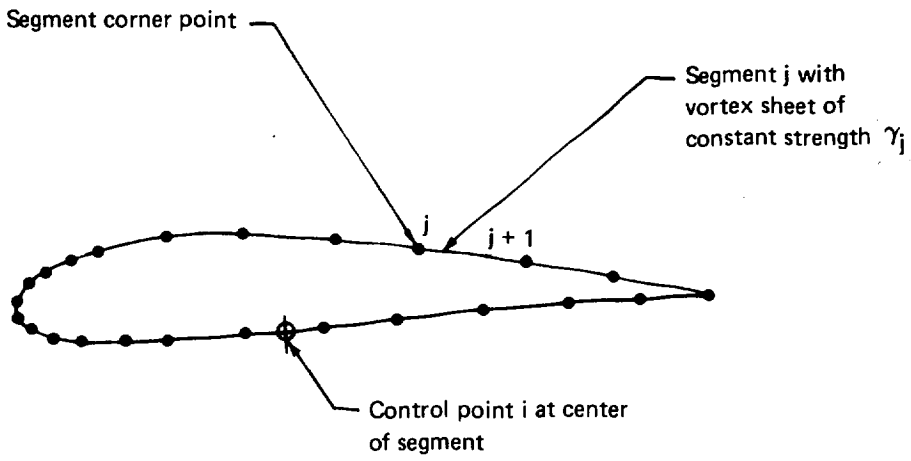

Figure 15. — Discretization Used in Potential Flow Method

Here, ψ_c is the value of the stream function at the contour of the airfoil; and the

$$K_{ij}^{V}\text{'s}$$

are the aerodynamic influence coefficients of a constant strength vortex sheet, defined by

$$K_{ij}^{V} = \frac{1}{2\pi} \int_{s_j}^{s_j + 1} \ell n\, r\,(s_i, s_j')ds' \tag{19}$$

The set of linear equations (18) contains N+1 unknowns, i.e., N unknown vortex strengths γ_j plus one unknown value of the stream function Ψ_c, but provides only N equations. The missing equation is supplied by the Kutta condition, which is formulated as

$$\gamma_1 + \gamma_N = 0 \tag{20}$$

This equation is not the classical Kutta condition, which, in potential flow past airfoils with a nonzero trailing edge angle, postulates the existence of a stagnation point at the trailing edge. Instead, equation (20) states the velocities at the upper and lower surface of the trailing edge are equal, but not necessarily zero as would be the case at a stagnation point.

VORTEX STRENGTH AND STREAM FUNCTION

The principles of Oeller's potential flow method are explained in the previous section. Modifications of the method to include source distributions along the airfoil surface and the wake centerline for the simulation of boundary layer and wake displacement effects are described next.

SINGLE AIRFOIL

Sources are distributed along the airfoil surface and along the wake centerline to represent the displacement effect of boundary layers and wake. The curvature of the wake is assumed to be negligible, so that vortices are only placed along the airfoil surface and not along the wake centerline. The stream function of the flow field must include the contribution of this source sheet.

Accordingly, equation (17) is modified to

$$\Psi = U_\infty \cos\alpha\, Z - U_\infty \sin\alpha\, X + \frac{1}{2\pi}\int_0^{s_{TE}} \gamma(s')\, \ell n\, r\,(s,s')\, ds' + \frac{1}{2\pi}\int_0^{s_E} \sigma(s')\, \varphi(s,s')\, ds' \quad (21)$$

Here, the symbol $\sigma(s)$ denotes the strength of the source distribution. The angle φ and the arc length s_E are illustrated in figure 16.

To solve for the unknown strength of the vortex sheet, the potential flow problem is discretized as follows. The airfoil surface is subdivided into N segments. In addition, there are N_W segments representing the wake centerline. Each of the N segments, which approximate the airfoil surface, carries a constant strength source sheet σ_j and a constant distribution of vortex strength γ_j. Only source sheets of constant strength are placed on the N_W wake segments.

Furthermore, to solve equation (21), a streamline of known position must be chosen along which the stream function will have a constant value Ψ_c. Knowing the position of this streamline, control points (X_i,Z_i) on the streamline can then be chosen. In the absence of sources, the airfoil surface itself represents without any doubt such a streamline. The question now arises: does the airfoil surface remain a streamline when sources are distributed along the surface? This is obviously not the case, since the sources model the displacement thickness of the boundary layer which, when added to the geometric airfoil surface, produce the so-called displacement body. That is to say, the presence of the sources has shifted the stagnation streamline from the airfoil surface to the surface of the displacement body. Figure 17 shows the qualitative pattern of the streamlines in the vicinity of the airfoil surface.

Nevertheless, control points that are located on the airfoil surface and, therefore, are fixed during the solution procedure are chosen for reasons of simplicity and computational efficiency. This choice can be justified as follows.

The objective of the potential flow calculation is to provide a solution of Laplace's equation with a known distribution of sources in the flow field simulating viscous flow displacement effects. The strengths of these sources represent boundary conditions prescribing the velocity normal to the airfoil surface and the wake centerline. When discretizing equation (21), one can make use of the fact that the source σ_i on the i-th segment already satisfies the specified normal velocity boundary condition. Hence, the superposition of the effects of all remaining vortices and sources of the flow field must satisfy the boundary condition of zero normal velocity at the i-th control point. Writing this condition as $\delta\Psi/\delta x = 0$, where x is the local Cartesian coordinate tangent to the

surface, one arrives at the boundary condition of a constant value of the stream function along the airfoil surface. This constant value of Ψ is denoted by Ψ_c.

The reader is reminded the potential flow problem in the presence of sources is solved as if the stream function had a constant value along the surface. The superposition of all vortices and sources of the flow field including σ_i will produce a stream function whose value changes along the airfoil surface.

Discretizing equation (21) as described results in

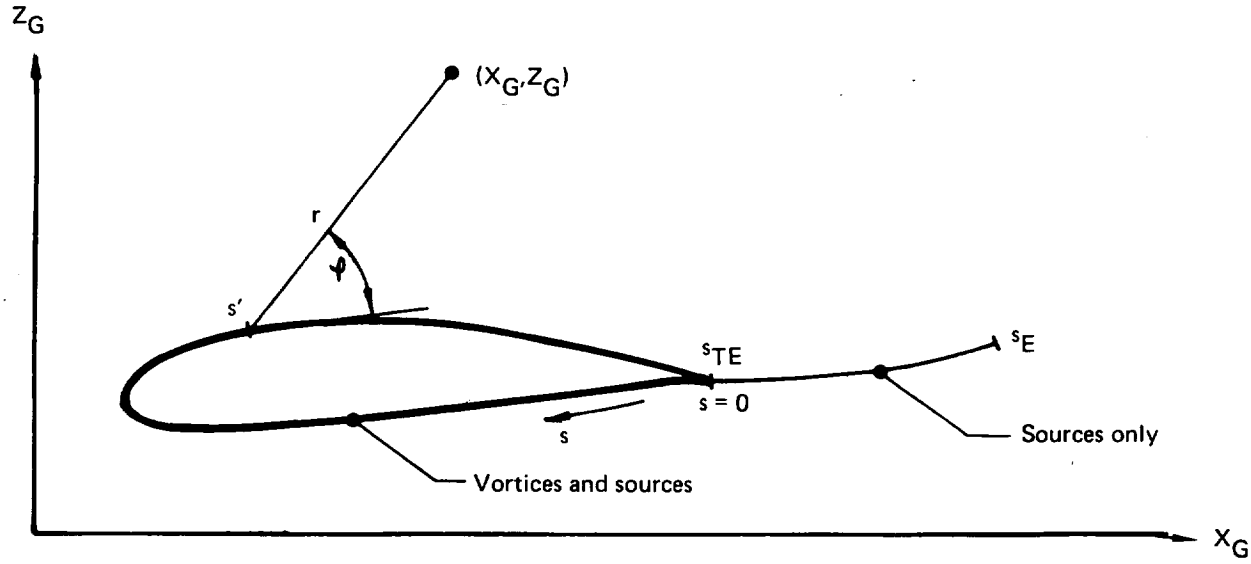

Figure 16. – Additional Notation for Source Distributions

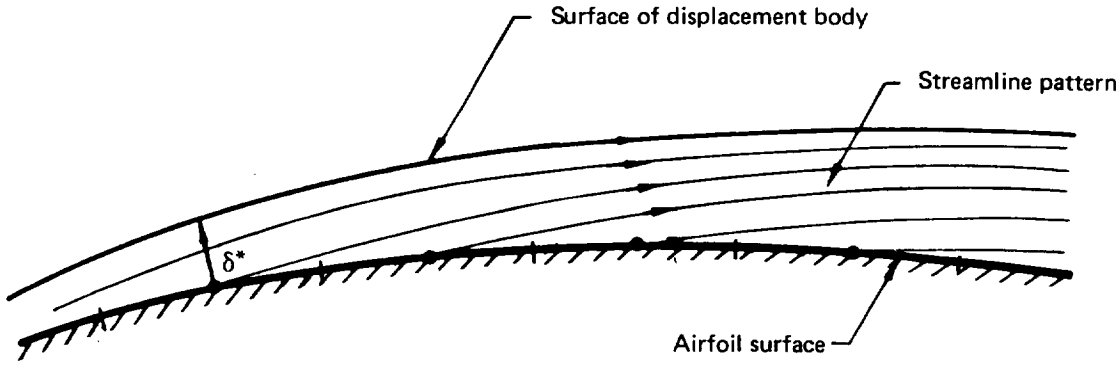

Figure 17. – Streamlines Near Airfoil Surface

$$\Psi_c - \sum_{j=1}^{N} K_{ij}^{V} \gamma_j = U_\infty \cos\alpha Z_i - U_\infty \sin\alpha X_i + \sum_{j=1}^{N+Nw} K_{ij}^{S} \sigma_j \qquad (i=1,2,\ldots N) \qquad (22)$$

where the stream function influence coefficients of sources are defined by

$$K_{ij}^{S} = \frac{1}{2\pi} \int_{s_j}^{s_{j+1}} \varphi(s_i, s_j') ds' \qquad (23)$$

According to the argument preceding equation (22) , this equation is a superposition of the effects of all vortices and sources of the flow field on the control point of the i-th segment, but does not include σ_i, whose influence is eliminated by formally setting $K_{ii}^{S} = 0$. The control points (X_i,Z_i) are the midpoints of the airfoil segments.

KUTTA CONDITION

When adding sources to the flow field the formulation of the Kutta condition must be modified. Requiring that the velocities on the upper- and lower-surface trailing edge are equal results in

$$\gamma_1 + \gamma_N = (\sigma_N - \sigma_1) \sin\epsilon \qquad (24)$$

The variable ϵ denotes the trailing edge closure angle (fig. 18). The symbols σ_1,σ_N represent the source strength of the first and last airfoil segment, respectively. The reader should note that the source strength σ_{N+1} of the neighboring wake centerline does not enter this formulation of the Kutta condition.

MULTIELEMENT AIRFOIL

The formulation of the potential flow method of a single airfoil is readily extended to airfoils consisting of several components. Noting that a multielement airfoil with N_c components has N_c stagnation streamlines with different values of the stream function, one arrives at

$$\Psi_m - \sum_{m=1}^{N_C} \sum_{j=1}^{N_m} K_{ij}^{V} \gamma_j = \cos\alpha (Z_i)_m - \sin\alpha (X_i)_m + \sum_{m=1}^{N_C} \sum_{j=1}^{(N+Nw)_m} K_{ij}^{S} \sigma_j \qquad (25)$$

$$(m=1,\ldots N_c)$$
$$(i=1,2,\ldots N_m)$$

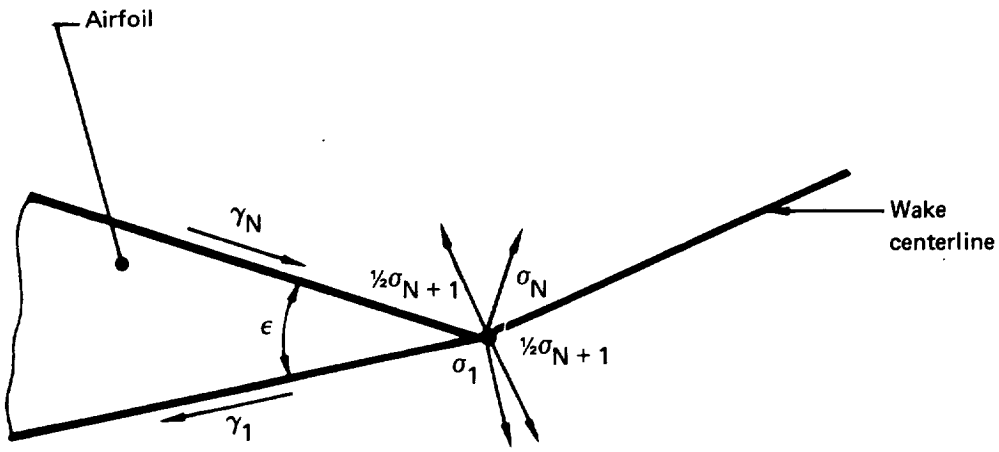

Figure 18. — Airfoil Trailing Edge

The subscript m indicates the m-th airfoil component. In particular, the coordinates of the N_m control points on the surface of the m-th component are denoted by $(X_i)_m$, $(Z_i)_m$ and the stream function value of the m-th component is Ψ_m. Furthermore, in equation (25) the singularity strengths γ_j, σ_j, as well as the stream function value Ψ_m, represent nondimensional quantities, referred to the magnitude of the freestream velocity U_∞.

Equation (25) represents a total of

$$N_T = \sum_{m=1}^{N_C} N_m$$

equations, but there are $N_T + N_C$ unknown vortices γ_j and stream functions Ψ_m. N_C additional equations are provided by the Kutta condition of each airfoil component, which reads

$$(\gamma_1 + \gamma_N)_m = (\sigma_N - \sigma_1)_m \sin \epsilon_m \tag{26}$$

where ϵ_m is the trailing edge closure angle of the m-th airfoil component.

INCOMPRESSIBLE SURFACE VELOCITY (BBBA)

The incompressible surface velocity is computed in subroutine POTLFE. Equations for the velocity components U, W in global coordinates are derived from

$$\Psi(X,Z) = \cos\alpha\, Z - \sin\alpha\, X + \sum_{m=1}^{N_C}\sum_{j=1}^{N_m} {}^{V}K_{ij}\,\gamma_j + \sum_{m=1}^{N_C}\sum_{j=1}^{(N+Nw)_m} {}^{S}K_{ij}\,\sigma_j \tag{27}$$

where Ψ, γ_j, σ_j, are nondimensional quantities, referred to U_∞.

From the equations defining the stream function

$$\frac{U_i}{U_\infty} = \left(\frac{\partial \Psi}{\partial Z}\right)_i$$

$$\frac{W_i}{U_\infty} = -\left(\frac{\partial \Psi}{\partial X}\right)_i \tag{28}$$

one obtains

$$\frac{U_i}{U_\infty} = \cos\alpha + \sum_{m=1}^{N_C}\sum_{j=1}^{N_m} \frac{\partial K_{ij}^V}{\partial Z}\gamma_j + \sum_{m=1}^{N_C}\sum_{j=1}^{(N+N_w)_m} \frac{\partial K_{ij}^S}{\partial Z}\sigma_j \tag{29}$$

$$\frac{W_i}{U_\infty} = \sin\alpha - \sum_{m=1}^{N_C}\sum_{j=1}^{N_m} \frac{\partial K_{ij}^V}{\partial X}\gamma_j - \sum_{m=1}^{N_C}\sum_{j=1}^{(N+N_w)_m} \frac{\partial K_{ij}^S}{\partial X}\sigma_j \tag{30}$$

The velocity influence coefficients

$$\frac{\partial K_{ij}^V}{\partial X}, \frac{\partial K_{ij}^V}{\partial Z}, \frac{\partial K_{ij}^S}{\partial X}, \frac{\partial K_{ij}^S}{\partial Z}$$

are discussed in the next section.

The incompressible surface velocity follows from

$$\frac{V_i}{U_\infty} = \sqrt{\left(\frac{U_i}{U_\infty}\right)^2 + \left(\frac{W_i}{U_\infty}\right)^2} \tag{31}$$

In computing the velocity components U_i, W_i at control points on the airfoil surface, the source induced velocity normal to the surface is not included

$$\frac{\partial K_{ij}^S}{\partial X} = 0, \frac{\partial K_{ii}^S}{\partial Z} = 0 .$$

Therefore, the surface velocity V_i is tangential to the airfoil surface.

AERODYNAMIC INFLUENCE COEFFICIENTS

The aerodynamic influence coefficients are computed in subroutine CPTAIC.

STREAM FUNCTION INFLUENCE COEFFICIENTS

These influence coefficients are defined by equations (19) and (23) for a vortex segment of constant strength and a source segment of constant strength, respectively. Introducing local segment coordinates, see figure 19, the influence coefficients can be rewritten as

$$K_{ij}^{V} = \frac{1}{2\pi} \int_{o}^{c_j} \ell n \sqrt{\left(\xi_j' - \xi_i\right)^2 + \eta_i^2}\, d\xi_j' \tag{32}$$

$$K_{ij}^{S} = \frac{1}{2\pi} \int_{o}^{c_j} \arctan \frac{\eta_i}{\xi_i - \xi_j'}\, d\xi_j' \tag{33}$$

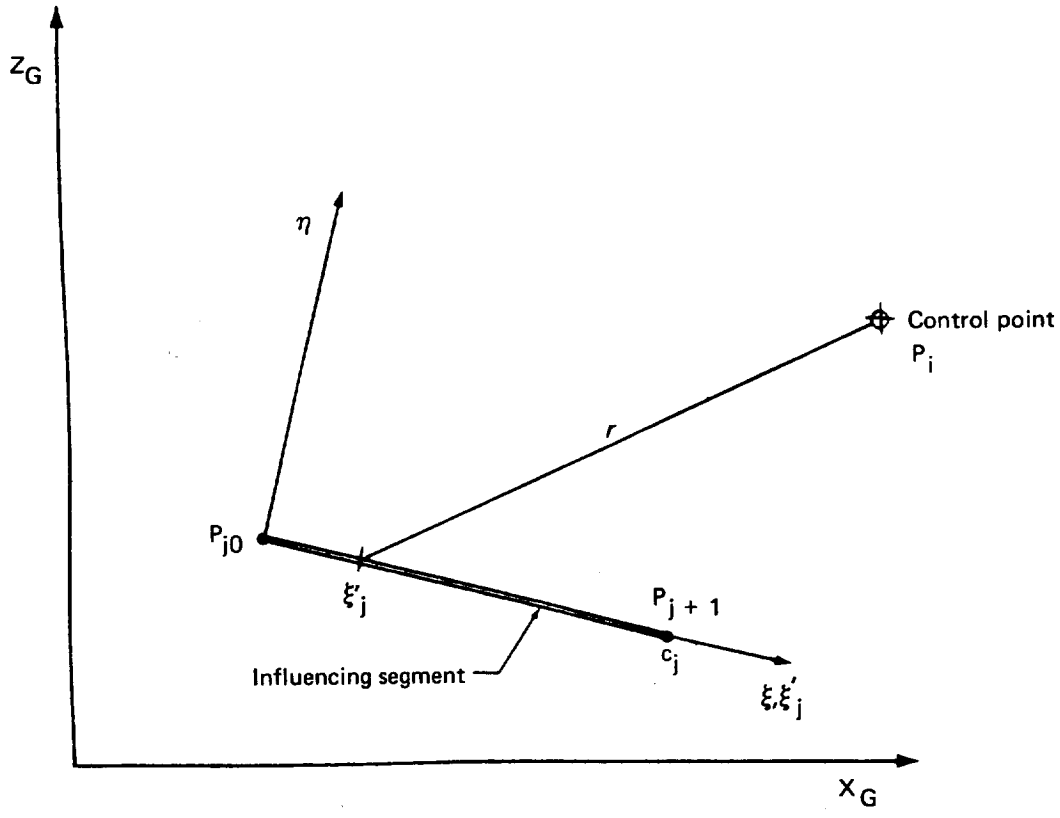

Figure 19. — Local Segment Coordinates ξ, η

Hence,

$$4\pi\, K_{ij}^{V} = \xi_i \ln\left(\xi_i^2 + \eta_i^2\right) - \left(\xi_i - c_j\right)\ln\left[\left(\xi_i - c_j\right)^2 + \eta_i^2\right] - 2\, c_j + 2\eta_i\left(\arctan\frac{\xi_i}{\eta_i} - \arctan\frac{\xi_i - c_j}{\eta_i}\right) \tag{34}$$

$$4\pi\, K_{ij}^{S} = \eta_i \ln\left(\xi_i^2 + \eta_i^2\right) - \eta_i \ln\left[\left(\xi_i - c_j\right)^2 + \eta_i^2\right] + \pi\, c_j - 2\,\xi_i \arctan\frac{\xi_i}{\eta_i} + 2\left(\xi_i - c_j\right)\arctan\frac{\xi_i - c_j}{\eta_i} \tag{35}$$

The control point coordinates (ξ_i,η_i) are expressed in terms of global coordinates as follows.

$$\xi_i = \frac{\left(X_{j+1} - X_j\right)\left(X_i - X_j\right) + \left(Z_{j+1} - Z_j\right)\left(Z_i - Z_j\right)}{c_j}$$

$$\eta_i = \frac{-\left(X_i - X_j\right)\left(Z_{j+1} - Z_j\right) + \left(X_{j+1} - X_j\right)\left(Z_i - Z_j\right)}{c_j} \tag{36}$$

with

$$c_j = \sqrt{\left(X_{j+1} - X_j\right)^2 + \left(Z_{j+1} - Z_j\right)^2}$$

Here, (X_j,Z_j), (X_{j+1},Z_{j+1}) are the segment corner points in global coordinates and (X_i,Z_i) is the control point in the same coordinate system.

The stream function influence coefficients K_{ij}^{v} and K_{ij}^{s} are calculated using the above equations. The latter coefficient is set to zero for source segments on the airfoil surface, i.e.,

$$K_{ii}^{S} = 0$$

VELOCITY INFLUENCE COEFFICIENTS

The derivatives of K_{ij}^{v} and K_{ij}^{s} with respect to the global coordinates X,Z (subscript G dropped for convenience), are termed velocity influence coefficients. They are expressed in terms of local segment coordinates ξ,η by

$$\frac{\partial K_{ij}^{V}}{\partial X} = \frac{\partial K_{ij}^{V}}{\partial \xi}\frac{\partial \xi}{\partial X} + \frac{\partial K_{ij}^{V}}{\partial \eta}\frac{\partial \eta}{\partial X}$$

$$\frac{\partial K_{ij}^{V}}{\partial Z} = \frac{\partial K_{ij}^{V}}{\partial \xi}\frac{\partial \xi}{\partial Z} + \frac{\partial K_{ij}^{V}}{\partial \eta}\frac{\partial \eta}{\partial Z} \qquad (37)$$

$$\frac{\partial K_{ij}^{S}}{\partial X} = \frac{\partial K_{ij}^{S}}{\partial \xi}\frac{\partial \xi}{\partial X} + \frac{\partial K_{ij}^{S}}{\partial \eta}\frac{\partial \eta}{\partial X}$$

$$\frac{\partial K_{ij}^{S}}{\partial Z} = \frac{\partial K_{ij}^{S}}{\partial \xi}\frac{\partial \xi}{\partial Z} + \frac{\partial K_{ij}^{S}}{\partial \eta}\frac{\partial \eta}{\partial Z}$$

Here, the coefficients of the Jacobian of the transformation from local to global coordinates are

$$\frac{\partial \xi}{\partial X} = \frac{X_{j+1} - X_j}{c_j} \qquad \frac{\partial \xi}{\partial Z} = \frac{Z_{j+1} - Z_j}{c_j} \qquad (38)$$

$$\frac{\partial \eta}{\partial X} = -\frac{Z_{j+1} - Z_j}{c_j} \qquad \frac{\partial \eta}{\partial Z} = \frac{X_{j+1} - X_i}{c_j}$$

The velocity influence coefficients in local segment coordinates read

$$\frac{\partial K_{ij}^{V}}{\partial \xi} = \frac{\partial K_{ij}^{S}}{\partial \eta} = \frac{1}{4\pi}\left\{ \ell n\left(\xi_i^2 + \eta_i^2\right) - \ell n\left[\left(\xi_i - c_j\right)^2 + \eta_i^2\right]\right\} \qquad (39)$$

$$\frac{\partial K_{ij}^{V}}{\partial \eta} = -\frac{\partial K_{ij}^{S}}{\partial \xi} = \frac{1}{2\pi}\left(\arctan\frac{\xi_i}{\eta_i} - \arctan\frac{\xi_i - c_j}{\eta_i}\right) \qquad (40)$$

In calculating the influence of a segment singularity distribution on its own control point, the vortex velocity influence coefficients are computed at $\eta = 0+$ and the source velocity influence coefficients are set to zero.

$$\frac{\partial K_{ii}^{S}}{\partial X} = \frac{\partial K_{ii}^{S}}{\partial Z} = 0 \tag{41}$$

STAGNATION POINTS

A stagnation point is a point on the airfoil surface where the velocity V_i is zero. The location of the N_C stagnation points is determined in subroutine STAGN by marching along the surface of each airfoil component from the lower to the upper surface trailing edge. A change in sign of the surface velocity V_i and linear interpolation between segment corner point coordinates determine the location of a stagnation point.

COMPRESSIBILITY CORRECTION

Compressible potential flow solutions are calculated in subroutine COMPR.

The well known Karman-Tsien rule (ref. 12) is used, which relates compressible and incompressible quantities of the same airfoil geometry. A scaling of the geometry is therefore not performed.

The compressible surface velocity, V_c, is obtained from the corresponding incompressible velocity V_i by means of the equation

$$\frac{V_c}{U_\infty} = \frac{\frac{V_i}{U_\infty}(1-\lambda)}{1-\lambda\left(\frac{V_i}{U_\infty}\right)^2} \tag{42}$$

where the parameter λ depends on the freestream Mach number M_∞

$$\lambda = \frac{M_\infty^2}{\left(1+\sqrt{1-M_\infty^2}\right)^2} \tag{43}$$

The way equation (42) is written indicates all velocities are nondimensionalized by the freestream velocity U_∞. Further, the local Mach number, M_e, and the surface pressure coefficient, c_p, are given by the isentropic flow relations.

$$M_e = \frac{M_\infty \left|\frac{V_c}{U_\infty}\right|}{\sqrt{T}} \tag{44}$$

$$c_P = \frac{2}{\gamma M_\infty^2}\left(T^{\frac{\gamma}{\gamma-1}} - 1\right) \qquad M_\infty \geq 0.001 \tag{45}$$

$$T = 1 + \frac{\gamma - 1}{2} M_\infty^2 \left[1 - \left(\frac{V_c}{U_\infty} \right)^2 \right] \quad ;\gamma = 1.4 \tag{46}$$

The code uses Bernoulli's equation

$$c_P = 1 - \left(\frac{V_i}{U_\infty} \right)^2$$

to compute the surface pressure coefficient for $M_\infty = 0$.

At a stagnation point, compressible variables are calculated from

$$V_c = 0 \qquad\qquad M_e = 0 \tag{47}$$

$$c_P = \frac{2}{\gamma M_\infty^2} \left[\left(1 + \frac{\gamma - 1}{2} M_\infty^2 \right)^{\frac{\gamma}{\gamma - 1}} - 1 \right]$$

Dimensional compressible surface velocities, V_c, in ft/sec are obtained from

$$V_c = \left(\frac{V_c}{U_\infty} \right) U_\infty \tag{48}$$

and

$$U_\infty = 49.02\, M_\infty \sqrt{\frac{T_o}{1 + .2\, M_\infty^2}} \quad \left[\frac{ft}{sec} \right] \tag{49}$$

The symbol T_0 stands for the freestream stagnation temperature in °R.

LAMINAR BOUNDARY LAYER (BBCA)

This section describes the calculation of compressible laminar boundary layer characteristics. The method is coded in OVERLAY (4,1), subroutine LAMNA.

COMPRESSIBLE LAMINAR BOUNDARY LAYER

COHEN AND RESHOTKO METHOD

The method used in LAMNA is based on the compressible analysis of Cohen and Reshotko (ref. 13) as modified by Goradia (ref. 1). Some results of the Pohlhausen method (ref. 14) for incompressible boundary layers are also utilized. The following assumptions are made:

- The laminar boundary layer flow is steady and two-dimensional
- Curvature effects are negligible
- Dynamic viscosity is a linear function of temperature
- Surface temperature is uniform
- Air is a perfect gas

Consequently, the equations governing compressible, steady, two-dimensional laminar boundary layer flow read

$$\frac{\partial}{\partial x}(\rho u) + \frac{\partial}{\partial y}(\rho v) = 0 \tag{50}$$

$$\rho u \frac{\partial u}{\partial x} + \rho v \frac{\partial u}{\partial y} = -\frac{dp}{dx} + \frac{\partial}{\partial y}\left(\mu \frac{\partial u}{\partial y}\right) \tag{51}$$

$$\rho c_p \left(u\frac{\partial T}{\partial x} + v \frac{\partial T}{\partial y}\right) = u \frac{dp}{dx} + \frac{\partial}{\partial y}\left(k\frac{\partial T}{\partial y}\right) + \mu\left(\frac{\partial u}{\partial y}\right)^2 \tag{52}$$

where the symbols denote

c_p	Specific heat at constant pressure
k	Heat transfer factor
p	Static pressure
T	Static temperature
u,v	Velocity components in x,y directions
x,y	Surface fitted coordinates
μ	Dynamic viscosity
ρ	Density

Two additional equations are given by the perfect gas law

$$p = \rho RT \tag{53}$$

and the assumption

$$\frac{\mu}{\mu_o} = \lambda \frac{T}{T_o} \tag{54}$$

The subscript o denotes freestream stagnation values. The coefficient λ is determined by matching the viscosity with the Sutherland value at the airfoil surface. Sutherland's viscosity formula reads

$$\frac{\mu}{\mu_o} = \frac{T_o + K_{Su}}{T + K_{Su}} \left(\frac{T}{T_o}\right)^{\frac{3}{2}} \tag{55}$$

$$K_{Su} = 198.6\ ^\circ R$$

Hence,

$$\lambda = \frac{T_o + K_{Su}}{T + K_{Su}} \sqrt{\frac{T_w}{T_o}} \tag{56}$$

The subscript w denotes values at the airfoil surface. The listed equations are solved subject to the following known boundary conditions. At the airfoil surface

$$u(x, 0) = v(x, 0) = 0 \qquad T(x, 0) = T_w$$

and at the outer edge of the boundary layer ($y = \delta$), denoted by the subscript e, they are

$$u(x, \delta) = V_c \qquad T(x, \delta) = T_e$$

The code uses the integral method of Cohen and Reshotko for the solution of the described flow problem. An outline of this method is given below.

The compressible boundary layer problem is converted into an equivalent incompressible problem by means of the Stewartson transformation, which reads

$$\frac{\partial \Psi}{\partial y} = \frac{\rho u}{\rho_o} \qquad \frac{\partial \Psi}{\partial x} = -\frac{\rho v}{\rho_o} \tag{57}$$

$$X = \int_o^x \lambda \frac{a_e}{a_o} \frac{p_e}{p_o}\, dx \qquad Y = \frac{a_e}{a_o} \int_o^y \frac{\rho}{\rho_o}\, dy \tag{58}$$

$$U = \frac{\partial \Psi}{\partial Y} \qquad V = -\frac{\partial \Psi}{\partial X} \tag{59}$$

The symbols Ψ and a represent the stream function and the speed of sound, respectively. Quantities of the equivalent incompressible problem are denoted by capital letters. i.e., U, V velocity components; X, Y surface fitted coordinates.

The Prandtl number

$$Pr = \frac{\mu\, c_p}{k}$$

and the specific heat c_p are assumed to be constant during this transformation.

An integral form of the momentum equation governing the momentum thickness θ_{tr} and the displacement thickness δ^*_{tr} can be derived for the transformed problem. Defining

$$\theta_{tr} = \int_o^{\Delta} \frac{U}{U_e}\left(1 - \frac{U}{U_e}\right) dY \tag{60}$$

$$\delta_{tr}^{*} = \int_{o}^{\Delta} \left(1 - \frac{U}{U_e} + S\right) dY \tag{61}$$

where

$$S = \frac{h_s}{h_o} - 1$$

is an enthalpy term involving the local stagnation enthalpy, h_s, and the freestream stagnation enthalpy, h_0, and the symbol Δ stands for the boundary layer thickness in the transformed space, the momentum integral equation takes the form

$$\frac{d\,\theta_{tr}}{dX} + \frac{1}{U_e}\frac{d\,U_e}{dX}\left(2\,\theta_{tr} + \delta_{tr}^{*}\right) = \frac{\nu_o}{U_e^2}\left(\frac{\partial U}{\partial Y}\right)_w \tag{62}$$

The symbol ν_0 is the freestream stagnation value of the kinematic viscosity.

Equation (62) can further be expressed in terms of two parameters, the shear parameter ℓ, defined by

$$\ell = \frac{\theta_{tr}}{U_e}\left(\frac{\partial U}{\partial Y}\right)_w \tag{63}$$

and the correlation number n, defined by

$$n = -\frac{\theta_{tr}^2}{\nu_o}\frac{d\,U_e}{dX} \tag{64}$$

Also, introducing the shape parameter

$$H_{tr} = \frac{\delta_{tr}^{*}}{\theta_{tr}}$$

yields the following momentum integral equation

$$-U_e\frac{d}{dX}\left(\frac{n}{\frac{d\,U_e}{dX}}\right) = 2\left[n\left(H_{tr} + 2\right) + \ell\right] \tag{65}$$

This equation is the basic equation of the solution method for the compressible laminar boundary layer calculation in subroutine LAMNA. It is solved for n assuming that the RHS is a function of n and S_W only, i.e.,

$$N\left(n, S_w\right) = 2\left[n\left(H_{tr} + 2\right) + \ell\right] \tag{66}$$

and that this functional relation provides sufficient accuracy by similar solutions investigated in reference 15 by Cohen and Reshotko.

The parameter S_W is the value of the enthalpy at the airfoil surface.

$$S_W = \frac{T_w}{T_o} - 1 \tag{67}$$

Numerical values of the function $N(n,S_W)$ are listed in table 2 and are plotted in figure 20 between the stagnation point and the separation point for two surface temperatures. The latter figure shows that the function $N(n,S_W)$ can be approximated by

$$N = A + Bn \tag{68}$$

for fixed values S_W. Hence, equation (65) can be integrated resulting in

$$n = - A\, U_e^{-B} \frac{d\, U_e}{dX} \int_o^X U_e^{B-1} dX_1 \tag{69}$$

Finally, equation (69) can be expressed in terms of physical compressible variables by means of the Stewartson transformation, (eqs. (57), (58), (59)).

$$n = - A\, M_e^{-B} \frac{d\, M_e}{dx}\, T_e^{-4} \int_o^x M_e^{B-1}\, T_e^{4}\, dx_1 \tag{70}$$

Here, $M_e = u_e/a_e$ is the local Mach number at the outer edge of the boundary layer and T_e is the temperature at the same location. Both T_e and M_e are related by

$$\frac{T_o}{T_e} = 1 + \frac{\gamma-1}{2} M_e^2 \tag{71}$$

Equation (70) is evaluated numerically in the computer code for known distributions of M_e. Having computed the correlation number, n, the other boundary layer parameters of interest (δ^*, θ, c_f, R_{e_θ}) can be calculated. Details of the calculations follow.

COMPUTATIONAL DETAILS

Step 1

The parameter S_W is obtained from

$$S_W = k \frac{1 + \frac{\gamma-1}{2} (Pr)^{\frac{1}{3}} M_\infty^2}{1 + \frac{\gamma-1}{2} M_\infty^2} - 1 \tag{72}$$

Table 2. — Numerical Values of the Function $N(n,S_W)$

S_W	n	ℓ	N
-0.8	0.1215	0	1.0305
	0.1304	0.0312	1.0606
	0.1298	0.0436	1.0499
	0.1260	0.0681	1.0185
	0.1212	0.0827	0.9885
	0.1017	0.1214	0.882
	0.0355	0.1935	0.5781
	0	0.220	0.44
	-0.0837	0.2678	0.1676
	-0.2008	0.3179	-0.1332
	-0.2522	0.3366	-0.2517
-0.4	0.0899	0	0.9087
	0.0894	0.0300	0.8968
	0.0826	0.0624	0.8519
	0.0615	0.1210	0.7379
	0	0.220	0.440
	-0.0722	0.3019	0.1442
	- 0.1733	0.3924	-0.1713
0	0.0681	0	0.822
	0.0487	0.1051	0.7068
	0	0.220	0.440
	-0.0602	0.3220	0.1232
	-0.8029	0.3556	0
	-0.1002	0.3808	-0.0748
	-0.1064	0.3892	-0.1040

Note: Reproduced from Table II of NACA-1294

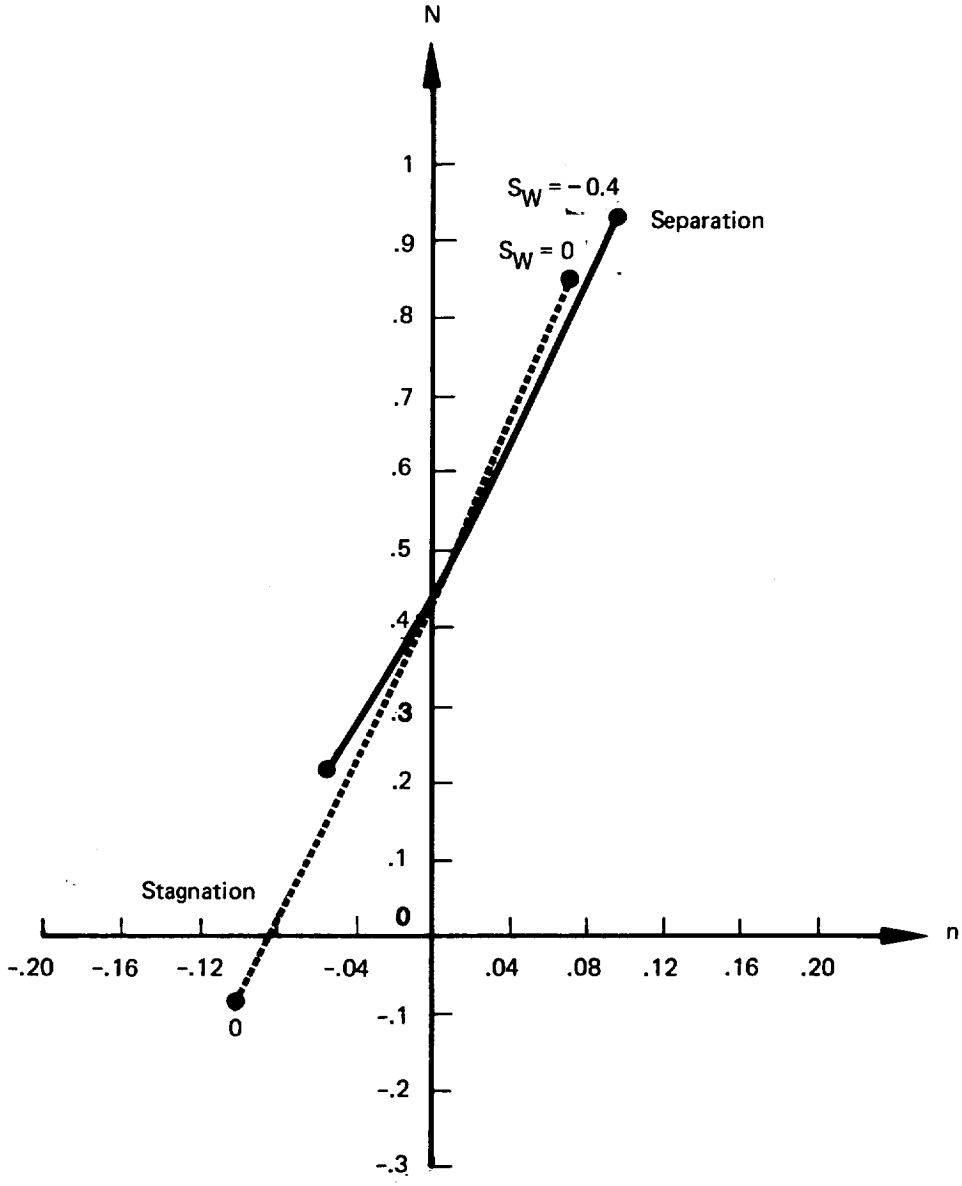

Figure 20. — Correlation of Dimensionless Momentum Equation, Function $N(n,S_W)$

with $\gamma = 1.4$ used for the ratio of specific heats. The remaining parameters, the heat transfer factor k, the Prandtl number Pr, and the freestream Mach number, M_∞, are input variables.

The values of the correlation number at the stagnation and separation points are

$$n_{stag} = -.1064 + .01725 S_w + .375 S_w^2 \tag{73}$$

$$n_{sep} = .06961058 - .0395712 S_w + .06717244 S_w^2 \tag{74}$$

and are shown in figure 21.

Step 2

The correlation number is calculated from equation (70) with the following equations for the coefficients A, B, which are assumed to depend on the last available value of n and S_W.

$$A(n, S_w) = a_1 - c_1 n^2 - 2 d_1 n^3$$
$$B(n, S_w) = b_1 + 2 c_1 n + 3 d_1 n^2 \tag{75}$$

with

$$a_1 = .44$$
$$b_1 = 5.56903 + 2.5138 S_w$$
$$c_1 = 3.195945 - 7.0807 S_w$$
$$d_1 = -6.358574 - 13.64784 S_w$$

Equation (70) is solved by marching along the surface of the airfoil beginning at the stagnation point. The step size is the distance between the computational surface points. For the first and second points, n is obtained from

$$n_1 = n_{stag} \tag{76}$$
$$n_2 = -A(n_1, S_w) \frac{1}{M_e} \left(\frac{d M_e}{dx}\right)_2 \frac{x_2}{2}$$

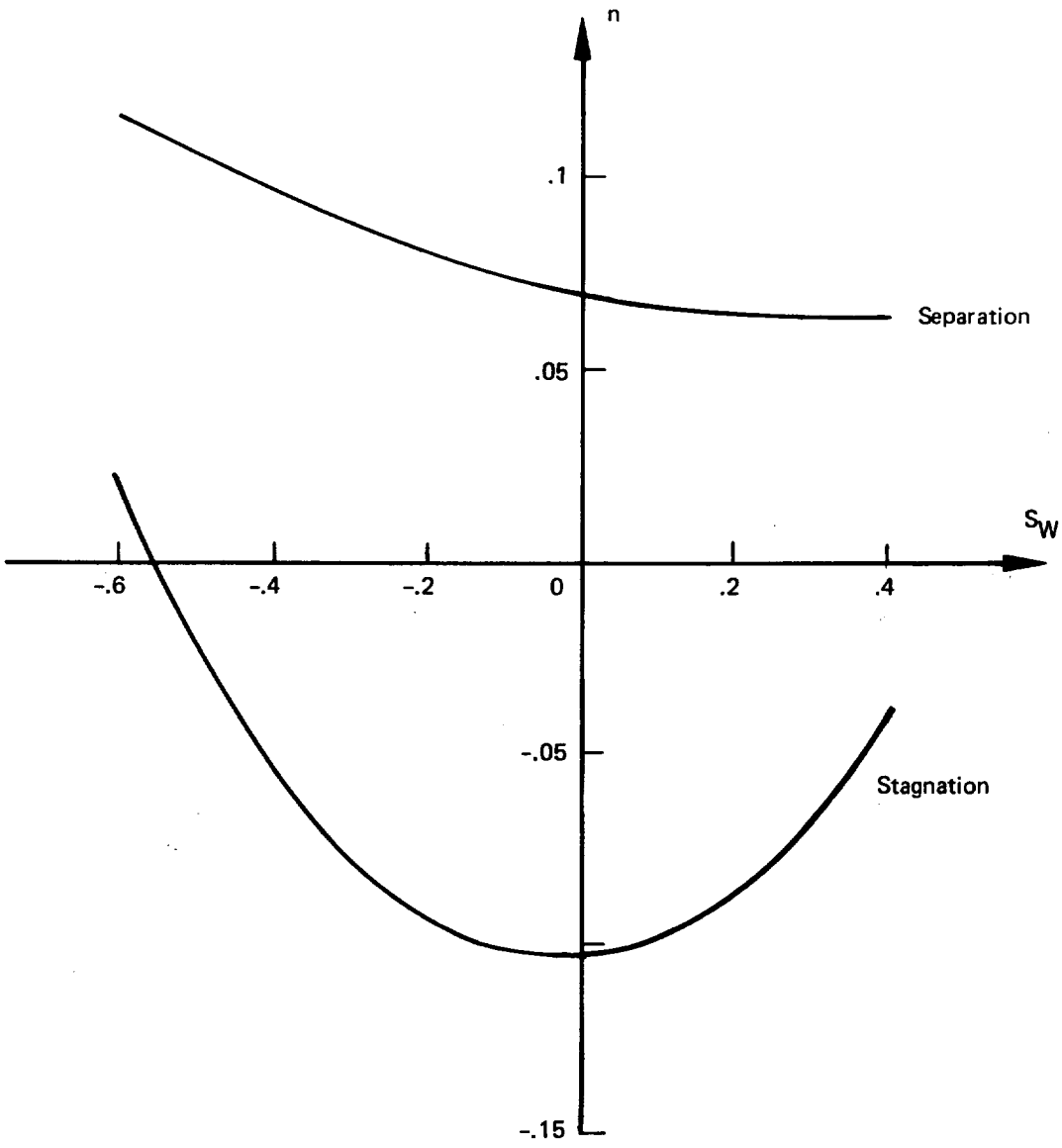

Figure 21. — Correlation Number n at Stagnation and Separation Conditions

From the third point on, the following numerical scheme is used. Equation (70) can be written as

$$F(x) = \int_0^x f(x_1)\, dx_1$$

with

$$F(x) = \frac{n\, M_e{}^B}{\frac{d\, M_e}{dx}\left(1 + \frac{\gamma-1}{2} M_e^2\right)^4}$$

and

$$f(x) = \frac{M_e{}^{B-1}}{\left(1 + \frac{\gamma-1}{2} M_e^2\right)^4}$$

Using the trapezoidal rule

$$F(x_{i+1}) = F(x_i) + \frac{1}{2}\left[f(x_{i+1}) + f(x_i)\right](x_{i+1} - x_i) \tag{77}$$

$n(x_{i+1}) = n_{i+1}$ $(i \geqslant 2)$ follows.

The value of n is restricted to the range

$$n_{stag} \leqslant n \leqslant 10\, n_{sep} \tag{78}$$

The factor 10 allows the numerical scheme to continue beyond the point of separation. This is done to avoid premature separation during the first cycles of the overall iteration procedure.

Step 3

The momentum thickness θ is calculated from

$$\theta = \sqrt{\left| \frac{-\lambda \nu_o}{a_o}\left(1 + \frac{\gamma-1}{2} M_e^2\right) \frac{2\, n}{\frac{d\, M_e}{dx}} \right|} \tag{79}$$

which can be derived from the definition of n and the relation between the momentum thicknesses θ and θ_{tr}.

$$\theta = \frac{p_o\, a_e}{p_e\, a_o}\,\theta_{tr}$$

In order to calculate θ, the variables λ, ν_0 and a_0 are obtained from

$$\lambda = \frac{T_o + K_{Su}}{T_w + K_{Su}}\sqrt{\frac{T_w}{T_o}} \qquad K_{Su} = 198.6\ ^\circ R \tag{80}$$

$$T_w = T_o\left(S_w + 1\right) \tag{81}$$

The freestream stagnation value of the kinematic viscosity ν_0 follows from the sequence of calculations listed below

$$T_\infty = \frac{T_o}{1 + \frac{\gamma-1}{2}M_\infty^2} \qquad \frac{\mu_\infty}{\mu_o} = \frac{T_o + K_{Su}}{T_\infty + K_{Su}}\left(\frac{T_\infty}{T_o}\right)^{\frac{3}{2}}$$

$$\frac{\rho_o}{\rho_\infty} = \left(1 + \frac{\gamma-1}{2}M_\infty^2\right)^{\frac{1}{\gamma-1}} \qquad a_\infty = 49.02\sqrt{T_\infty}\ \text{[ft/sec]} \tag{82}$$

$$\nu_\infty = \frac{M_\infty\, a_\infty}{Re_{ft}} \qquad \nu_o = \frac{\nu_\infty}{\frac{\mu_\infty}{\mu_o}\frac{\rho_o}{\rho_\infty}}$$

The freestream stagnation value of the speed of sound is given by

$$a_o = 49.02\sqrt{T_o}\ \text{[ft/sec]} \tag{83}$$

It should be noted that the dimension of the speed of sound,a,is ft/sec, since

$$\sqrt{\gamma R} = 49.02\left[\frac{ft}{sec\sqrt{^\circ R}}\right]$$

is used.

Step 4

The shape factor H is calculated from

$$H = (-1.1138n + 2.38411)\left[1 + 1.18\left(\frac{T_w}{T_e} - 1\right)\right] + \frac{\gamma-1}{2}(Pr)^\alpha M_e^2 \tag{84}$$

where the exponent α of the Prandtl number is obtained from

$$\alpha = \frac{1}{3} + b_t n + cn^2 \tag{85}$$

with

$$b_t = -\frac{2\,n_{sep} - n_{stag}}{12\,n_{sep}\left(n_{stag} - n_{sep}\right)} + \frac{1}{n_{stag}} \qquad c = \frac{2\,n_{sep} - n_{stag}}{12\,n_{sep}\,n_{stag}\left(n_{stag} - n_{sep}\right)}$$

Then the displacement thickness δ^* follows from

$$\delta^* = \theta H \tag{86}$$

Step 5

The shear parameter ℓ is needed to determine the skin friction coefficient. The value of ℓ is computed from the following cubic equation in subroutine PROOT.

$$p_o + p_1 \ell + p_2 \ell^2 + p_3 \ell^3 - n = 0 \tag{87}$$

where

$$\begin{aligned}
p_o &= 0.0715016 - 0.04559\,S_w + 0.04871\,S_w^2 \\
p_1 &= -0.088925 + 0.3898894\,S_w + 1.11892\,S_w^2 \\
&\quad +0.990225\,S_w^3 + 1.219532\,S_w^4 \\
p_2 &= -1.227559 - 1.662158\,S_w - 9.193\,S_w^2 \\
&\quad -13.197\,S_w^3 - 17.78815\,S_w^4 \\
p_3 &= 0.7312 + 4.32497\,S_w + 12.251\,S_w^2 \\
&\quad +21.8919\,S_w^3 + 30.92805\,S_w^4
\end{aligned}$$

The shear parameter ℓ is chosen as the lowest real value in the range

$$0 \leqslant \ell \leqslant 0.7 \tag{88}$$

with the assumption that $\ell = 0$ if no real value exists in that range. Figure 22 shows plots of the shear parameter for various values of S_W.

Two different skin friction coefficients, c_{f_i} and $\bar{c}_{f_i}$, are computed in subroutine LAMNA. They are defined by

$$c_{f_i} = \frac{\tau_w}{\frac{\rho_w}{2} V_c^2} \qquad \tau_w = \mu_w \left(\frac{\partial u}{\partial y}\right)_w \tag{89}$$

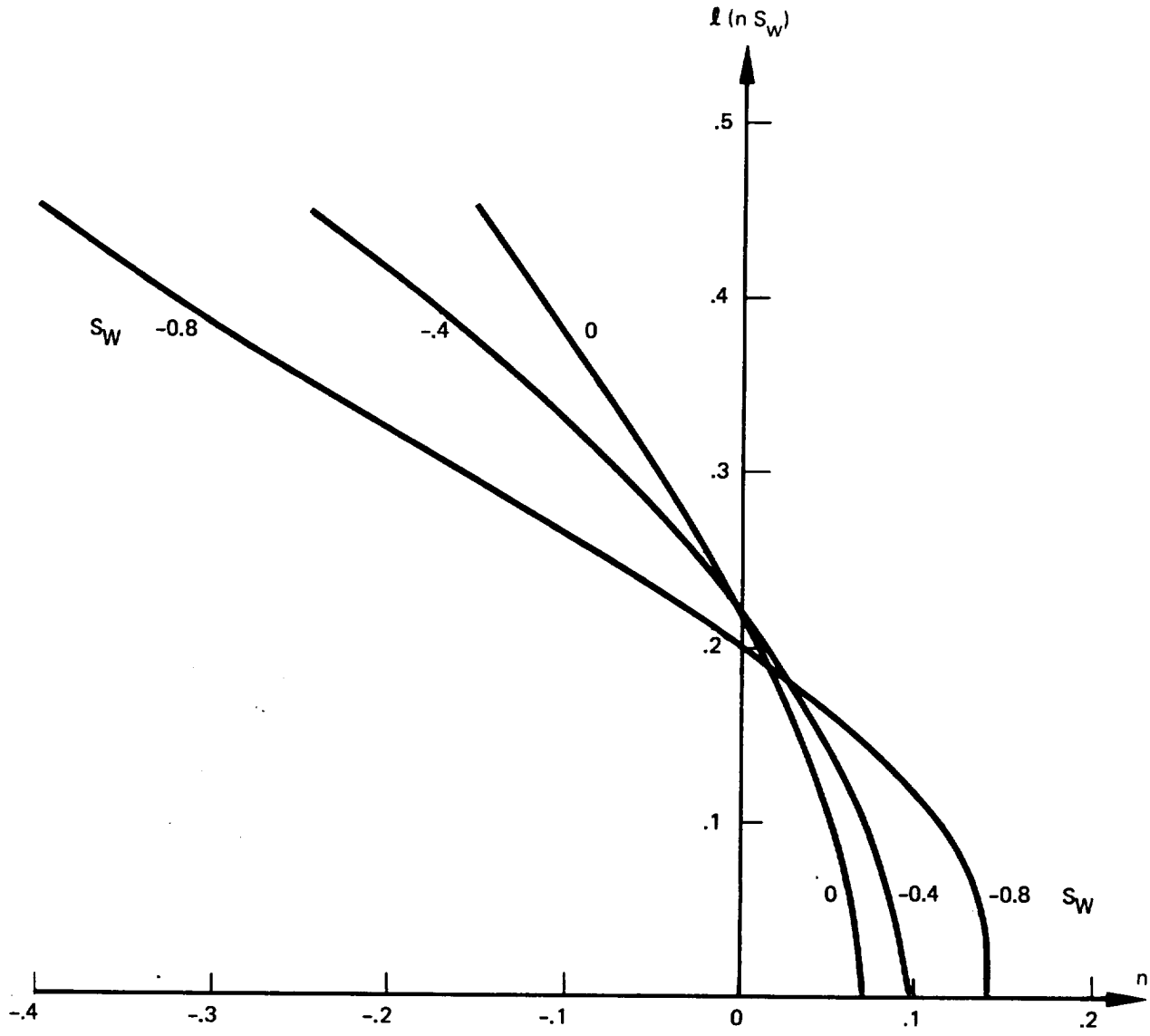

Figure 22. — Shear Parameter ℓ (n,S_W)

and

$$\bar{c}_{f_i} = c_{f_i} \frac{q_e}{q_\infty} \tag{90}$$

Here, q_e and q_∞ denote the local dynamic pressure and the freestream dynamic pressure, respectively. The skin friction coefficient c_{f_i} is printed, whereas $\bar{c}_{f_i}$ is used in the load calculations.

$$c_{f_i} = \frac{2\ell}{\sqrt{Re_x}} \sqrt{\frac{x}{n} \left| \frac{1}{M_e} \frac{dM_e}{dx} \right|} \tag{91}$$

$$\frac{q_e}{q_\infty} = \left(\frac{M_e}{M_\infty} \right)^2 \left(1 + \frac{\gamma}{2} M_e^2 \, c_p \right) \tag{92}$$

In the last equation c_p is the surface pressure coefficient. The Reynolds number Re_x in equation (91) is calculated by means of

$$Re_x = Re_\theta \frac{x}{\theta} \tag{93}$$

$$Re_\theta = \frac{a_o \, \theta M_e}{\left(1 + \frac{\gamma - 1}{2} M_e^2 \right)^4 \nu_o \lambda \left(1 + S_w \right)^2}$$

Step 6

The boundary layer thickness is found utilizing results of the Pohlhausen theory (ref. 14) for incompressible boundary layers. In incompressible flow (subscript i)

$$\frac{\delta_i}{\theta_i} = \frac{1}{\frac{37}{315} - \frac{\Lambda_i}{945} - \frac{\Lambda_i^2}{9072}} \tag{94}$$

Here, Λ_i is the Pohlhausen parameter, defined by

$$\Lambda_i = \left(\frac{\delta^2}{\nu} \frac{dU}{dx} \right)_i$$

and related to the shape factor H_i as shown in table 3. In calculating δ of compressible boundary layers, the assumption is made that equation (94) also holds in compressible flow, i.e.,

Table 3. — Auxiliary Functions for the Calculation of Incompressible Laminar Boundary Layers

Λ_i	$H_i = \delta_i^*/\theta_i$
12.0	2.250
11.0	2.253
10.0	2.260
9.0	2.273
8.0	2.289
7.8	2.293
7.6	2.297
7.4	2.301
7.2	2.305
Stagnation Point → 7.052	2.308
7.0	2.309
6.8	2.314
6.6	2.318
6.4	2.323
6.2	2.328
6.0	2.333
5.0	2.361
4.0	2.392
3.0	2.427
2.0	2.466
1.0	2.508
0	2.554
-1.0	2.604
-2.0	2.647
-3.0	2.716
-4.0	2.779
-5.0	2.847
-6.0	2.921
-7.0	2.999
-8.0	3.085
-9.0	3.176
-10.0	3.276
-11.0	3.383
Separation Point → -12.0	3.500
-13.0	3.627
-14.0	3.765
-15.0	3.916

$$\delta = \frac{\theta}{\frac{37}{315} - \frac{\Lambda}{945} - \frac{\Lambda^2}{9072}} \tag{95}$$

where the compressible parameter Λ is obtained from the compressible shape factor H by means of table 3 assuming $\Lambda(H) = \Lambda_i(H_i)$. The following restrictions are imposed on Λ:

$\Lambda = 12 \quad H \leq 2.250$
$\Lambda = -15 \quad H \geq 3.916$

SYMBOLS OF THE LAMINAR BOUNDARY LAYER SECTION

Theory	Code	Definition
A,B	A,B	Coefficients of the momentum parameter N
a_0	AO	Freestream stagnation value of speed of sound
a_e		Speed of sound at edge of boundary layer
a_∞	AINF	Speed of sound of freestream
c_{f_i}	SG	Skin friction coefficient based on q_e
$\bar{c}_{f_i}$	CFI	Skin friction coefficient based on q_∞
c_p		Specific heat at constant pressure
c_p	CP	Surface pressure coefficient
H	H	Shape factor
H_{tr}		Transformed shape factor
h		Enthalpy
K_{Su}	198.6	Sutherland's constant
k	XK	Heat transfer factor
ℓ	AL	Shear parameter
M_e	AME	Local Mach number
M_∞	AMEIF	Freestream Mach number
	(FSMCH)	
N		Momentum parameter
n	CN	Correlation number
n_{sep}	SEP	Value of n at separation
n_{stag}	CNSTAG	Value of n at the stagnation point

Theory	Code	Definition
Pr	PRR	Prandtl number
p		Static pressure
p_0	P	Stagnation pressure
p_e		Surface pressure
q_e		Local value of dynamic pressure
q_∞		Freestream value of dynamic pressure
R		Gas constant
Re_{ft}		Reynolds number per foot
	RN	Reynolds number per foot in millions
Re_x	REW	Reynolds number, $u_e x/\nu$
Re_θ	REMOM	Reynolds number, $u_e \theta/\nu$
S		Enthalpy parameter
S_W	SW	Surface value of S
T		Static temperature
T_W		[illegible]erature
T_0	TO	Freestream stagnation temperature in °R
T_e		Temperature at edge of boundary layer
T_∞	TINF	Freestream temperature
U		Transformed velocity component parallel to surface
U_e		Value of U at the outer edge of the boundary layer
u		Compressible velocity component parallel to surface
V_e	UE	Compressible velocity at the outer edge of the boundary layer
u_∞		Freestream velocity
v		Compressible velocity component normal to surface
V		Transformed velocity component normal to surface

Theory	Code	Definition
x	SUMS	Arc length, surface coordinate
X,Y		Transformed coordinates
x,y		Boundary layer coordinates
α	ALFA	Angle of attack in radians
α	ALPHA	Exponent of Prandtl number
γ	1.4	Ratio of specific heats
δ		Boundary layer thickness
	DELT	Nondimensional boundary layer thickness
δ^*	DISP	Displacement thickness
θ	AMTK	Momentum thickness
Λ	G1K	Pohlhausen parameter
λ	AMU	Coefficient of viscosity temperature relation
μ		Dynamic viscosity
ν		Kinematic viscosity
ν_0	VO	Freestream stagnation value of kinematic viscosity
ρ		Density
τ_W		Wall shear stress

Subscripts

e	Outer edge of boundary layer	stag	Stagnation point
i	Incompressible	tr	Transformed value
o	Freestream stagnation value	w	Value at surface
s	Local stagnation value	∞	Freestream
sep	Separation		

TRANSITION AND LAMINAR SEPARATION (BBCAB)

The following calculations are performed in subroutine BLTRAN, OVERLAY (4,1).

- Natural transition location
- Laminar separation location
- Laminar bubble properties
  - Short bubble with turbulent reattachment
  - Long bubble with laminar separation
- Check for user input fixed transition location

Subroutine BLTRAN is used in conjunction with the laminar boundary layer routine LAMNA, which calls BLTRAN at each surface point.

Boundary layer transition is calculated using a standard two step approach.

1. The laminar instability point must be located, and
2. Once the laminar boundary layer has become unstable, the search for natural transition is started.

Laminar separation and stall is predicted using both Cohen-Reshotko and Curle criteria. Laminar bubble properties are calculated using the Goradia-Lyman criterion. The following paragraphs will give the details of each calculation.

NATURAL TRANSITION

Natural transition location is calculated using a two step approach. The first step is to locate the laminar instability point, i.e., that point on the surface where disturbances of the laminar boundary layer will be amplified. Schlichting (ref. 16) has solved the Orr-Sommerfeld equation, assuming Polhausen laminar velocity profiles. The results of this linearized stability analysis are presented in figure 23. Correlation of the theoretical results has been done in terms of

$$Re_\theta = \frac{U_e \theta}{\nu}$$

versus

$$k = \frac{\theta^2}{\nu} \frac{d U_e}{dx}$$

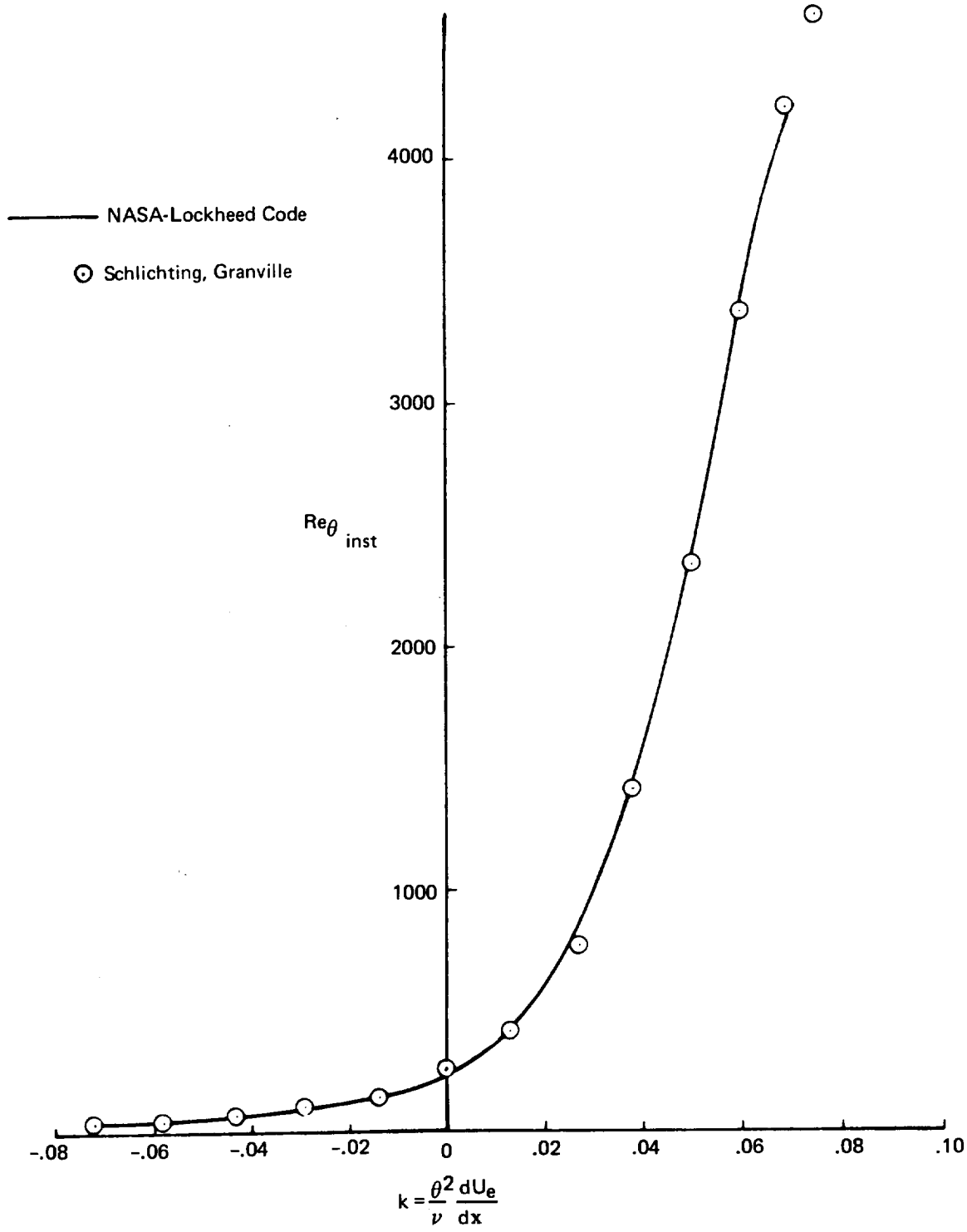

Figure 23. — Stability Curve

The solid line in figure 23 is a curve fit to the stability data made by Goradia and given by:

$$\left(\overline{Re_\theta}\right)_{crit} = \exp\left(5.46963 + 43.37458\,k + 218.28\,k^2 - 1934.6k^3 - 23980k^4\right) \quad (96)$$

for $-.1567 \leq k \leq .0767$

$$\left(Re_\theta\right)_{crit}$$

is the critical momentum thickness Reynolds number, i.e., if the local value of

$$Re_\theta < \left(Re_\theta\right)_{crit},$$

then the laminar boundary layer is stable, if

$$Re_\theta \geq \left(Re_\theta\right)_{crit},$$

the laminar boundary layer is unstable. The first point at which the laminar boundary layer is unstable is called the instability point. Once the instability point has been found, the search for the transition point begins. Granville (ref. 17) correlated

$$\Delta\left(Re_\theta\right)_{tran} = \left(Re_\theta\right)_{tran} - \left(Re_\theta\right)_{inst}$$

against an average pressure gradient parameter, $\overline{k}$, which is equal to:

$$\overline{k} = \frac{1}{s - s_{inst}} \int_{s_{inst}}^{s} k\,ds \quad (97)$$

The symbols in figure 24 represent the correlation of experimental data by Granville. The solid line represents a curve fit to this data made by Goradia given by the expression,

$$\Delta\left(Re_\theta\right)_{tran} = 825.45 + 28183.5\,\overline{k} + 721988\,\overline{k}^2 + 6317380\,\overline{k}^3 \quad (98)$$

for $-.05 \leq k \leq .0767$.

Thus, the first point at which

$$\Delta Re_\theta = \left(Re_\theta\right)_{local} - \left(Re_\theta\right)_{inst} \geq \Delta\left(Re_\theta\right)_{tran}$$

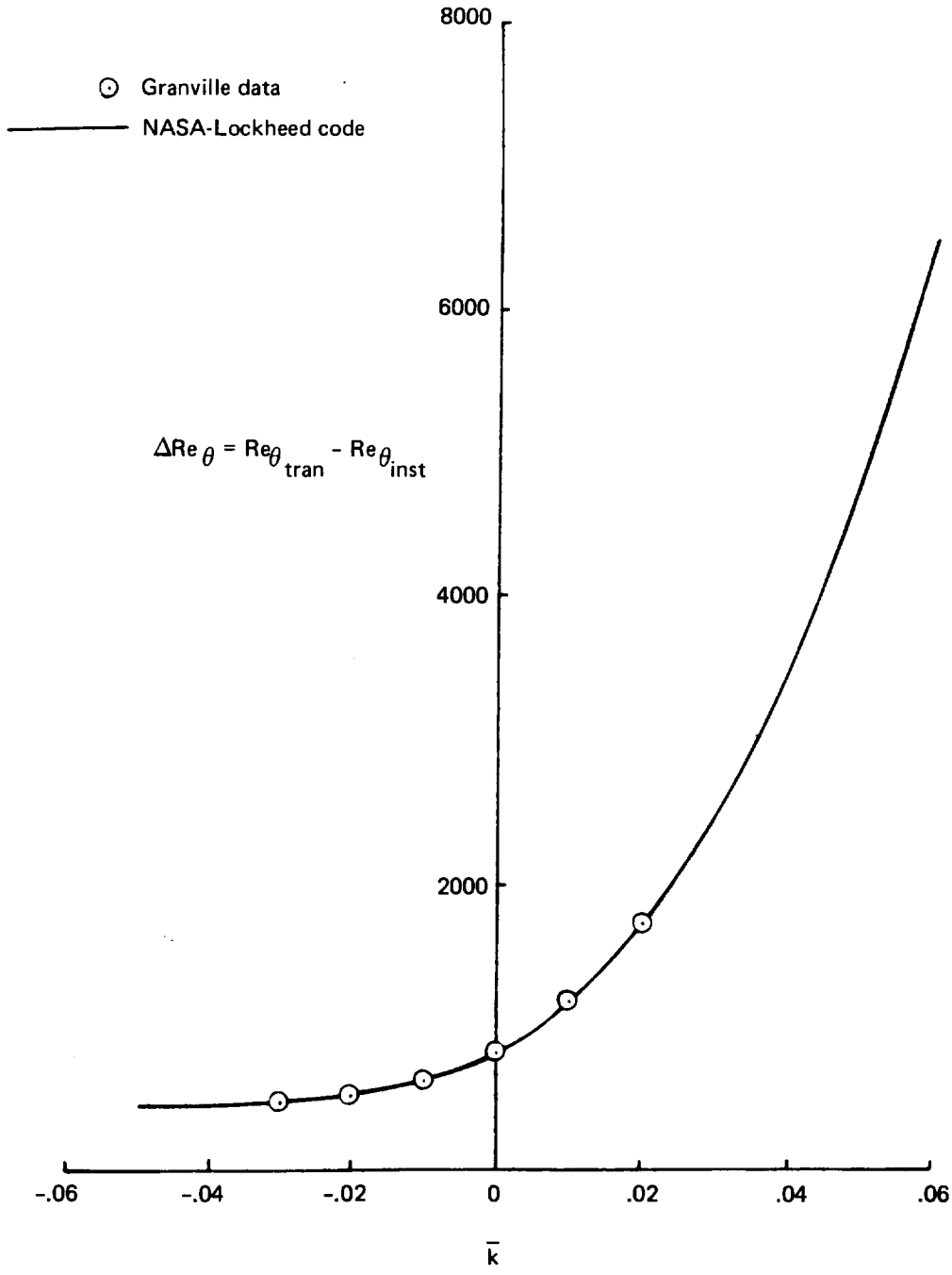

Figure 24. — Transition Curve

is called the transition point. Upon location of the natural transition point, subroutine LAMNA calculates the initial values of θ and H to start the prediction of the turbulent flow.

LAMINAR SEPARATION

Laminar separation is calculated two ways:

1. The local value of the correlation number n is compared with the separation value of n. If

$$n \geqslant n_{sep},$$

then separation has occured according to the Cohen and Reshotko analysis.

2. Curle writes the shear stress as:

$$\tau_w = \frac{\mu U_e \ell}{\theta} \tag{99}$$

where

$$\ell^2 = F_1(k) - (MU)\, G_1(k)$$

The parameter MU is defined by

$$MU = k^2 \frac{U_e U_e''}{(U_e')^2} \qquad U_e' = \frac{dU_e}{dx} \qquad U_e'' = \frac{d^2 U_e}{dx^2}$$

$$k = \frac{\theta^2}{\nu} U_e'$$

At separation

$$\ell = o \qquad MU = \frac{F_1(k)}{G_1(k)}$$

Thus, if the local value of MU is greater than $(MU)_{sep}$, separation has occurred according to the Curle criteria. Goradia's curve fits of the function $F_1(k)$ and $G_1(k)$ are shown in figures 25 and 26.

LAMINAR BUBBLE CRITERIA

Laminar bubble criteria (long with stall or short with turbulent reattachment) are based on the work of Goradia and Lyman (ref. 18). They have correlated dM_e/ds with Re_θ to come up with a critical dM_e/ds to determine bubble characteristics. The following test is used:

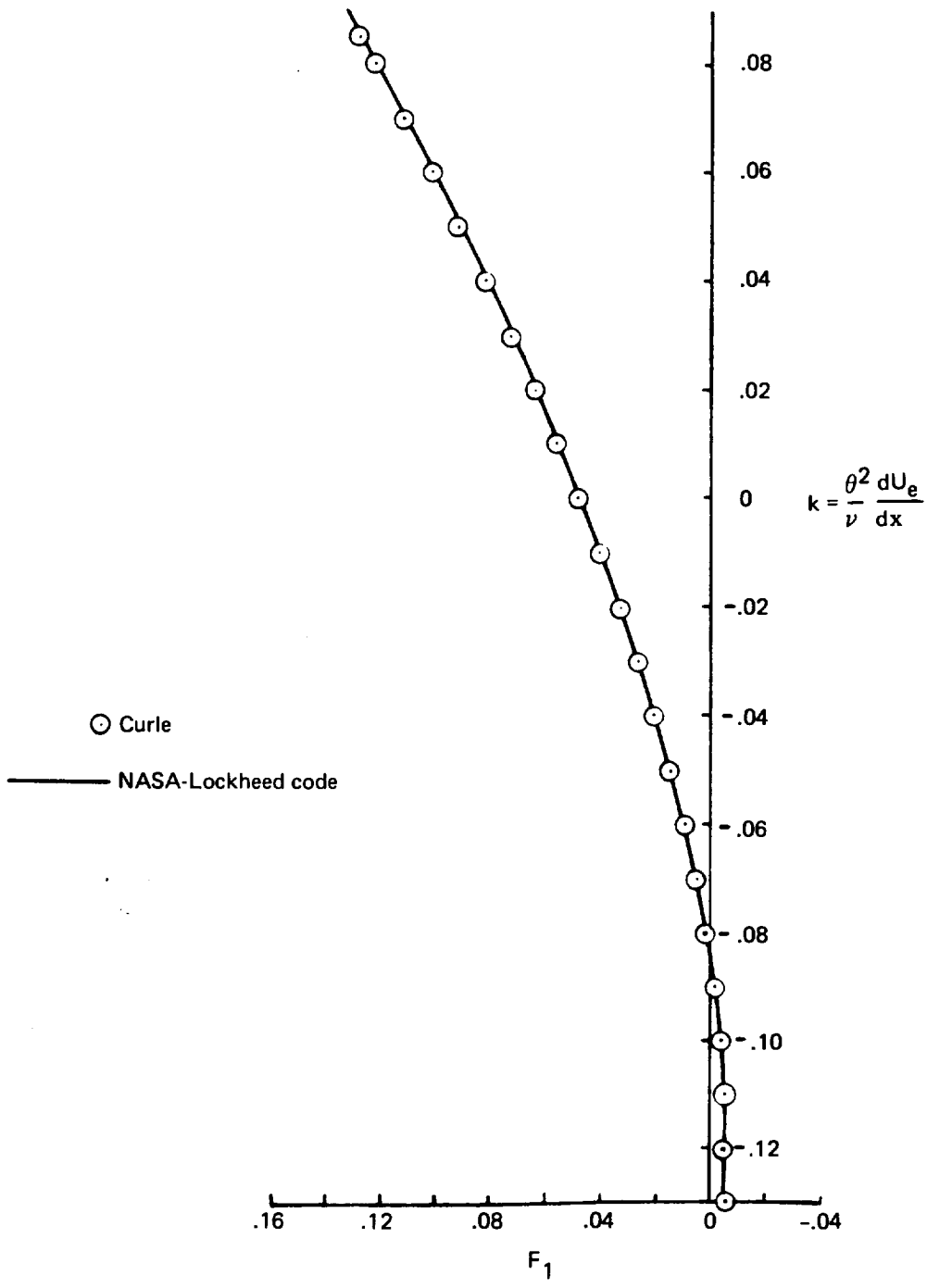

Figure 25. — Function $F_1(k)$

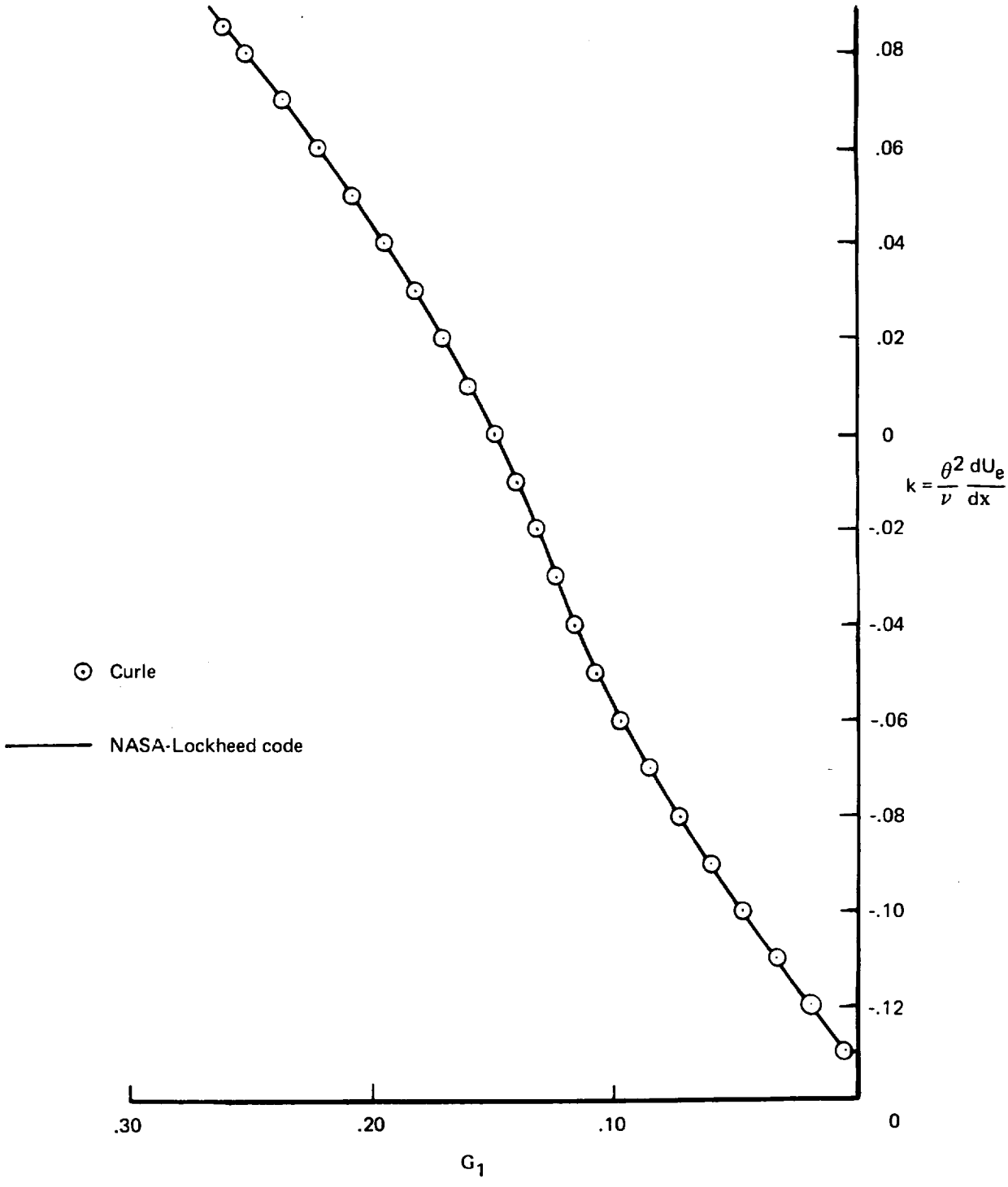

Figure 26. – Function $G_1(k)$

Long bubble if

$$-.02\ Re_\theta - 1 - \frac{dM_e}{ds} \geqslant 0 \tag{100}$$

Short bubble if

$$-.02\ Re_\theta - 1 - \frac{dM_e}{ds} < 0 \tag{101}$$

SYMBOLS OF TRANSITION AND LAMINAR SEPARATION

Theory	Code	Definition
F_1, G_1	F1,G1	Functions of Curles' boundary layer analysis
H	HMEAN	Boundary layer shape factor
k	LBL	Pressure gradient parameter
$\bar{k}$	KBAR	Average pressure gradient parameter, defined by equation (97)
ℓ	MBL	Parameter in Curles' analysis
M_e		Local Mach number
MU		Parameter
n	CN	Correlation number of the Cohen and Reshotko analysis
n_{sep}	SEP	Value of n at separation
Re_θ	REMOM	Momentum thickness Reynolds number
s	SUMS	Arc length along the airfoil surface
U_e	UE	Velocity at the outer edge of the boundary layer
θ	AMTK	Boundary layer momentum thickness
μ		Viscosity
ν	XNUX1	Kinematic viscosity
τ_W		Wall shear stress

Subscripts

crit	Critical value
inst	Instability point
local	Local value
tran	Transition

TURBULENT BOUNDARY LAYER (BBCB)

Ordinary turbulent boundary layer calculations are performed in subroutines TURBL and TURB of OVERLAY (4,2).

Subroutine TURBL uses the method of Truckenbrodt with some modifications made by Goradia aimed at avoiding program failures in regions of flow separation. Subroutine TURB uses the method of Nash and Hicks, but is only employed in the last iteration cycle for the purpose of predicting separation.

Method of Truckenbrodt (BBCBA)

Truckenbrodt's turbulent boundary layer analysis is an incompressible integral method based on the momentum integral equation and the energy integral equation (refs. 16 and 19). Details of this method follow, including the modifications made by Goradia to the original analysis.

In incompressible, two-dimensional flow, the momentum integral and the energy integral equations read

$$\frac{d\theta}{dx} + (H+2)\frac{\theta}{U_e}\frac{dU_e}{dx} = \frac{\tau_w}{\rho U_e^2} \tag{102}$$

$$\frac{1}{U_e^3}\frac{d}{dx}\left(U_e^3\ \delta^{**}\right) = 2\int_0^{\delta}\frac{\tau}{\rho\ U_e^2}\frac{\partial}{\partial y}\left(\frac{u}{U_e}\right)dy \tag{103}$$

The momentum thickness ,θ, and the energy dissipation thickness, δ^{**}, are defined by

$$U_e^2\ \theta = \int_0^{\delta} u\left(U_e - u\right)dy \tag{104}$$

$$U_e^3\ \delta^{**} = \int_0^{\delta} u\left(U_e^2 - u^2\right)dy \tag{105}$$

Furthermore, U_e denotes the velocity at the outer edge of the boundary layer, the symbol ρ stands for the density, and the shear stress is denoted by τ having the value τ_w at the airfoil surface. H is the ordinary shape factor, i.e., the ratio of displacement and momentum thicknesses.

In Truckenbrodt's analysis the shear stress integral of equation (103) is approximated by

$$\int_0^{\delta}\frac{\tau}{\rho\ U_e^2}\frac{\partial}{\partial y}\left(\frac{u}{U_e}\right)dy \approx \frac{0.0056}{\left(\frac{U_e\ \theta}{\nu}\right)^{\frac{1}{6}}} \tag{106}$$

and the wall shear is obtained from the Ludwieg-Tillmann formula

$$\frac{\tau_w}{\rho U_e^2} = 0.123 \quad 10^{-.678\,H}\left(\frac{U_e\,\theta}{\nu}\right)^{-.268} \tag{107}$$

Defining a second shape factor $\tilde{H}$ by

$$\tilde{H} = \frac{\delta^{**}}{\theta} \tag{108}$$

and substituting the empirical formula equation (106) into equation (103), the energy integral equation takes the form

$$\frac{d}{dx}\left(U_e^3\,\tilde{H}\,\theta\right) = z\,\frac{U_e^3}{\left(\frac{U_e\,\theta}{\nu}\right)^n} \tag{109}$$

with

$$z = 0.0112$$

$$n = \frac{1}{6}$$

Assuming an average value of the shape factor $\tilde{H}_{av}$, the last equation can be integrated in closed form. The result is

$$\theta = \left[\left(\frac{U_{e_t}}{U_e}\right)^{3+3n}\left(\frac{\nu}{\nu_t}\right)^n \theta_t^{\,1+n} + \frac{A\nu^n}{U_e^{3+3n}}\int_{x_t}^{x} U_e^{3+2n}\,dx\right]^{\frac{1}{1+n}} \tag{110}$$

The subscript t refers to the initial turbulent point. The coefficient A combines the values of n, z, and $\tilde{H}_{av}$ according to

$$A = (1+n)\frac{z}{\tilde{H}_{av}} = 0.0076 \tag{111}$$

In addition to the quadrature formula (110) for the calculation of θ the Truckenbrodt method utilizes a differential equation to determine the shape factor $\tilde{H}$. This shape factor equation can be derived by combining the momentum integral and the energy integral equations. It reads

$$\theta\frac{d\tilde{H}}{dx} = \frac{z}{\left(\frac{U_e\,\theta}{\nu}\right)^{\frac{1}{6}}} - \tilde{H}\,\frac{\tau_w}{\rho U_e^2} + (H-1)\,\frac{\tilde{H}\,\theta}{U_e}\frac{dU_e}{dx} \tag{112}$$

The two shape factors, H and $\tilde{H}$, are related by the following empirical equation

$$\tilde{H} = \frac{1.269\,H}{H - 0.379} \tag{113}$$

Up to this point, the described method is entirely that of Truckenbrodt. There are several differences between equations (110), (112) and the equations programmed in subroutine TURBL. These differences are:

Truckenbrodt	Subroutine TURBL
$A = 0.0076$	$A = 0.0079$
$\dfrac{z}{\left(\dfrac{U_e\,\theta}{\nu}\right)^{\frac{1}{6}}}$	$1.1\,\dfrac{z}{\left(\dfrac{U_e\,\theta}{\nu}\right)^{\frac{1}{6}}}$
$(H-1)\dfrac{\tilde{H}\,\theta}{U_e}\dfrac{dU_e}{dx}$	$(H-1.1)\dfrac{\tilde{H}\,\theta}{U_e}\dfrac{dU_e}{dx}$

The effects of these small changes are unknown, but they are not expected to be significant.

One of the major areas of concern in a coupled viscous-inviscid analysis of the interactive type is premature boundary layer separation during the first few cycles of the iteration procedure. This problem is avoided by constraining the shape factor $\tilde{H}$ to the range

$$1.55 \leqslant \tilde{H} \leqslant 1.85 \tag{114}$$

which, according to equation (113), corresponds to the following restrictions for the shape factor H.

$$1.21 \leqslant H \leqslant 2.09 \tag{115}$$

These constraints can also be viewed as an artificial way of modeling the flow in the separated region.

NASH AND HICKS METHOD (BBCBB)

The method is an integral method (ref. 20) for the prediction of ordinary turbulent boundary layer characteristics. It is basically incompressible, but uses simple correction terms to account approximately for compressibility effects. The following description outlines the method.

EQUATIONS

The Nash and Hicks method uses the momentum integral equation

$$\int_0^{\delta} \left\{ u \frac{\partial u}{\partial x} - \frac{\partial u}{\partial y} \int_0^{y} \frac{\partial u}{\partial x}\, dy_1 \right\} dy = \delta\, U_e \frac{d\, U_e}{dx} + \frac{1}{\rho} \int_0^{\delta} \frac{\partial \tau}{\partial y}\, dy \qquad (116)$$

and the moment of momentum integral equation

$$\int_0^{\delta} \left\{ u \frac{\partial u}{\partial x} - \frac{\partial u}{\partial y} \int_0^{y} \frac{\partial u}{\partial x}\, dy_1 \right\} y\, dy = \frac{\delta^2}{2}\, U_e \frac{d\, U_e}{dx} + \frac{1}{\rho} \int_0^{\delta} y \frac{\partial \tau}{\partial y}\, dy \qquad (117)$$

The u-velocity is approximated by Coles' two-parameter velocity profile (ref. 8), which reads

$$u = \frac{u_\tau}{\kappa} \left\{ \ell n \frac{y\, u_\tau}{\nu} + C \right\} + \frac{u_\beta}{2} \left\{ 1 - \cos\left(\frac{\pi y}{\delta} \right) \right\}$$

with

$$\kappa = 0.41$$
$$C = 2.05$$

The two parameters in Coles' formula are the friction velocity u_τ, which is related to the wall shear τ_w by

$$u_\tau = \sqrt{\frac{\tau_w}{\rho}}$$

and the velocity parameter u_β.

The shear stress integral is determined from the following empirical first order differential equation which allows the shear stress to lag behind the equilibrium value for a given value of the shape factor H.

$$\frac{d\, C_\tau}{dx} = \frac{0.15}{\delta} \left(\hat{C}_\tau - C_\tau \right) \qquad (119)$$

where

$$C_\tau = \frac{1}{\frac{\rho}{2} U_e^2\, \delta} \int_0^{\delta} \tau\, dy \qquad (120)$$

and the equilibrium value of C_τ is provided by

$$\hat{C}_\tau = 0.025 \left(1 - \frac{1}{H}\right)^2 \tag{121}$$

From equations (116), (117), (118), a set of three ordinary first order differential equations can be derived for the calculation of the unknowns u_τ, u_β and the boundary layer thickness δ. The derivation is outlined as follows.

Nondimensional variables α and β are defined by

$$\alpha = \frac{u_\tau}{\kappa\ U_e} \qquad \beta = \frac{u_\beta}{U_e} \tag{122}$$

a Coles' velocity profile, equation (118), is introduced to the momentum and moment of momentum integral equations. This procedure provides two of the desired ordinary differential equations. A third equation, the so-called differentiated skin friction law, is obtained from Coles' velocity profile by putting $y=\delta$ in equation (118) and differentiating the result with respect to x.

The resulting three equations read

$$[A]\begin{Bmatrix} \frac{d\alpha}{dx} \\ \frac{d\beta}{dx} \\ \frac{d\delta}{dx} \end{Bmatrix} = \{b\} \tag{123}$$

with the following coefficients of $[A]$ and $\{b\}$.

$$A_{11} = -4\alpha + 1 - 1.58949\beta$$

$$A_{12} = -1.58949\ \alpha + 0.5 - 0.75\beta$$

$$A_{13} = \frac{1}{\delta}\left(-2\alpha^2 + \alpha - 1.58949\ \alpha\beta + 0.5\beta - 0.375\ \beta^2\right)$$

$$b_1 = \frac{1}{U_e}\frac{dU_e}{dx}\left(4\alpha^2 - 3\alpha + 3.17898\ \alpha\beta - 1.5\ \beta + 0.75\beta^2\right) + \frac{\alpha^2\ \kappa^2}{\delta}$$

$$A_{21} = \alpha - \frac{1}{4} + \beta\left(\frac{5}{8} + \frac{2}{\pi^2} - 0.250515\right)$$

$$A_{22} = \left(\frac{1}{2} - \frac{3}{\pi^2}\right)\left(\beta - \frac{1}{2}\right) + \alpha\left(\frac{3}{8} + \frac{2}{\pi^2} - 0.083505\right)$$

$$A_{23} = \frac{1}{\delta}\left[\frac{3}{4}\alpha^2 - \frac{\alpha}{2} + \alpha\beta\left(\frac{3}{4} + \frac{2}{\pi^2} - 0.16701\right) + \frac{\beta^2}{16} + \beta\ (\beta - 2)\left(\frac{1}{4} - \frac{1}{\pi^2}\right)\right]$$

$$b_2 = -\frac{1}{U_e}\frac{dU_e}{dx}\left[\alpha(\alpha-1)+\alpha\beta\left(1-\frac{4}{\pi^2}-0.33402\right)+\beta(\beta-2)\left(\frac{1}{2}-\frac{2}{\pi^2}\right)\right]-\frac{C_\tau}{2\delta}$$

$$A_{31} = \ell n\left(\frac{\delta\, U_e\ \kappa\,\alpha}{\nu}\right)+C+1$$

$$A_{32} = 1$$

$$A_{33} = \frac{\alpha}{\delta}$$

$$b_3 = -\frac{\alpha}{U_e}\frac{dU_e}{dx}$$

Knowing the variables α, β, and δ, the boundary layer momentum thickness, and the displacement thickness, and the skin friction coefficient are calculated from

$$\theta = \delta\left(-2\,\alpha^2+\alpha-1.5849\,\alpha\beta+\frac{\beta}{2}-\frac{3}{8}\beta^2\right) \tag{124}$$

$$\delta^* = \delta\left(\alpha+\frac{\beta}{2}\right) \tag{125}$$

$$c_f = 2\ \kappa^2\alpha^2 \tag{126}$$

INITIAL VALUES

The turbulent analysis is started, assuming the value of the momentum thickness θ at the last laminar point is equal to the momentum thickness at the transition point. Thus a plot of θ will be smooth through transition, while H, c_f, and δ^* will show a certain discontinuity as they go through transition. The turbulent starting process consists of the following steps:

1. The compressible laminar momentum thickness is converted to the incompressible value;

$$\theta_{inc} = \theta_{comp}\left(1+0.065\ M_{e_t}^2\right) \tag{127}$$

where M_{e_t} is the local Mach number at transition

2. The initial value of the incompressible turbulent shape factor is calculated using the expression

$$\left(H_{initial}\right)_{turb} = \frac{1.4754}{\log_{10} Re_\theta} + 0.9698 \tag{128}$$

where

$$Re_\theta = \frac{U_e\,\theta}{\nu}$$

3. The initial value of c_f is calculated using the Ludwieg-Tillman formula:

$$c_f = 0.246\left(Re_\theta\right)^{-.268} e^{-1.561\,H} \tag{129}$$

4. Initial values of α and β are obtained from

$$\alpha_1 = \sqrt{\frac{c_f}{2}}\ \frac{-1}{\kappa}$$

and

$$\beta_1 = \left[\left(\frac{H-1}{2} - 1.58949\,\alpha\,H\right) + \left\{\left(\frac{H-1}{2} - 1.58949\,\alpha\,H\right)^2 + 1.5\,H\left(\alpha(H-1) - 2\,\alpha^2 H\right)\right\}^{\frac{1}{2}}\right]\frac{1}{0.75\,H} \tag{130}$$

The equation for β_1 comes from the expression for

$$\frac{\delta^* - \theta}{\delta}$$

which is solved for β.

Once the initial values (actual guesses) at α and β have been obtained, a Newton iteration technique is used to find the values of α and β which are roots of the equations:

$$\alpha\left\{\ell n\left(Re_{\delta^*}\,\kappa\ \frac{\alpha}{\alpha + \beta/2}\right) + C\right\} + \beta - 1 = 0 \tag{131}$$

$$\alpha + \frac{\beta}{2} + H\left(2\alpha^2 - \alpha + 1.58949\,\alpha\beta - \beta/2 + 0.375\,\beta^2\right) = 0 \tag{132}$$

A maximum of 50 iterations is permitted in the starting routine. Upon success in starting, new values of α, β, c_f, and δ are computed and the solution proceeds using the described predictor-corrector technique.

SOLUTION METHOD

The parameters α, β, δ, and C_τ are obtained from the first order ordinary differential equations (119) and (123), which can be written in the form

$$\frac{d\phi}{dx} = f\left(\alpha, \beta, \delta, C_\tau\right)$$

where ϕ denotes any of the four unknowns. The equations are integrated using the following predictor-corrector technique having a maximum step size 2δ. The solution is advanced from x to $x+\Delta x$ using the predictor step

$$\phi_{x+\frac{\Delta x}{2}} = \phi_x + \left(\frac{d\phi}{dx}\right)_x \frac{\Delta x}{2} \tag{133}$$

and the corrector step

$$\phi_{x+\Delta x} = \phi_x + \left(\frac{d\phi}{dx}\right)_{x+\frac{\Delta x}{2}} \Delta x \tag{134}$$

COMPRESSIBILITY CORRECTION

The Nash-Hicks analysis is incompressible, so it becomes necessary to correct the computed viscous flow parameters for compressibility effects. The corrections read

$$\delta^*_{comp} = \delta^*_{inc}\left(1 + 0.30\, M_e^2\right) \tag{135}$$

$$H_{comp} = H_{inc}\left(1 + 0.365\, M_e^2\right) \tag{136}$$

$$c_{f_{comp}} = c_{f_{inc}} \frac{1}{1 + .065\, M_e^2} \tag{137}$$

$$\theta_{comp} = \theta_{inc} \frac{1}{1 + .065\, M_e^2} \tag{138}$$

where M_e is the local Mach number at the edge of the boundary layer.

SEPARATION

Boundary layer separation is predicted when

$$\alpha < 0.023 \text{ or } \beta > 1 \tag{139}$$

The [illegible] equation (139) are used in place of the theoretical values obtained from Coles' profile of $\alpha = 0$ and $\beta = 1$. Practical experience has shown that $\alpha = .023$ is more reasonable ($\alpha = .023$ corresponds to $c_f < .000\,18$.)

SYMBOLS OF THE ORDINARY TURBULENT BOUNDARY LAYER CALCULATION

Theory	Code	Definition of Symbol
C	2.05	Constant in Coles' velocity profile
c_f	CF	Skin friction coefficient
C_τ	CFI	Shear stress integral
$\hat{C}_\tau$		Equilibrium value of shear stress integral
H	HMEAN H	Shape factor, δ^*/θ
$\tilde{H}$	[illegible]	Shape factor, δ^{**}/θ
M_e	ML, AME	Local Mach number
n		Exponent
Re_{δ^*}		Displacement thickness Reynolds number
Re_θ		Momentum thickness Reynolds number
U_e	UE	Velocity at the outer edge of the boundary layer
u_β		Wake component of velocity profile
u_τ		Friction velocity
u		Velocity component in x-direction
x,y	XTEMP, YTEMP	Boundary layer coordinates
α	ALPHAI	$u_\tau/(U_e\kappa)$
β	BETAI	u_β/U_e
δ	DLTA	Boundary layer thickness
δ^*	DLTAS	Displacement thickness
	DELSTR	
δ^{**}		Energy dissipation thickness
θ	TTA, THETA	Momentum thickness

Theory	Code	Definition of Symbol
κ	0.41	Constant in Coles' velocity profile
ν	XNUXI	Kinematic viscosity
ρ		Density
τ		Shear stress
τ_W		Wall shear stress
ϕ		General variable

Subscripts

comp	Compressible
e	Outer edge of boundary layer
inc	Incompressible
t	Transition

CORE REGION

The core region is that part of the flow field where the wake of one airfoil component is separated from the boundary layer of the next downstream airfoil by a potential core, (fig. 27). The following four problems are solved to determine the details of the flow in this region.

- Wake centerline geometry
- Wake flow
- Boundary layer growth
- End-of-core region

Theoretical methods of predicting boundary layer characteristics on the surface of the aft airfoil component are described previously in this document. The reader should note that transition of the boundary layer from laminar to turbulent flow may take place in the core region. This section of the document contains a detailed account of the method used to trace the potential flow streamline leaving the trailing edge of the upstream airfoil (wake centerline). It further contains a brief outline of the lag entrainment method of Green which provides the pertinent parameters of the wake flow and describes the geometric scheme for determining the downstream boundary of the core region (end of core).

WAKE CENTERLINE

The wake centerline is that potential flow streamline which is attached to the average trailing edge point of an airfoil component. The problem of determining the geometry of the wake centerline must be solved for each component of the multielement airfoil during each cycle of the overall iterative solution procedure. The computer code is contained in subroutine WAKCL of OVERLAY (1,0) and subroutines WAKEG, WAKEJ, WAKES, WAKET of OVERLAY (3,0).

STREAMLINE TRACING

Since the potential flow problem is solved on the basis of a stream function method, which among other results provides the value of the stream function Ψ_m for each stagnation streamline, it is a natural approach to also use the stream function to calculate the position of the wake centerline. The following assumptions are made.

- The values and locations of all vortices γ_j and sources σ_j are known and have a fixed value during the calculation of the streamline.
- The chord length of each segment representing the wake centerline and the total chord length are constant.

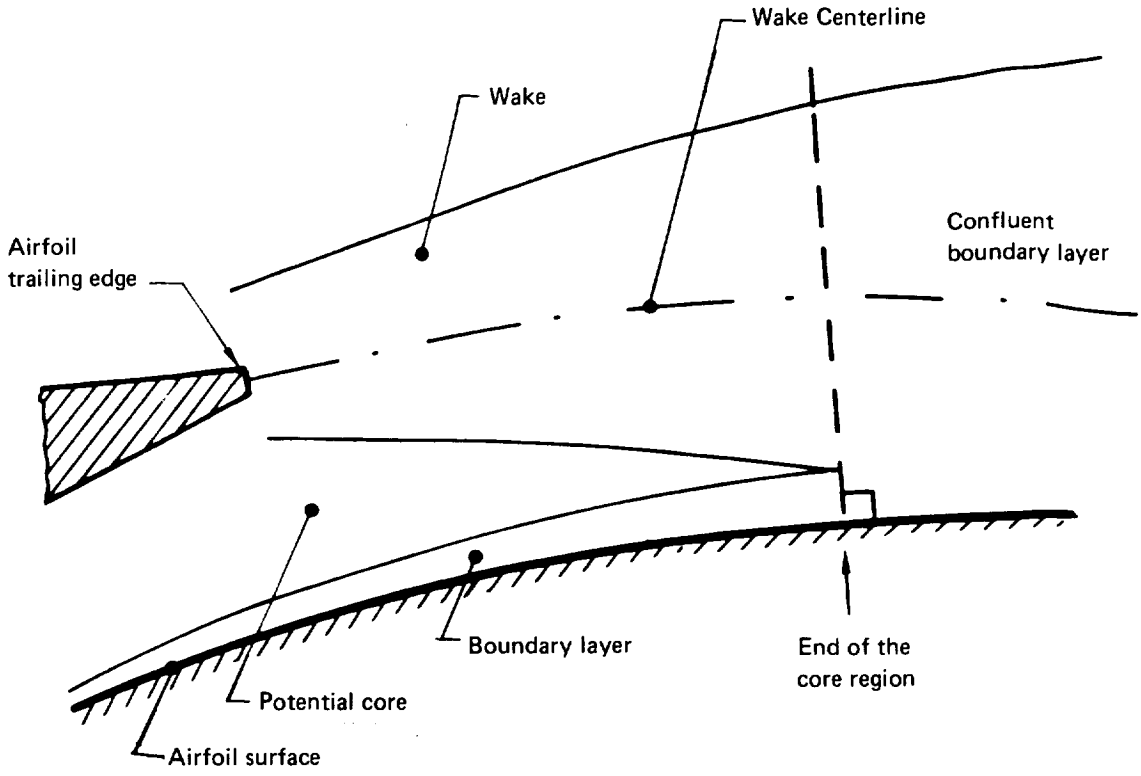

Figure 27. — Core Region

- The source distribution simulating the displacement effect of the viscous wake occupies either part or the whole length of the wake centerline.

The wake centerline is discretized as shown in figure 28, where each segment of the polygon is inclined to the X_G-axis of the global coordinate system at an angle θ_i. The equation of the stream function along the wake centerline can therefore be written in parametric form as

$$\Psi_m = \Psi \left[X\left(\theta_i\right), Z\left(\theta_i\right) \right] \tag{140}$$

where Ψ_m is known for each airfoil component. The problem of calculating the centerline coordinates is nonlinear, since in equation (140) the stream function depends in nonlinear fashion on these coordinates. This can be seen more clearly by writing the value of Ψ at a field point (X,Z)

$$\Psi(X,Z) = \cos\alpha\, Z - \sin\alpha\, X + \sum_{m=1}^{N_c} \sum_{j=1}^{N_m} K_{ij}^{V} \gamma_j + \sum_{m=1}^{N_c} \sum_{j=1}^{(N+N_w)_m} K_{ij}^{S} \sigma_j \tag{141}$$

This equation is derived in the Potential Flow section which also contains the definitions and illustrations of all variables. In particular, it is shown there that the stream function influence coefficients K_{ij}^{V} and K_{ij}^{S} are nonlinear functions of the field point coordinates (X,Z).

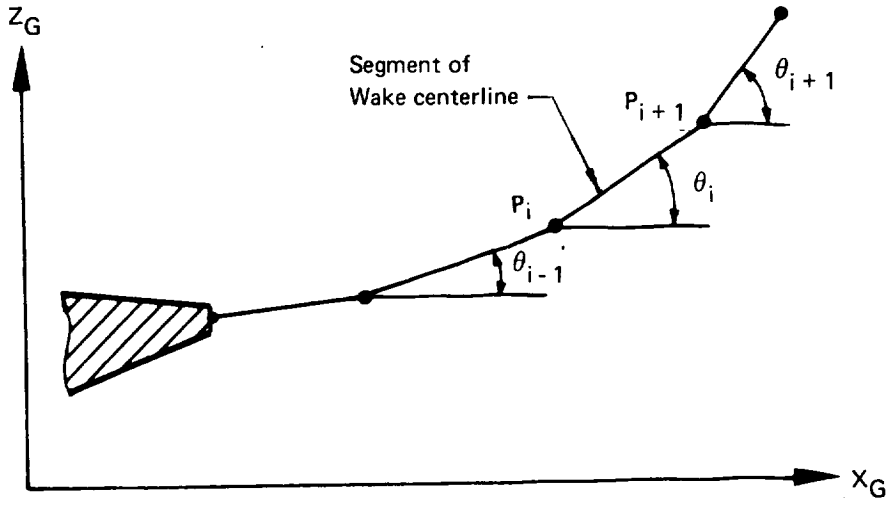

Figure 28. — Discretization of Wake Centerline

Beginning from some assumed initial position of the wake centerline, the solution of the nonlinear equation (140) for the desired wake centerline geometry is arrived at by iteration. During a step of this iteration procedure, incremental values $\Delta\theta$ of the segment angles are computed from

$$\left[\left(\frac{\partial\Psi}{\partial X}\frac{\partial X}{\partial\theta}+\frac{\partial\Psi}{\partial Z}\frac{\partial Z}{\partial\theta}\right)^{(k-1)}\right]\left\{\Delta\theta\right\}=\left\{\Psi_m-\Psi_i^{(k-1)}\right\} \tag{142}$$

The superscript (k-1) denotes coefficients that are known from the previous, i.e., the (k-1)st iteration cycle. The matrix

$$\left[\left(\frac{\partial\Psi}{\partial X}\frac{\partial X}{\partial\theta}+\frac{\partial\Psi}{\partial Z}\frac{\partial Z}{\partial\theta}\right)\right]$$

is the so-called Jacobian, whose coefficients are determined as follows.

The derivatives of the stream function, with respect to the coordinates X and Z, are the potential flow velocities

$$U_i=\left.\frac{\partial\Psi}{\partial Z}\right|_i \qquad -V_i=\left.\frac{\partial\Psi}{\partial X}\right|_i \tag{143}$$

at the corner points of the wake centerline segments due to the combined effect of the freestream, and all vortices γ_j and sources σ_j of the flow field. It should be emphasized at this point that, during the calculation of the centerline geometry, the wake sources remain fixed along the assumed initial position of the wake centerline.

The derivatives $\partial X/\partial\theta$ and $\partial Z/\partial\theta$ represent a shift of the coordinates of the i-th corner point caused by a change in inclination of the j-th segment of the wake centerline. Denoting a segment corner point by

$$P_i = \left(X_i,\ Z_i \right),$$

the desired derivatives are calculated as follows.

$$\frac{\partial P_i}{\partial \theta_j} = \begin{Bmatrix} 0 \\ 0 \end{Bmatrix} \quad (j \geqslant i) \tag{144}$$

$$\frac{\partial P_i}{\partial \theta_j} = \begin{Bmatrix} -c_j \sin\theta_j \\ c_j \cos\theta_j \end{Bmatrix} \quad (j < i) \tag{145}$$

It should be noticed that the property expressed by equation (144) leads to a triangular Jacobian with obvious advantages for the economy of the streamline calculation.

The angles $\Delta\theta_i$ are calculated from equation (142) utilizing a modification of the familiar Newton method, that is known in the literature as the Quasi-Newton method (ref. 21).

Having computed the angles $\Delta\theta_i$, the shift of the segment corner points parallel to the global X,Z-coordinates are obtained from

$$\begin{aligned} \Delta X_i &= \sum_{j=1}^{(N_w)_m} \frac{\partial X_i}{\partial \theta_j} \Delta\theta_j \\ \Delta Z_i &= \sum_{j=1}^{(N_w)_m} \frac{\partial Z_i}{\partial \theta_j} \Delta\theta_j \end{aligned} \tag{146}$$

INITIAL POSITION

Two cases have to be distinguished when selecting the initial position of the wake centerline and its total length. The calculations are performed by subroutine WAKCL of OVERLAY (1,0).

Case a

During the first cycle of the overall iteration procedure, the initial position of the wake centerlines is chosen as shown in figure 29 for a two-component airfoil. The first wake centerline is assumed to be parallel to the surface of the adjacent airfoil component. The distance is

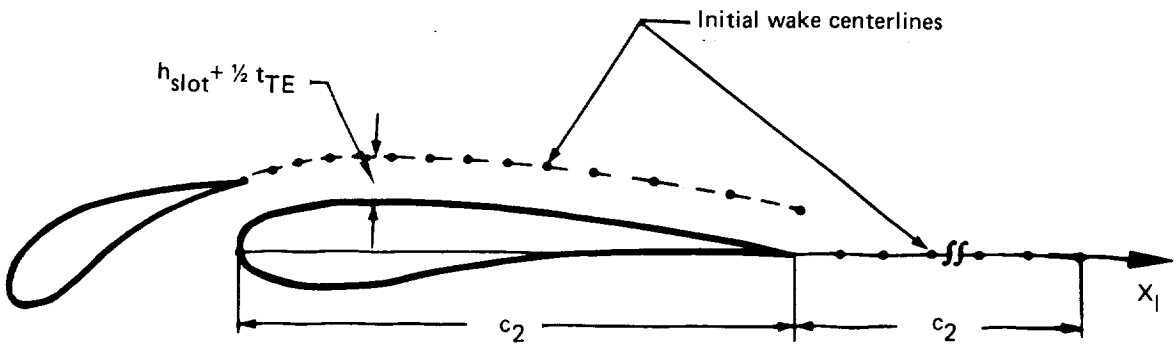

Figure 29. – Initial Position and Length of Wake Centerlines

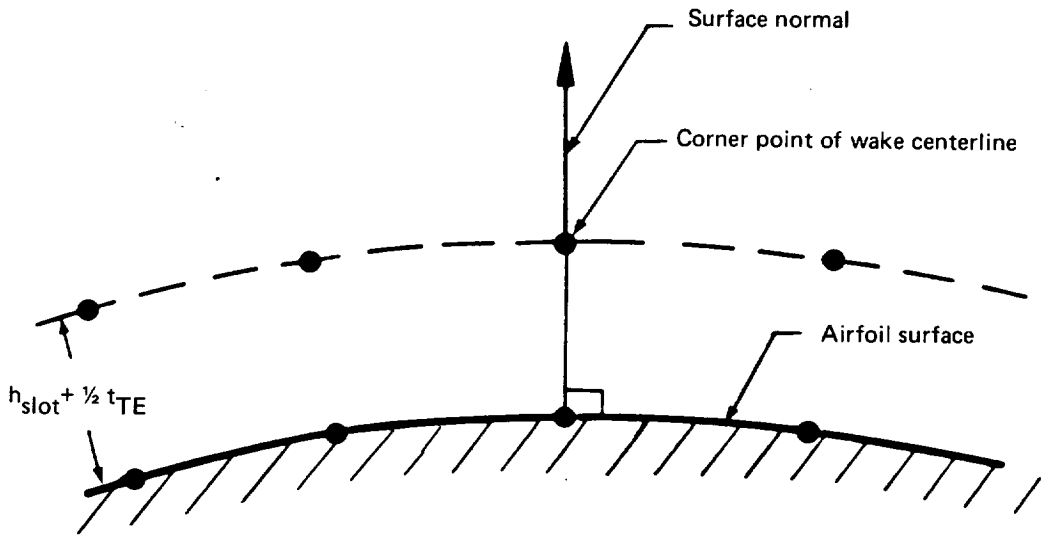

Figure 30. – Selection of Segment Corner Points of Initial Wake Centerline

$$h_{slot} + \frac{1}{2} t_{TE}$$

where the symbols h_{slot} and t_{TE} stand for the slot height at the upstream slot exit and the trailing edge thickness of the upstream airfoil, respectively. The corner points of wake segments are chosen, as illustrated in figure 30, by shifting the corresponding airfoil surface points along the surface normal. This procedure gives a wake centerline which extends from the slot exit to the trailing edge of the neighboring airfoil.

The initial position and the total length of the last wake centerline are selected by extending the chord length of the last airfoil by 100%. All segments representing this wake centerline are of equal length. Their total number equals the number of segments on the upper surface of the last airfoil.

Case b

Beginning with the second cycle of the overall iteration procedure, the initial position of the wake centerlines is the computed position for the previous cycle.

WAKE VELOCITY

Wake velocity is the potential flow velocity computed at points on the wake centerline. The wake centerline velocity approximates the velocities at the outer edges of the viscous wake, which are equal, since the effect of wake curvature is neglected. The inviscid wake centerline velocity is the correct inner limit of the outer potential flow solution, and should not be confused with the viscous flow velocity along the wake centerline.

COMPRESSIBILITY EFFECT

In applying the Karman-Tsien compressibility correction, the airfoil geometry is not scaled from a compressible to an equivalent incompressible geometry. This is justified by the theoretical result that the Karman-Tsien compressibility correction does not distort streamlines to any significant degree during the transformation from the compressible to the incompressible flow domain. For the same reason, the geometry of the wake centerline need not be corrected for compressibility effects. The wake velocity, of course, is transformed to a compressible velocity as described in the section on the Potential Flow solution.

WAKE FLOW (BBCC)

The method is coded in subroutines WAKEI, WAKED, WADEP of OVERLAY (4,3).

The properties of the wake behind each airfoil component are calculated using a version of the Green method, reference 7, which is based on the following assumptions.

- Wake flow is two-dimensional and incompressible

- Wake curvature effects are neglected
- Thin boundary layer approximations apply to wake flow
- Secondary effects on the turbulence structure of the wake are neglected

LAG ENTRAINMENT METHOD OF GREEN (BBCCA)

The following description of the Green method applies to the wake flow on one side of the wake centerline.

It is an integral method formulated in terms of the following three dependent variables. The first variable is the momentum thickness, θ, defined by

$$U_w^2\,\theta = \int_0^{\delta} (U_w - u)\,u\,dy \tag{147}$$

where U_w is the potential flow velocity at the outer edge of the wake. The coordinate y is measured perpendicular to the wake centerline and the symbol δ represents the distance from the wake centerline to the outer edge of the wake.

The second variable is the shape factor H, defined by

$$H = \frac{\delta^*}{\theta} \tag{148}$$

where the displacement thickness δ^* has the familiar definition

$$U_w\,\delta^* = \int_0^{\delta} (U_w - u)\,dy \tag{149}$$

The third main variable of the prediction method is the so-called entrainment coefficient c_E defined by

$$U_w\,c_E = \frac{d}{dx}\left(\int_0^{\delta} u\,dy\right) \tag{150}$$

The three variables θ, H, and c_E are governed by the momentum integral equation, the entrainment equation, and an equation for the streamwise rate of change of the entrainment coefficient. The three equations are briefly described below. The momentum integral equation reads

$$\frac{d\theta}{dx} = -(H+2)\,\frac{\theta}{U_w}\,\frac{dU_w}{dx} \tag{151}$$

The coordinate x is tangent to the wake centerline. The entrainment equation can be [illegible] from the definitions of the entrainment coefficient c_E, equation (150) and the [illegible] shape parameter

$$H_1 = \frac{\delta - \delta^*}{\theta} \tag{152}$$

[illegible]

$$\frac{dH}{dx} = \frac{1}{\theta} \frac{dH}{dH_1} \left(c_E + H_1 (H + 1) \frac{\theta}{U_w} \frac{dU_w}{dx} \right) \tag{153}$$

The shape factors H and H_1 are related by an empirical equation, which reads

$$H_1 = 3.15 + \frac{1.72}{H - 1} - 0.01 (H - 1)^2 \tag{154}$$

Hence,

$$\frac{dH}{dH_1} = - \frac{(H - 1)^2}{1.72 + 0.02 (H - 1)^3} \tag{155}$$

The equation for the streamwise rate of change of the entrainment coefficient, the so-called lag equation, is also an empirical equation. The equation takes into account the influence of the upstream flow history on the turbulent stresses and reads

$$\frac{dc_E}{dx} = \frac{F}{\theta} \left[\frac{2.8}{H + H_1} \left\{ \left(c_\tau \right)^{\frac{1}{2}}_{EQ_o} - \lambda \left(c_\tau \right)^{\frac{1}{2}} \right\} + \left(\frac{\theta}{U_w} \frac{dU_w}{dx} \right)_{EQ} - \frac{\theta}{U_w} \frac{dU_w}{dx} \right] \tag{156}$$

The various terms in equation (156) are calculated from

$$\lambda = \frac{1}{2} \tag{157}$$

$$F = \frac{\left(0.024 + 1.2\, c_E \right) c_E}{0.012 + 1.2\, c_E} \tag{158}$$

$$c_\tau = 0.024\, c_E + 1.2\, c_E^2 \tag{159}$$

$$\left(\frac{\theta}{U_w}\frac{dU_w}{dx}\right)_{EQ_o} = -\frac{1.25}{H}\left(\frac{H-1}{6.432\,H}\right)^2 \tag{160}$$

$$\left(c_E\right)_{EQ_o} = -H_1\,(H+1)\left(\frac{\theta}{U_w}\frac{dU_w}{dx}\right)_{EQ_o} \tag{161}$$

$$\left(c_\tau\right)_{EQ_o} = 0.024\left(c_E\right)_{EQ_o} + 1.2\left(c_E\right)^2_{EQ_o} \tag{162}$$

$$\left(c_E\right)_{EQ} = \sqrt{\frac{\left(c_\tau\right)_{EQ_o}}{1.2\,\lambda^2} + 0.0001} - 0.01 \tag{163}$$

$$\left(\frac{\theta}{U_w}\frac{dU_w}{dx}\right)_{EQ} = -\frac{\left(c_E\right)_{EQ}}{H_1\,(H+1)} \tag{164}$$

INITIAL VALUES

Initial values for θ and H are provided by the boundary layer calculations at the upper- and lower-surface trailing edge. An initial value for the entrainment coefficient is assumed to be given by its equilibrium value $(c_E)_{EQ}$ which can be calculated from equations (154), (157), (160), (161), (162), and (163).

COMPLETE WAKE SOLUTION

The wake flow is calculated on both sides of the wake centerline solving the differential equations (151), (153), and (156) in marching fashion beginning at the trailing edge of the upstream airfoil. At each point of the wake centerline, the wake parameters of both sides are calculated before the integration procedure advances to the next point.

The main result of the wake calculation is the total displacement thickness of the wake

$$\delta^*_w = \delta^*_u + \delta^*_l \tag{165}$$

which is the sum of δ^* of the upper side (subscript u) and lower side (subscript l) of the wake.

In addition, the distance from the wake centerline to the lower edge of the wake, denoted by the symbol δ_l, is needed to predict the end of the core region. δ is obtained from

$$\delta_l = \theta_l\left(H_l\right)_l + \delta^*_l \tag{166}$$

At the end of the potential core region, δ_l and its corresponding value at the upper side of the wake, δ_u, are saved as initial values for the confluent boundary layer calculation.

END OF CORE (BBCCB)

The method is programmed in subroutine ECORE, OVERLAY (4,3).

The physical boundaries of the core region are shown in figure 27. The downstream boundary of that region is termed the end of the core. It is defined by the normal to the surface of the aft airfoil which passes through the point of intersection of wake and boundary layer edges. This definition is consistent with the aerodynamic model of the confluent boundary layer for which initial values must be provided along the same surface normal.

The notation used in determining the end of the core is illustrated in figure 31. It is assumed that properties of the boundary layer beneath the potential core are known. The wake flow calculation proceeds in marching fashion along the wake centerline. At each step of the calculation it is checked whether or not the end of the core region has been reached. Knowing the properties of the wake at a point P_i, which include the half width of the wake δ_l, the following calculation is performed.

The distance $\overline{P_i P_N}$ along the surface normal is determined as described in the geometry section of the program for the slot height calculation. Further, the distance d along the the surface normal measured from the point P_i to the edge of the wake is obtained from

$$d = \frac{\Delta s \ \delta_{l_i}}{\Delta s \cos\gamma + \left(\delta_{l_i} - \delta_{l_{i-1}}\right) \sin\gamma} \tag{167}$$

The symbol Δs denotes the arc length between the points P_i and P_{i-1} on the wake centerline. The angle γ is formed by the normal to the wake centerline at point P_i and the surface normal of the aft airfoil, see figure 31.

The end of the core region has been reached if

$$d + \delta_{BL} \geqslant \overline{P_i P_N} \tag{168}$$

where δ_{BL} is the thickness of the boundary layer at the point P_N.

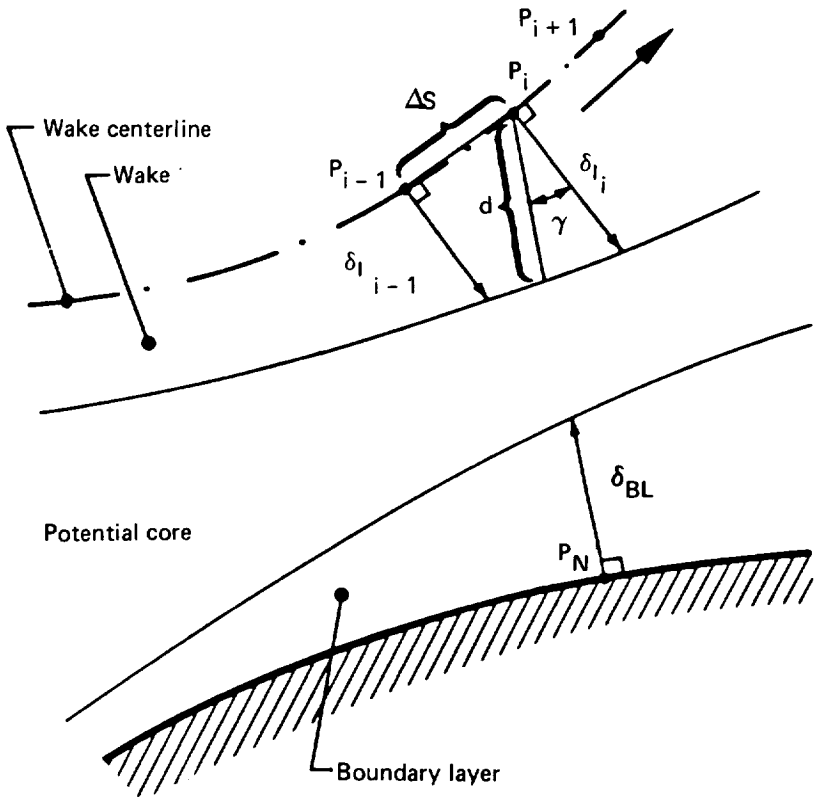

Figure 31. — On the Calculation of the End of the Core Region

CONFLUENT BOUNDARY LAYER (BBCD)

FLOW MODEL

FLOW REGIONS

The flow downstream of the slot of a two-element airfoil configuration consists of three regions, shown in figure 32. These regions are termed

- Core region
- Confluent boundary layer
- Ordinary turbulent boundary layer

In general, all these flow regions can exist above the surface of the second airfoil component. Their existence depends on many influencing parameters involving airfoil geometry and flight conditions. Most regions shown in figure 32 are expected to exist if the relative chord length of the second airfoil is large, the gap between the two airfoils and the angle of attack are such that only a relatively small potential core develops, and, in addition, the wake of the upstream airfoil does not entirely dominate the spreading of the confluent boundary layer. This flow condition is often encountered on a wing with a leading edge flap (slat). On the other hand, for a wing with a single trailing edge flap and a relatively large gap, the potential core often extends beyond the flap trailing edge and, consequently, only the core region develops.

The flow models of the core region and of the ordinary turbulent boundary layer are described previously in this document. This section describes the model of the confluent boundary layer, developed by Goradia (refs. 2 and 22).

Goradia divides the confluent boundary layer into two regions – main regions I and II.

Main region I is that flow region immediately downstream of the potential core. The confluent boundary layer in main region I consists of three layers, figure 33, that are termed

- Wall layer
- Jet layer
- Wake layer

The wall layer is the continuation of the upstream boundary layer. The jet layer and wake layer represent the remainder of the inner and outer part of the viscous wake of the upstream airfoil component, respectively. Figure 33 shows a representative velocity

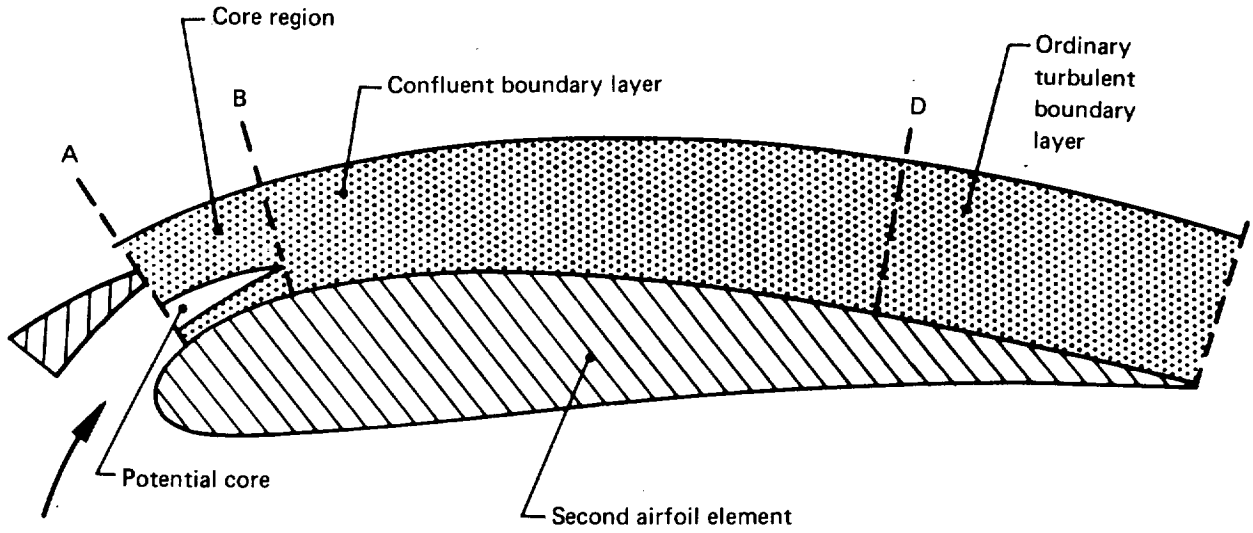

Figure 32. – Flow Regions Above Surface of Two-Element Airfoil

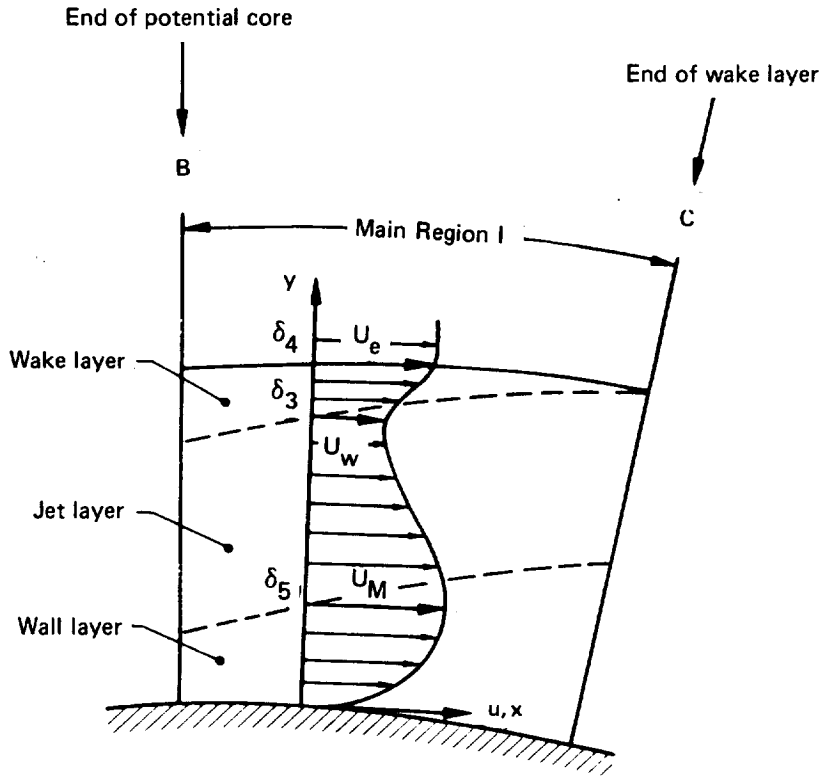

Figure 33. – Layers of the Flow Model in Main Region I

profile of this region. The velocity at the outer edge of the wall layer is denoted by U_M. The symbol U_W denotes the velocity at the common boundary of jet layer and wake layer. The outer edges of the three layers are denoted by the variables δ_5, δ_3, and δ_4.

Main region II is the confluent boundary layer region downstream of the point where the wake layer disappeared. The velocity profile of this region is that of a simple wall jet featuring a velocity maximum only, see figure 34. The influence of the wake of the upstream airfoil component is not noticeable. At the end of main region II, the jet layer disappears and the confluent boundary layer degenerates into an ordinary turbulent boundary layer.

Having discussed the basic confluent boundary layer model of an airfoil with two components, its application to the more complex flow field above a multielement airfoil shall now be described. Figure 35 illustrates the flow model above a high-lift airfoil consisting of four airfoil components, a wing with a leading edge flap, and a double-slotted trailing edge flap. Above the main wing and above the surface of each of the two trailing edge flaps, the flow field is modeled by the described basic model, which in general consists of a core region, main regions I and II of the confluent boundary layer, and an ordinary turbulent boundary layer. In other words, it is assumed that at each slot exit a new flow field develops, simulated by the basic flow model. This representation of the flow above the surface of multielement airfoils ignores the detailed structure of the wakes and potential cores that might still exist at the trailing edge of the upstream airfoil component, i.e., it is assumed that near the trailing edge of each airfoil component the viscous flow has always degenerated into an ordinary turbulent boundary layer.

ASSUMPTIONS AND LIMITATIONS

The following assumptions are made in the prediction of the confluent boundary layer characteristics.

- The flow is two-dimensional and incompressible.
- The effect of surface curvature is neglected.
- The development of the various viscous layers comprising the confluent boundary layer is governed by the turbulent boundary layer equations for a steady mean flow. This and the previous assumption imply that the static pressure is constant in direction normal to the surface along which the confluent boundary layer develops.
- The confluent boundary layer is attached to the surface over which it develops.
- The velocity profiles of the individual viscous layers are self-similar in each region of the confluent boundary layer.

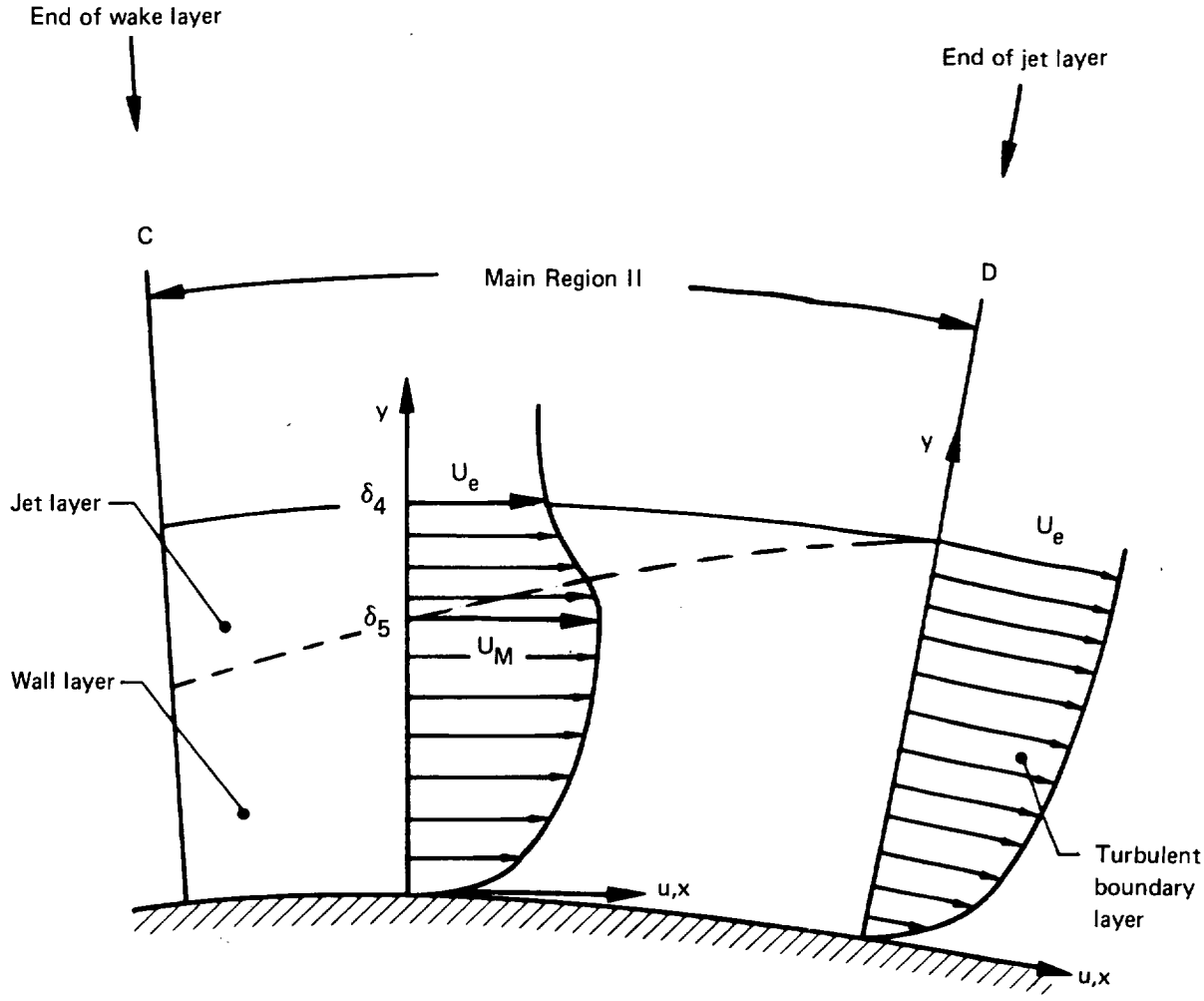

Figure 34. — Layers of the Flow Model in Main Region II

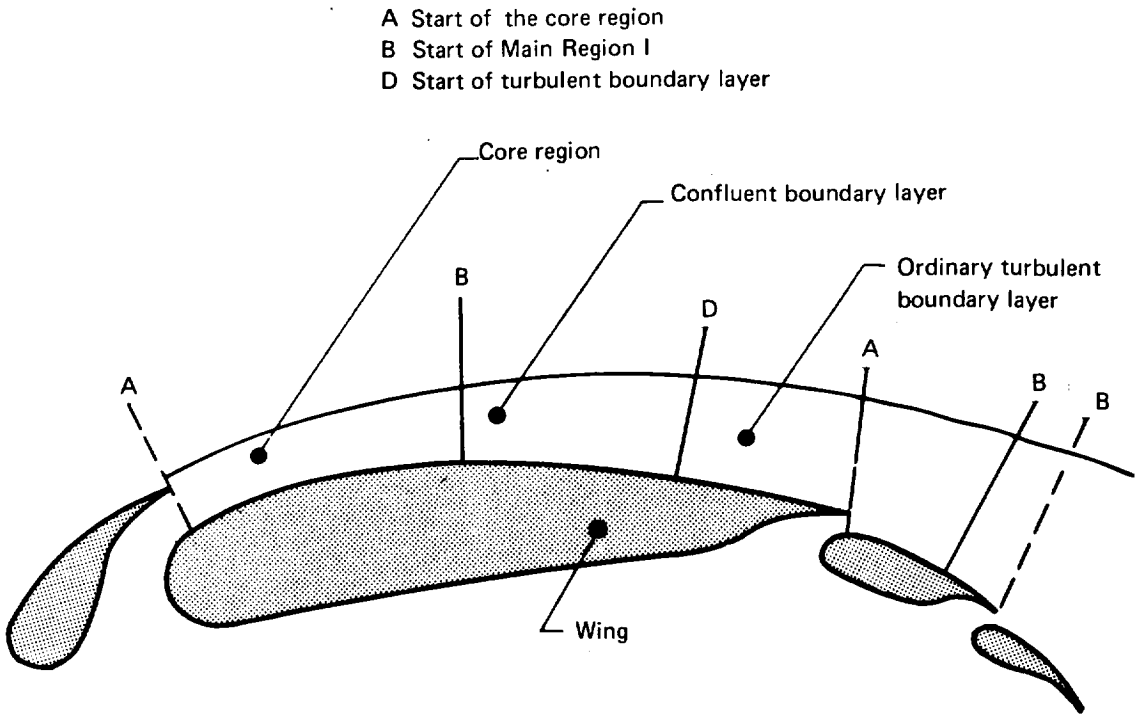

Figure 35. — Application of the Basic Flow Model to a Multielement Airfoil

The following features of the flow model of the confluent boundary layer represent additional limitations of its applicability.

- The characteristics of the predicted growth of the confluent boundary layer depend strongly on the empirical content of the turbulent flow model.
- The model does not account for multiple potential cores and/or multiple wakes which might exist above slotted flaps.

BASIC FLOW EQUATIONS

The governing equations of all viscous layers of the confluent boundary layer are the two-dimensional incompressible turbulent boundary layer equations. They read

$$\frac{\partial u}{\partial x} + \frac{\partial v}{\partial y} = 0 \tag{169}$$

$$u \frac{\partial u}{\partial x} + v \frac{\partial u}{\partial y} = U_e \frac{dU_e}{dx} + \frac{\partial}{\partial y} \left(\frac{\tau}{\rho} \right) \tag{170}$$

where u and v are the mean values of the velocity components in x- and y-directions. The symbols τ and ρ denote the shear stress and fluid density, respectively. U_e is the velocity at the outer edge of the confluent boundary layer. The coordinates x,y are the usual boundary layer coordinates, where x is measured in the direction parallel to the airfoil surface and y along the surface normal.

In order to solve these equations, different initial conditions and boundary conditions will be specified for each layer of the confluent boundary layer in subsequent sections of this document. The empirical input to these equations will also be given.

MAIN REGION I (BBCDA)

The equations used to predict confluent boundary layer characteristics of main region I are listed and discussed here. The method is coded in subroutine CONF7 of OVERLAY (4, 4). Three viscous layers comprise the confluent boundary layer of this region, the wall layer, the jet layer, and the wake layer (fig. 33). The governing equations of these layers are coupled and must be solved simultaneously, since the wall layer is not separated from the jet layer by a potential core. The velocity U_M at the outer edge of the wall layer is obtained as part of the solution.

The governing equations of the viscous layers of this region are the turbulent boundary layer equations (169) and (170). The equations of each layer are solved utilizing an integral method and the assumption of a self-similar velocity profile. Turbulence is modeled by empirical relations (refs. 2 and 22) for the following quantities.

- Growth functions for the widths of the jet layer and the wake layer
- Shear stress terms
- Velocity profiles and their integrals

WALL LAYER

The solution of the wall layer has to satisfy the following boundary conditions

$$\begin{aligned} y = 0 \quad & u = v = 0 \quad && \tau = \tau_w \\ y = \delta_5 \quad & u = U_M \quad && \tau = \tau(\delta_5) \end{aligned} \tag{171}$$

The subscript 5 is used for parameters of the wall layer in main region I. The growth of the momentum thickness θ_5 is governed by the momentum integral equation of the wall layer

$$\frac{d\theta_5}{dx} = \frac{2\theta_5}{H_5 - 1}\frac{1}{U_M}\frac{dU_M}{dx} - \frac{U_e}{U_M^2}\frac{dU_e}{dx}\theta_5 H_5 \frac{H_5 + 1}{H_5 - 1} + \frac{\tau_w - \tau(\delta_5)}{\rho U_M^2} \tag{172}$$

where the shape factor H_5 is defined by

$$H_5 = \frac{\delta_5^*}{\theta_5} \tag{173}$$

and the displacement thickness δ_5^* and momentum thickness are defined by

$$U_M \, \delta_5^* = \int_o^{\delta_5} \left(U_M - u \right) dy \tag{174}$$

$$U_M^2 \, \theta_5 = \int_o^{\delta_5} u \left(U_M - u \right) dy \tag{175}$$

The momentum integral equation (172) can be derived by integrating the x-momentum equation (170) across the width of the wall layer utilizing the continuity equation (169), the boundary conditions (171), and the assumption of a one parameter velocity profile

$$\frac{u}{U_M} = \left(\frac{y}{\delta_5} \right)^{\frac{1}{n}} \tag{176}$$

The empirical equation

$$\frac{\tau_W - \tau(\delta_5)}{\rho \, U_M^2} = 1.385 \, Y^{-45.79} \, e^{-0.918 H_5 + 17.21 \, Y - 0.743 \, Y^2} \tag{177}$$

with

$$Y = \ln \frac{U_M \, \theta_5}{\nu}$$

represents the difference of the wall shear stress τ_W and the shear stress at the outer edge of the wall layer $\tau(\delta_5)$ in equation (172).

The energy dissipation thickness δ_5^{**} is computed by means of

$$\frac{d \, \delta_5^{**}}{dx} = -3 \, \delta_5^{**} \frac{1}{U_M} \frac{d \, U_M}{dx} + 2 \, \delta_5^{**} \frac{1}{2 - \tilde{H}_5} \frac{1}{U_M} \frac{d \, U_M}{dx} \tag{178}$$

$$- 2 \, \delta_5^{**} \frac{1}{2 - \tilde{H}_5} \frac{U_e}{U_M^2} \frac{d \, U_e}{dx} + 2 \int_o^{\delta_5} \frac{\tau}{\rho \, U_M^2} \frac{\partial}{\partial y} \left(\frac{u}{U_M} \right) dy - 2 \frac{\tau(\delta_5)}{\rho \, U_M^2}$$

This equation is the energy integral equation of the wall layer. δ^{**}_5 is defined by

$$U_M^3 \, \delta_5^{**} = \int_o^{\delta_5} u \left(U_M^2 - u^2 \right) \tag{179}$$

and $\tilde{H}_5$ is the shape factor

$$\tilde{H}_5 = \frac{\delta_5^{**}}{\theta_5} \tag{180}$$

The energy integral equation (178) can be derived by first multiplying the x-momentum equation (170) by the velocity component u and then integrating it across the wall layer. The definitions of the wall layer parameters, δ_5, θ_5, H_5, δ_5^{**}, $\tilde{H}_5$, the boundary conditions (eq. (171)), the continuity equation (169), and the velocity profile (eq. (176)) are utilized during that derivation.

The shear stress integral in equation (178) is given by the empirical formula

$$\int_o^{\delta_5} \frac{\tau}{\rho U_M^2} \frac{\partial}{\partial y} \left(\frac{u}{U_M} \right) dy = 0.889 \quad 10^{23} \, Y^{-158.7} \, e^{-0.636 H_5 + 48.55 Y - 1.82 Y^2} \tag{181}$$

with

$$Y = \ell n \frac{U_M \theta_5}{\nu}$$

The shear stress $\tau(\delta_5)$ follows from

$$\frac{\tau(\delta_5)}{\rho U_M^2} = \frac{\tau_w}{\rho U_M^2} - \frac{\tau_w - \tau(\delta_5)}{\rho U_M^2} \tag{182}$$

in which the wall shear is obtained from

$$\frac{\tau_w}{\rho U_M^2} = 0.943 \quad 10^{16} \, Y^{-114.6} \, e^{-1.819 H_5 + 35.68 Y - 1.365 Y^2} \tag{183}$$

and the second term is given by equation (177).

Knowing the parameters δ^{**}_5 and θ_5 the shape factor $\tilde{H}_5$ can be calculated from its definition, but is restricted in the code to the range

$$1.63 \leqslant \tilde{H}_5 \leqslant 1.80 \tag{184}$$

The ordinary shape factor H_5 of the wall layer, in turn is calculated from the empirical equation

$$H_5 = 16.133 - \frac{56.91}{\tilde{H}_5} + \frac{54.54}{\tilde{H}_5^2} \tag{185}$$

Finally, the thickness δ_5 of the wall layer in main region I is calculated using

$$\delta_5 = 0.00434 + 9.492 \quad \theta_5 \tag{186}$$

The displacement thickness δ_5^* follows from the definition of H_5

$$\delta_5^* = H_5 \, \theta_5$$

Having solved all parameters of the confluent boundary layer in main region I the wall shear stress is calculated from the Ludwieg-Tillmann formula

$$\frac{\tau_w}{\rho \, U_M^2} = 0.123 \; 10^{-0.678 \, H_5} \left(Re_{\theta_5} \right)^{-0.268} \tag{187}$$

and not from equation (183).

The described formulation of the wall layer problem contains the velocity U_M at the outer edge of the wall layer for which no equation is given. The missing equation is provided by the formulation of the jet layer problem.

JET LAYER

The momentum integral equation of the jet layer (fig. 33) can be derived assuming a self-similar velocity profile $f(\eta)$, defined by

$$u = U_M - \left(U_M - U_w \right) f(\eta) \tag{188}$$

$$\eta = \frac{\delta_3 - y}{\delta_3 - \delta_5} \tag{189}$$

$$f(\eta) = 1.002 - 0.164 \, \eta - 1.967 \, \eta^2 + 1.338 \, \eta^3 - 0.209 \, \eta^4 \tag{190}$$

The pertinent boundary conditions of the jet layer are

$$\begin{array}{lllll} y = \delta_5 & \eta = 1 & u = U_M & f(\eta) = 0 & \tau = \tau(\delta_5) \\ y = \delta_3 & \eta = 0 & u = U_w & f(\eta) = 1 & \tau = \tau(\delta_3) \end{array} \tag{191}$$

Integrating the x-momentum equation (170) from $y = \delta_5$ to $y = \delta_3$ and using the formulation of the jet layer and wall layer problems yields the momentum integral equation of the jet layer. Defining nondimensional velocities by

$$\bar{U}_M = \frac{U_M}{U_e} \qquad \bar{U}_w = \frac{U_w}{U_e} \tag{192}$$

and the width of the jet layer by the symbol

$$b_j = \delta_3 - \delta_5 \tag{193}$$

the equation takes the following form

$$c_1 \frac{d\,\bar{U}_M}{dx} = c_2 \frac{d\,b_j}{dx} + c_3 \frac{d\,\bar{U}_w}{dx} + c_4 \frac{d\,U_e}{dx} + c_5 \tag{194}$$

where the coefficients are

$$c_1 = 2\,b_j\;\bar{U}_M\,S_{M4} - S_{M4}\,b_j\;\bar{U}_w - 2\,S_{M3}\,b_j\left(\bar{U}_M - \bar{U}_w\right)$$
$$+ 2\,S_{M5}\,b_j\left(\bar{U}_M - \bar{U}_w\right) + 2\,\theta_5\,H_5\frac{H_5 + 1}{(H_5 - 1)^2}\left(\bar{U}_M - \bar{U}_w\right)$$

$$c_2 = -\,S_{M4}\left(\bar{U}_M - \bar{U}_w\right)\bar{U}_M - S_{M5}\left(\bar{U}_M - \bar{U}_w\right)^2 + S_{M3}\left(\bar{U}_M - \bar{U}_w\right)^2$$

$$c_3 = S_{M4}\,b_j\,\bar{U}_M - S_{M3}\,b_j\left(\bar{U}_M - \bar{U}_w\right) + 2\,S_{M5}\,b_j\left(\bar{U}_M - \bar{U}_w\right) - \bar{U}_M\,b_j$$

$$c_4 = \frac{1}{U_e}\left[b_j - \frac{2\,H_5}{(H_5 - 1)^2}\left(2\,H_5^2 - 5\,H_5 + 1\right)\theta_5\left(\bar{U}_M - \bar{U}_w\right)\frac{1}{\bar{U}_M} - 2\,S_{M4}\,b_j\,\bar{U}_M\left(\bar{U}_M - \bar{U}_w\right)\right.$$
$$+ 2\,S_{M3}\,b_j\left(\bar{U}_M - \bar{U}_w\right)^2 - \bar{U}_M\,b_j\,\bar{U}_w - 2\,S_{M5}\,b_j\left(\bar{U}_M - \bar{U}_w\right)^2$$
$$\left. + S_{M3}\,b_j\,\bar{U}_w\left(\bar{U}_M - \bar{U}_w\right) - 2\left(\bar{U}_M - \bar{U}_w\right)\theta_5\frac{H_5^2 + H_5}{(H_5 - 1)^2}\;\bar{U}_M\right]$$

$$c_5 = 4\,\bar{U}_M\left(\bar{U}_M - \bar{U}_w\right)\frac{H_5^2}{(H_5 - 1)^2}\,\frac{\tau_w}{\rho\,U_M^2} + \bar{U}_M^2\left(\frac{\tau(\delta_3)}{\rho\,U_M^2} - \frac{\tau(\delta_5)}{\rho\,U_M^2}\right)$$
$$+ \bar{U}_M\left(\bar{U}_M - \bar{U}_w\right)\frac{5\,H_5 - 1}{H_5 - 1}\,\frac{\tau(\delta_5)}{\rho\,U_M^2}$$

$$- \bar{U}_M \left(\bar{U}_M - \bar{U}_w\right) \left(\frac{3\,H_5 - 1}{H_5 - 1}\right)^2 \int_o^{\delta_5} \frac{\tau}{\rho\, U_M^2} \frac{\partial}{\partial y} \left(\frac{u}{\bar{U}_M}\right) dy$$

with

$$S_{M3} = \int_o^1 f(\eta)\, d\eta = 0.5644 \tag{195}$$

$$S_{M4} = 1 - S_{M3} = 0.4356$$

$$S_{M5} = \int_o^1 f^2(\eta)\, d\eta = 0.4331$$

The shear stress terms contained in the coefficient c_5 are represented by the previously listed empirical equations of the wall layer problem. In addition, the assumption is made that the shear stress at the outer edge of the jet layer is

$$\tau(\delta_3) = 0.3\tau_w \tag{196}$$

The width of the jet layer is calculated from the empirical growth function

$$\frac{d\, b_j}{dx} = 0.17 \frac{U_M - U_w}{U_M + U_w} \tag{197}$$

The formulation of the jet layer problem in main region I is completed by defining the contributions of the jet layer to the displacement thickness and the momentum thickness of the confluent boundary layer.

$$\delta_j^* = b_j \left[1 - \bar{U}_M + S_{M3} \left(\bar{U}_M - \bar{U}_w\right)\right] \tag{198}$$

$$\theta_j = b_j \left[\bar{U}_M \left(1 - \bar{U}_M\right) + S_{M3}\, \bar{U}_M \left(\bar{U}_M - \bar{U}_w\right)\right.$$

$$\left. - S_{M3} \left(1 - \bar{U}_M\right) \left(\bar{U}_M - \bar{U}_w\right) - S_{M5} \left(\bar{U}_M - \bar{U}_w\right)^2\right] \tag{199}$$

WAKE LAYER

The coupling of the equations of the jet layer and the wake layer is accomplished by the velocity U_W at their common boundary. A momentum integral equation of the wake layer governing the development of U_W can be obtained by using the following definition of the self-similar velocity profile $g(\eta)$.

$$u = U_e - \left(U_e - U_w\right) g(\eta) \tag{200}$$

$$\eta = \frac{y - \delta_3}{y_{1/2} - \delta_3} \tag{201}$$

$$g(\eta) = 1.0194 - 0.450\,\eta - 0.2029\,\eta^2 + 0.1543\,\eta^3 - 0.024\,\eta^4 \tag{202}$$

The symbol $y_{1/2}$ denotes the half velocity point of the wake layer, i.e., the y-location where

$$\overline{u = \frac{1}{2}\left(U_w + U_e\right)}$$

The boundary conditions of the wake layer problem are

$$\begin{array}{lllll} y = \delta_3 & \eta = 0 & u = U_w & g(\eta) = 1 & \tau = \tau(\delta_3) \\ y = \delta_4 & \eta = K_2 & u = U_e & g(\eta) = 0 & \tau = 0 \end{array} \tag{203}$$

Integration of the momentum equation (170) and utilization of most of the hitherto introduced equations of main region I yields the desired momentum equation of the wake layer. Defining the width of that layer by

$$b_w = y_{1/2} - \delta_3 \tag{204}$$

the equation takes the form

$$d_1 \frac{d\,\bar{U}_w}{dx} = d_2 \frac{d\,b_w}{dx} + d_3 \frac{d\,b_j}{dx} + d_4 \frac{d\,\bar{U}_M}{dx} + d_5 \frac{d\,U_e}{dx} + d_6 \tag{205}$$

with

$$d_1 = S_{M1}\,b_w - 2\,b_w\,S_{M2}\left(1 - \bar{U}_w\right) - S_{M3}\left(1 - \bar{U}_w\right) b_j$$

$$d_2 = S_{M1}\left(1 - \bar{U}_w\right) - S_{M2}\left(1 - \bar{U}_w\right)^2$$

$$d_3 = \left(1 - \bar{U}_w\right)\bar{U}_M - S_{M3}\left(1 - \bar{U}_w\right)\left(\bar{U}_M - \bar{U}_w\right)$$

$$d_4 = 2\left(1 - \bar{U}_w\right)\theta_5\,H_5\,\frac{H_5 + 1}{\left(H_5 - 1\right)}\,2 - S_{M3}\left(1 - \bar{U}_w\right) b_j + b_j\left(1 - \bar{U}_w\right)$$

$$d_5 = \frac{1}{U_e}\Big[3\,S_{M1}\left(1 - \bar{U}_w\right) b_w - 2\,S_{M2}\left(1 - \bar{U}_w\right)^2 b_w + b_j\left(1 - \bar{U}_w\right)\bar{U}_M$$

$$- S_{M3}\left(1-\bar{U}_w\right) b_j \left(\bar{U}_M - \bar{U}_w\right) + 2\left(1-\bar{U}_w\right)\theta_5 H_5 \frac{H_5+1}{(H_5-1)^2}\bar{U}_M$$

$$+ 2\left(1-\bar{U}_w\right)\frac{1}{\bar{U}_M}\theta_5 H_5 \frac{2H_5^2 - 5H_5 + 1}{(H_5-1)^2}\Bigg]$$

$$d_6 = -4\bar{U}_M\left(1-\bar{U}_w\right)\frac{H_5^2}{(H_5-1)^2}\frac{\tau_w}{\rho U_M^2} - \bar{U}_M\left(1-\bar{U}_w\right)\frac{5H_5-1}{H_5-1}\frac{\tau(\delta_5)}{\rho U_M^2}$$

$$- \bar{U}_M^2\frac{\tau(\delta_3)}{\rho U_M^2} + \bar{U}_M\left(1-\bar{U}_w\right)\left(\frac{3H_5-1}{H_5-1}\right)^2 \int_o^{\delta_5} \frac{\tau}{\rho U_M^2}\frac{\partial}{\partial y}\left(\frac{u}{\bar{U}_M}\right) dy$$

and

$$S_{M1} = \int_o^{K_2} g(\eta)\, d\eta = 1.178 \qquad S_{M2} = \int_o^{K_2} g^2(\eta)\, d\eta = 0.786 \qquad (206)$$

The width of the wake layer is governed by the empirical growth function

$$\frac{d\, b_w}{dx} = .185\frac{U_e - U_w}{U_e + U_w} \qquad (207)$$

The contributions of the wake layer to the displacement thickness and momentum thickness of the confluent boundary layer are computed from

$$\delta_w^* = S_{M1}\, b_w\left(1-\bar{U}_w\right) \qquad (208)$$

$$\theta_w = b_w\left[S_{M1}\left(1-\bar{U}_w\right) - S_{M2}\left(1-\bar{U}_w\right)^2\right] \qquad (209)$$

The true width of the wake layer is

$$\delta_4 - \delta_3 = 2.5\, b_w \qquad (210)$$

which follows directly from the definition of K_2

$$K_2 = \frac{\delta_4 - \delta_3}{b_w} \qquad (211)$$

The symbol K_2 is used to indicate the value of η, see equation (201), at the outer edge of the wake layer δ_4.

INITIAL VALUES

The computer code contains two different sets of initial values of the variables in main region I. They are chosen depending on whether or not main region I is preceded by a core region.

- Main region I is preceded by a core region: The flow parameters at the end of the core region are saved as initial conditions for main region I. The variables δ^{**}_5 and H_5 are recomputed using

$$\delta_5^{**} = 1.73\,\theta_5 - 0.00005$$

$$\tilde{H}_5 = \frac{\delta_5^{**}}{\theta_5} \qquad 1.63 \leqslant \tilde{H}_5 \leqslant 1.80 \tag{212}$$

$$H_5 = 4.411 - \frac{23.9}{\tilde{H}_5} + \frac{33.11}{\tilde{H}_5^2}$$

In addition, the velocity U_W is obtained from

$$U_W = 0.8\,U_{wake}\,(x_e) \tag{213}$$

where $U_{wake}\,(x_e)$ denotes the potential flow wake centerline velocity at the end of the core, x_e.

- Main region I is entered directly: Some of the initial values are given by the flow conditions at the slot exit, others are simply assumed.

Wall layer parameters

$$\theta_5 = \theta_{s_2} \qquad \delta_5^{**} = 1.68\,\theta_5 \tag{214}$$
$$H_5 = 1.6 \qquad \delta_5 = 7\,\theta_5$$

The symbol θ_{s_2} is the momentum thickness of the wall layer at the slot exit.

Jet layer parameters

$$U_M = 1.01\,U_e \qquad b_j = \delta_{s_1} \tag{215}$$

δ_{s_1} is the boundary layer thickness at the lower surface trailing edge of the upstream airfoil.

Wake layer parameters

$$U_W = 0.8\,U_e \qquad b_W = 0.4\,\delta_F \tag{216}$$

δ_F is the boundary layer thickness at the upper surface trailing edge of the upstream airfoil.

The empirical equation (186) for the thickness of the wall layer is replaced by

$$\delta_5 = 0.00596 + 12.88\,\theta_5 + 15.97\,\theta_5^2 \tag{222}$$

JET LAYER

The wake layer has disappeared, so that

$$U_w = U_e \tag{223}$$

$$\tau(\delta_4) = \tau(\delta_3) = 0 \tag{224}$$

Hence,

$$\bar{U}_w = \frac{U_w}{U_e} = 1 \qquad\qquad \frac{d\,\bar{U}_w}{dx} = 0$$

and the momentum integral equation of the jet layer reduces to

$$c_1 \frac{d\,\bar{U}_M}{dx} = c_2 \frac{d\,b_j}{dx} + c_4 \frac{d\,U_e}{dx} + c_5 \tag{225}$$

with

$$c_1 = 2\,b_j\,\bar{U}_M\,S_{M4} - S_{M4}\,b_j\,\bar{U}_M - 2\,S_{M3}\,b_j\left(\bar{U}_M - 1\right) + 2\,S_{M5}\,b_j\left(\bar{U}_M - 1\right) + 2\,\theta_5\,H_5\,\frac{H_5 + 1}{(H_5 - 1)^2}\left(\bar{U}_M - 1\right)$$

$$c_2 = -\,S_{M4}\left(\bar{U}_M - 1\right)\bar{U}_M - S_{M5}\left(\bar{U}_M - 1\right)^2 + S_{M3}\left(\bar{U}_M - 1\right)^2$$

$$c_4 = \frac{1}{U_e}\left[b_j - \frac{2\,H_5}{(H_5 - 1)^2}\left(2\,H_5^2 - 5\,H_5 + 1\right)\theta_5\left(\bar{U}_M - 1\right)\frac{1}{\bar{U}_M} - 2\,S_{M4}\,b_j\,\bar{U}_M\left(\bar{U}_M - 1\right) + 2\,S_{M3}\,b_j\left(\bar{U}_M - 1\right)^2 - \bar{U}_M\,b_j - 2\,S_{M5}\,b_j\left(\bar{U}_M - 1\right)^2 + S_{M3}\,b_j\left(\bar{U}_M - 1\right) - 2\left(\bar{U}_M - 1\right)\theta_5\,\frac{H_5^2 + H_5}{(H_5 - 1)^2}\,\bar{U}_M\right]$$

$$c_5 = 4\,\bar{U}_M\left(\bar{U}_M - 1\right)\frac{H_5^2}{(H_5 - 1)^2}\,\frac{\tau_w}{\rho\,U_M^2} - \bar{U}_M^2\,\frac{\tau(\delta_5)}{\rho\,U_M^2}$$

DISPLACEMENT THICKNESS AND MOMENTUM THICKNESS

The displacement thickness δ^* of the confluent boundary layer in main region I is the sum of the contributions of the wall layer, the jet layer, and the wake layer to δ^*,

$$\delta^* = \delta_5^* + \delta_j^* + \delta_w^* \tag{217}$$

Similarly, the momentum thickness is calculated using

$$\theta = \theta_5 + \theta_j + \theta_w \tag{218}$$

MAIN REGION II (BBCDB)

The properties of the confluent boundary layer of this region are computed in OVERLAY (4,4), subroutine CONF8. The formulation of the problem of main region II is very similar to that of main region I. The differences are:

- The formulation does not contain equations for the wake layer, since the wake layer has disappeared at the end of main region I.
- Some empirical coefficients used in the wall layer and jet layer formulations are different.

In the remainder of this section, only those equations that are different from the equations of main region I are discussed.

WALL LAYER

The first coefficient of each of the empirical equations (177), (181), and (183) for the shear stress terms is different.

$$\frac{\tau_w - \tau(\delta_5)}{\rho U_M^2} = 1.234\, Y^{-45.79}\, e^{-0.918 H_5 + 17.21 Y - 0.743 Y^2} \tag{219}$$

$$\int_0^{\delta_5} \frac{\tau}{\rho U_M^2} \frac{\partial}{\partial y}\left(\frac{u}{U_M}\right) dy = 1.050 \times 10^{23}\, Y^{-158.7}\, e^{-0.636 H_5 + 48.55 Y - 18.2 Y^2} \tag{220}$$

$$\frac{\tau_w}{\rho U_M^2} = 0.982 \times 10^{16}\, Y^{-114.6}\, e^{-1.819 H_5 + 35.68 Y - 1.365 Y^2} \tag{221}$$

$$+ \bar{U}_M \left(\bar{U}_M - 1\right) \frac{5\,H_5 - 1}{H_5 - 1} \frac{\tau(\delta_5)}{\rho\, U_M^2}$$

$$- \bar{U}_M \left(\bar{U}_M - 1\right) \left(\frac{3\,H_5 - 1}{H_5 - 1}\right)^2 \int_o^{\delta_5} \frac{\tau}{\rho\, U_M^2} \frac{\partial}{\partial y} \left(\frac{u}{U_M}\right) dy$$

Further, the growth function for b_j has a slightly different empirical coefficient. It now reads

$$\frac{d\,b_j}{dx} = 0.185 \frac{U_M - U_e}{U_M + U_e} \tag{226}$$

INITIAL VALUES

Main region II is never entered directly. It is either preceded by main region I or by the core region. The parameters at the end of the upstream region are saved as initial conditions for main region II. In addition

$$\delta_5^{**} = 1.73\,\theta_5 - 0.00005 \tag{227}$$

$$\tilde{H}_5 = \frac{\delta_5^{**}}{\theta_5} \qquad 1.63 \leqslant \tilde{H}_5 \leqslant 1.80$$

$$H_5 = 16.133 - \frac{56.91}{\tilde{H}_5} + \frac{54.54}{\tilde{H}_5^2}$$

The last equation is different from equation (213) of main region I.

NUMERICAL INTEGRATION METHOD

The mathematical problem of the confluent boundary layer is formulated in terms of a set of n first-order ordinary differential equations and a number of algebraic equations. The differential equations can be written as

$$\frac{d\,y^j}{dx} = f^j\left(y^1, y^2, \ldots, y^n\right) \qquad j = 1, 2, \ldots n \tag{228}$$

for the n unknowns y^j. Initial values

$$y_o^j = y^j\left(x_o\right)$$

at the initial x-location x_o are assumed to be known.

The equations are integrated numerically using a modification of the Euler method. For this purpose, discrete points x_i (i=0,1,2...) are chosen that coincide with the computational surface points that are also used as segment corner points in the potential flow calculation. Assuming all variables are known at the point x_{i-1} the

variables y_i^j (j=1,2,...n) at the next point x_i are calculated using the following predictor-corrector type iteration procedure.

The predictor step reads

$$\left(y_i^j\right)^{(1)} = y_{i-1}^j + \Delta x\, f^j\left(y_{i-1}^1, y_{i-1}^2, \ldots y_{i-1}^n\right) \tag{229}$$

with

$$\Delta x = x_i - x_{i-1}$$

The corrector step is

$$\left(y_i^j\right)^{(k)} = y_{i-1}^j + \Delta x\, f^j\left(y_{mean}^1, y_{mean}^2, \ldots, y_{mean}^n\right) \tag{230}$$

where

$$y_{mean}^j = \frac{1}{2}\left[y_{i-1}^j + \left(y_i^j\right)^{(k-1)}\right]$$

Having computed (N-1)-values of $(y^j_i)^{(k)}$ (k=2,...n) and also $(y^j_i)^{(1)}$, the variables y^j_i are calculated by taking the average

$$y_i^j = \frac{1}{N}\left\{\sum_{k=2}^{N}\left(y_i^j\right)^{(k)} + \left(y_i^j\right)^{(1)}\right\} \tag{231}$$

The code uses N=6. The term dU_e/U_e is approximated by

$$\frac{d\,U_e}{U_e} = 2\,\frac{Ue_i - Ue_{i-1}}{Ue_i + Ue_{i-1}} \tag{232}$$

in the integration procedure.

MODIFIED CONFLUENT BOUNDARY LAYER METHOD

This section contains a description of a modification of the confluent boundary layer model, described previously, which was developed for the purpose of predicting separation of the confluent boundary layer. The major modification concerns the velocity profile of the wall layer. The power law profile of the wall layer is replaced by Coles' two parameter velocity profile, which is known, for ordinary turbulent boundary layers, to be a realistic representation near the point of separation. Most of the empirical content of Goradia's confluent boundary layer model is retained. The computer code is contained in OVERLAY (4,5), subroutines CONFI1, CONFI2, CONFD1, CONFD2, CONFP1, CONFP2.

COLES' VELOCITY PROFILE

To predict the point of separation of the confluent boundary layer, the power law velocity profile used for the wall layer is replaced by Coles' two-parameter velocity profile (ref. 8). With the wake function approximated by a cosine, it reads

$$u = \frac{u_\tau}{\kappa}\left\{\ln\frac{y\,u_\tau}{\nu} + C\right\} + \frac{u_\beta}{2}\left\{1 - \cos\frac{\pi\,y}{\delta_5}\right\} \tag{233}$$

where u_τ is the friction velocity, which is defined in terms of the wall shear τ_W and density ρ.

$$u_\tau = \sqrt{\frac{\tau_W}{\rho}} \tag{234}$$

u_β is an unknown parameter with the dimensions of velocity. The constants κ and C have the following values

$$\kappa = 0.41 \qquad C = 2.05 \tag{235}$$

Furthermore, in equation (233) the symbols ν and δ_5 denote the kinematic viscosity of air and the thickness of the wall layer, respectively.

Introducing the velocity profile of equation (233) to the definition of displacement thickness, δ_5^*, momentum thickness, θ_5, and energy dissipation thickness, δ^{**}_5, of the wall layer results in the following three equations.

$$U_M\,\delta_5^* = \left(\frac{u_\tau}{\kappa} + \frac{u_\beta}{2}\right)\delta_5 \tag{236}$$

$$U_M^2\,\theta_5 = \left[U_M\frac{u_\tau}{\kappa} + U_M\frac{u_\beta}{2} - K_1\frac{u_\tau}{\kappa}u_\beta - 2\left(\frac{u_\tau}{\kappa}\right)^2 - \frac{3}{8}u_\beta^2\right]\delta_5 \tag{237}$$

$$U_M^3\,\delta_5^{**} = \left[\frac{5}{16}u_\beta^3 - \frac{9}{8}U_M u_\beta^2 + U_M^2 u_\beta + 2U_M^2\frac{u_\tau}{\kappa} - 3K_1 U_M\frac{u_\tau}{\kappa}u_\beta - 6U_M\left(\frac{u_\tau}{\kappa}\right)^2 + 3K_2\frac{u_\tau}{\kappa}u_\beta^2 + 3K_3\left(\frac{u_\tau}{\kappa}\right)^2 u_\beta + 6\left(\frac{u_\tau}{\kappa}\right)^3\right]\delta_5 \tag{238}$$

where

$$K_1 = 1.589490$$
$$K_2 = 0.697958 \tag{239}$$
$$K_3 = 1.846111$$

MAIN REGION I

The confluent boundary layer method is formulated as a set of eight first order ordinary differential equations governing the following unknowns:

U_M	Velocity at the outer edge of the wall layer
θ_5	Momentum thickness of the wall layer
δ^{**}_5	Energy dissipation thickness of the wall layer
δ_5	Thickness of the wall layer
δ^*_5	Displacement thickness of the wall layer
U_W	Velocity at the outer edge of the jet layer
u_τ	Friction velocity
u_β	Parameter of Coles' velocity profile

The equations are the

- Momentum integral equation of the wall layer
- Energy integral equation of the wall layer
- Momentum integral equation of the jet layer
- Momentum integral equation of the wake layer
- Equation (236) differentiated with respect to x
- Equation (237) differentiated with respect to x
- Equation (238) differentiated with respect to x
- Differentiated skin friction law obtained from Coles velocity profile

The momentum and energy integral equations are very similar to the ones described previously. However, they are given below in their most general form, i.e., they have not been specialized to any particular velocity profile chosen for the wall layer. Furthermore, most of the empirical content of the confluent boundary layer method of Goradia is still contained in those equations.

The set of eight ordinary differential equations can be written as

$$[A]\left\{\frac{d\phi}{dx}\right\} = \{B\} \tag{240}$$

with

$$\phi = (U_M, \theta_5, \delta_5^{**}, \delta_5, \delta_5^{*}, U_w, u_\tau, u_\beta).$$

Details of the equations are given below in terms of the coefficients of the matrices [A] and {B}.

The momentum integral equation of the wall layer reads

$$A_{11}\frac{d\,U_M}{dx} + A_{12}\frac{d\,\theta}{dx} = B_1 \tag{241}$$

where

$$A_{11} = \frac{2\,\theta_5 - \delta_5 + \delta_5^{*}}{U_M} \qquad A_{12} = 1$$

$$B_1 = -U_e\frac{d\,U_e}{dx}\frac{\delta_5}{U_M^2} + \frac{\tau_w - \tau(\delta_5)}{\rho\,U_M^2}$$

The shear stress term is represented by the empirical equation

$$\frac{\tau_w - \tau(\delta_5)}{\rho\,U_M^2} = 1.385\,Y\,e^{-45.79 - 0.918\,H_5 + 17.21\,Y - 0.743\,Y^2} \tag{242}$$

with

$$Y = \ln\frac{U_M\,\theta_5}{\nu}$$

and the shape factor

$$H_5 = \frac{\delta_5^{*}}{\theta_5}$$

The energy integral equation of the wall layer is

$$A_{21}\frac{d\,U_M}{dx} + A_{23}\frac{d\,\delta_5^{**}}{dx} = B_2 \tag{243}$$

where

$$A_{21} = \frac{3\,\delta_5^{**} - 2\,\delta_5 + 2\,\delta_5^{*}}{U_M} \qquad\qquad A_{23} = 1$$

$$B_2 = -2\,U_e \frac{d\,U_e}{dx} \frac{\delta_5 - \delta_5^{*}}{U_M^2} - 2\frac{\tau(\delta_5)}{\rho\,U_M^2} + 2\int_o^{\delta_5} \frac{\tau}{\rho\,U_M^2} \frac{\partial}{\partial y}\left(\frac{u}{U_M}\right) dy$$

The shear stress integral is given by the empirical equation

$$\int_o^{\delta_5} \frac{\tau}{\rho\,U_M^2} \frac{\partial}{\partial y}\left(\frac{u}{U_M}\right) dy = 0.889\;\; 10^{23}\; Y^{-158.7}\; e^{-0.636\,H_5 + 48.55\,Y - 1.82\,Y^2} \tag{244}$$

Further, the value of the shear stress at the outer edge of the wall layer follows from

$$\frac{\tau(\delta_5)}{\rho\,U_M^2} = \frac{\tau_w}{\rho\,U_M^2} - \frac{\tau_w - \tau(\delta_5)}{\rho\,U_M^2} \tag{245}$$

in which the wall shear is obtained from

$$\frac{\tau_w}{\rho\,U_M^2} = 0.943\;\; 10^{16}\; Y^{-114.6}\; e^{-1.819\,H_5 + 35.68\,Y - 1.365\,Y^2} \tag{246}$$

and the second term on the right hand side of equation (245) is given by equation (242).

The momentum integral equation of the jet layer reads

$$A_{31}\frac{d\,U_M}{dx} + A_{34}\frac{d\,\delta_5}{dx} + A_{35}\frac{d\,\delta_5^{*}}{dx} + A_{36}\frac{d\,U_w}{dx} = B_3 \tag{247}$$

The coefficients are

$$A_{31} = b_j\left[2\,U_M - U_w - 4\,U_M\,S_{M3} + 3\,U_w\,S_{M3} + 2\left(U_M - U_w\right)S_{M5}\right] + \left(U_M - U_w\right)\left(\delta_5 - \delta_5^{*}\right)$$

$$A_{34} = U_M\left(U_M - U_w\right)$$

$$A_{35} = -U_M\left(U_M - U_w\right)$$

$$A_{36} = b_j \left[2\, U_M\, S_{M3} - U_w\, S_{M3} - 2 \left(U_M - U_w \right) S_{M5} \right]$$

$$B_3 = U_e \frac{d\, U_e}{dx}\, b_j + U_M^2 \frac{\tau(\delta_3)}{\rho\, U_M^2} - U_M^2 \frac{\tau(\delta_5)}{\rho\, U_M^2}$$

$$- \left(U_M - U_w \right) \left[U_M - 2\, U_M\, S_{M3} + U_w\, S_{M3} + \left(U_M - U_w \right) S_{M5} \right] \frac{d\, b_j}{dx}$$

with

$$S_{M3} = 0.5644 \qquad S_{M5} = 0.4331$$

The shear stress at the outer edge of the jet layer, $\tau(\delta_3)$, is obtained from the assumption

$$\tau(\delta_3) = 0.3\, \tau_w \tag{248}$$

and equation (246) for the wall shear.

The shear stress at the outer edge of the wall layer, $\tau(\delta_5)$, is given by equation (245) in conjunction with equations (246) and (242).

The growth of the jet layer is calculated from the empirical function

$$\frac{d\, b_j}{dx} = 0.17\, \frac{U_M - U_w}{U_M + U_w} \tag{249}$$

The momentum integral equation of the wake layer reads

$$A_{41} \frac{d\, U_M}{dx} + A_{44} \frac{d\, \delta_5}{dx} + A_{45} \frac{d\, \delta_5^*}{dx} + A_{46} \frac{d\, U_w}{dx} = B_4 \tag{250}$$

with

$$A_{41} = \left(U_w - U_e \right) \left(b_j - b_j\, S_{M3} + \delta_5 - \delta_5^* \right)$$

$$A_{44} = U_M \left(U_w - U_e \right)$$

$$A_{45} = - U_M \left(U_w - U_e \right)$$

$$A_{46} = b_w U_e S_{M1} + 2 b_w \left(U_w - U_e\right) S_{M2} + b_j \left(U_w - U_e\right) S_{M3}$$

$$B_4 = \left[U_e S_{M1} - 2 \left(U_w - U_e\right) S_{M1} + 2 \left(U_w - U_e\right) S_{M2}\right] b_w \frac{d U_e}{dx}$$

$$- U_M^2 \frac{\tau(\delta_3)}{\rho U_M^2} + \left(U_w - U_e\right)\left[\left(U_M - U_w\right) S_{M3} - U_M\right] \frac{d bj}{dx}$$

$$- \left(U_w - U_e\right)\left[U_e S_{M1} + \left(U_w - U_e\right) S_{M2}\right] \frac{d b_w}{dx}$$

$S_{M1} = 1.178 \qquad S_{M2} = 0.786$

The growth of the wake layer follows from

$$\frac{d b_w}{dx} = 0.185 \frac{U_e - U_w}{U_e + U_w} \tag{251}$$

The following three equations are obtained by differentiating equations (236), (237), and (239) with respect to the downstream coordinate x.

$$A_{51} \frac{d U_M}{dx} + A_{54} \frac{d \delta_5}{dx} + A_{55} \frac{d \delta_5^*}{dx} + A_{57} \frac{d u_\tau}{dx} + A_{58} \frac{d u_\beta}{dx} = 0 \tag{252}$$

where

$$A_{51} = \delta_5^* \qquad A_{54} = -\left(\frac{u_\tau}{\kappa} + \frac{u_\beta}{2}\right) \qquad A_{55} = U_M \qquad A_{57} = -\frac{\delta_5}{\kappa} \qquad A_{58} = -\frac{\delta_5}{2} \tag{253}$$

$$A_{61} \frac{d U_M}{dx} + A_{62} \frac{d \theta_5}{dx} + A_{64} \frac{d \delta_5}{dx} + A_{67} \frac{d u_\tau}{dx} + A_{68} \frac{d u_\beta}{dx} = 0$$

with

$$A_{61} = 2 U_M \theta_5 - \delta_5 \left(\frac{u_\tau}{\kappa} + \frac{u_\beta}{2}\right) \qquad A_{62} = U_M^2$$

$$A_{64} = - U_M^2 \frac{\theta_5}{\delta_5} \qquad A_{67} = -\frac{\delta_5}{\kappa}\left(U_M - K_1 u_\beta - 4 \frac{u_\tau}{\kappa}\right)$$

$$A_{68} = - \delta_5 \left(\frac{U_M}{2} - K_1 \frac{u_\tau}{\kappa} - \frac{3}{4} u_\beta\right)$$

$$A_{71}\frac{d\,U_M}{dx} + A_{73}\frac{d\,\delta_5^{**}}{dx} + A_{74}\frac{d\,\delta_5}{dx} + A_{77}\frac{d\,u_\tau}{dx} + A_{78}\frac{d\,u_\beta}{dx} = 0 \qquad (254)$$

with

$$A_{71} = 3\,U_M^2\,\delta_5^{**} + \frac{9}{8}\delta_5\,u_\beta^2 - 2\,\delta_5\,U_M\,u_\beta - 4\,\delta_5\,U_M\,\frac{u_\tau}{\kappa}$$

$$+ 3\,\delta_5\,K_1\,\frac{u_\tau}{\kappa}\,u_\beta + 6\,\delta_5\left(\frac{u_\tau}{\kappa}\right)^2$$

$$A_{73} = U_M^3 \qquad A_{74} = -\,U_M^3\,\frac{\delta_5^{**}}{\delta_5}$$

$$A_{77} = -\,\frac{\delta_5}{\kappa}\left(2\,U_M^2 - 3\,K_1\,U_M\,u_\beta - 12\,U_M\,\frac{u_\tau}{\kappa} + 3\,K_2\,u_\beta^2\right.$$

$$\left. + 6\,K_3\,\frac{u_\tau}{\kappa}\,u_\beta + 18\,\frac{u_\tau^2}{\kappa^2}\right)$$

$$A_{78} = -\,\delta_5\left(\frac{15}{16}\,u_\beta^2 - \frac{9}{4}\,U_M\,u_\beta + U_M^2 - 3\,K_1\,U_M\,\frac{u_\tau}{\kappa}\right.$$

$$\left. + 6\,K_2\,\frac{u_\tau}{\kappa}\,u_\beta + 3\,K_3\,\frac{u_\tau^2}{\kappa^2}\right)$$

The skin friction law is obtained from equation (233) by setting $u=U_M$ at $y=\delta_5$.

$$U_M = \frac{u_\tau}{\kappa}\left(\ln\frac{\delta_5\,u_\tau}{\nu} + C\right) + u_\beta \qquad (255)$$

Differentiation with respect to x yields the last desired equation.

$$A_{81}\frac{d\,U_M}{dx} + A_{84}\frac{d\,\delta_5}{dx} + A_{87}\frac{d\,u_\tau}{dx} + A_{88}\frac{d\,u_\beta}{dx} = 0 \qquad (256)$$

where

$$A_{81} = 1 \qquad A_{84} = -\,\frac{u_\tau}{\kappa\,\delta_5} \qquad A_{87} = -\left(\frac{U_M - u_\beta}{u_\tau} + \frac{1}{\kappa}\right) \qquad A_{88} = -\,1$$

The reader should note, that the particular order in which equations and unknowns are arranged seems to be most efficient for the numerical solution of the set of ordinary differential equations (240). The chosen arrangement yields a coefficient matrix [A] which approximates a triangular matrix as closely as possible.

MAIN REGION II

The wake layer does not exist in this region. Hence,

$$U_w = U_e \qquad \tau\left(\delta_3\right) = 0 \tag{257}$$

The number of unknowns reduces to seven, which are

$$\bar{\phi} = \left(U_M, \theta_5, \delta_5^{**}, \delta_5, \delta_5^{*}, u_\tau, u_\beta\right)$$

The governing equations of main region II are derived from those of main region I by eliminating the momentum integral equation of the wake layer and rewriting the momentum integral equation of the jet layer using equation (257). All other equations remain the same. In particular, the empirical coefficients in the shear-stress terms and the growth function for the jet-layer thickness are not changed. Writing the set of ordinary differential equations as

$$[\bar{A}]\left\{\frac{d\bar{\phi}}{dx}\right\} = \left\{\bar{B}\right\} \tag{258}$$

the coefficients of the matrices $[\bar{A}]$ and $\{\bar{B}\}$ are obtained from their counterparts in main region I as follows.

$$\bar{A}_{11} = A_{11} \qquad \bar{A}_{12} = A_{12} \qquad \bar{B}_1 = B_1$$

$$\bar{A}_{21} = A_{21} \qquad \bar{A}_{23} = A_{23} \qquad \bar{B}_2 = B_2$$

The coefficients of the momentum integral equation of the jet layer are

$$\bar{A}_{31} = b_j\left[2\,U_M - U_e - 4\,U_M\,S_{M3} + 3\,U_e\,S_{M3} + 2\left(U_M - U_e\right)S_{M5}\right] + \left(U_M - U_e\right)\left(\delta_5 - \delta_5^{*}\right)$$

$$\bar{A}_{34} = U_M\left(U_M - U_e\right)$$

$$\bar{A}_{35} = -U_M\left(U_M - U_e\right)$$

$$\bar{A}_{36} = 0$$

$$\bar{B}_3 = b_j\left[U_e - 2\,U_M\,S_{M3} + U_e\,S_{M3} + 2\left(U_M - U_e\right)S_{M5}\right]\frac{dU_e}{dx} - U_M^2\,\frac{\tau\left(\delta_5\right)}{\rho\,U_M^2} - \left(U_M - U_e\right)\left[U_M - 2\,U_M\,S_{M3} + U_e\,S_{M3} + \left(U_M - U_e\right)S_{M5}\right]\frac{db_j}{dx}$$

with

$$\frac{d\,b_j}{dx} = 0.17\,\frac{U_M - U_e}{U_M + U_e}$$

The coefficients of the remaining equations are

$$\overline{A}_{41} = A_{51} \qquad \overline{A}_{44} = A_{54} \qquad \overline{A}_{45} = A_{55}$$

$$\overline{A}_{46} = A_{57} \qquad \overline{A}_{47} = A_{58}$$

$$\overline{A}_{51} = A_{61} \qquad \overline{A}_{52} = A_{62} \qquad \overline{A}_{54} = A_{64}$$

$$\overline{A}_{56} = A_{67} \qquad \overline{A}_{57} = A_{68}$$

$$\overline{A}_{61} = A_{71} \qquad \overline{A}_{63} = A_{73} \qquad \overline{A}_{64} = A_{74}$$

$$\overline{A}_{66} = A_{77} \qquad \overline{A}_{67} = A_{78}$$

$$\overline{A}_{71} = A_{81} \qquad \overline{A}_{74} = A_{84}$$

$$\overline{A}_{76} = A_{87} \qquad \overline{A}_{77} = A_{88}$$

All other coefficients are zero.

INITIAL VALUES

It is assumed that main region II is always preceded by main region I. Therefore, only initial values for the latter region need be specified. The initial values for the main region II calculation are simply the values of the variables at the end of main region I.

In specifying initial values for main region I, two cases are distinguished depending on whether or not a potential core exists at the slot exit. A potential core exists at the slot exit if

$$\delta_{BL}(x_o) + \delta_{S1} < h_{slot}$$

The symbols have the meaning,

$\delta_{BL}(x_o)$	Thickness of the boundary layer on the upper surface of the downstream airfoil at the slot exit
δ_{s1}	Boundary layer thickness at the lower surface trailing edge of the upstream airfoil
h_{slot}	Slot height at the slot exit

Case a

$$\delta_{BL}(x_o) + \delta_{S1} < h_{slot}$$

Main region I is preceded by a core region. Denoting the location of the end of the core by x_e the initial values read

$$U_M = V_c(x_e) \qquad \theta_5 = \theta_{BL}(x_e) \qquad \delta_5^{**} = 1.73\,\theta_{BL}(x_e)$$

$$\delta_5 = \delta_{BL}(x_e) \qquad \delta_5^{*} = \delta_{BL}^{*}(x_e) \qquad U_w = 0.8\,U_{wake}(x_e) \tag{259}$$

$$u_\tau = U_M\sqrt{\frac{\tau_w}{\rho\,U_M^2}} \qquad u_\beta = U_M - \frac{u_\tau}{\kappa}\left(\ell n\,\frac{\delta_5\,u_\tau}{\nu} + C\right)$$

$$\frac{\tau_w}{\rho\,U_M^2} = 0.123\;10^{-0.678\,H_5}\left(Re_{\theta_5}\right)^{-0.268}$$

$$H_5 = \frac{\delta_5^*}{\theta_5}$$

$$Re_{\theta_5} = \frac{U_M\,\theta_5}{\nu}$$

Note that $V_c(x_e)$ is the compressible surface velocity of the downstream airfoil at the slot exit. U_{wake} is the compressible wake centerline velocity.

In addition, initial values for the thicknesses of the jet layer and wake layer are needed.

$$b_j = (\delta_1)_{wake} \qquad b_w = \frac{(\delta_u)_{wake}}{K_2} \tag{260}$$

with

$$K_2 = 2.5$$

The symbol $(\delta_u)_{wake}$ denotes the distance between the wake centerline and the upper edge of the wake; $(\delta_l)_{wake}$ denotes the corresponding value of the lower part of the wake.

Case b

$$\delta_{BL}(x_o) + \delta_{S1} \geq h_{slot}$$

A potential core does not exist. The computation enters main region I directly at the slot exit. The initial values at the slot exit x_o are

$$U_M = V_c(x_o) \qquad \theta_5 = \theta_{BL}(x_o) = \theta_{S2} \qquad \delta_5^{**} = 1.68\,\theta_5$$
$$\delta_5 = \delta_{BL}(x_o) = \delta_{S2} \qquad \delta_5^{*} = \delta_{BL}^{*}(x_o) \qquad U_w = 0.8\,V_c(x_o) \tag{261}$$

$$u_\tau = U_M\sqrt{\frac{\tau_w}{\rho\,U_M^2}} \qquad u_\beta = U_M - \frac{u_\tau}{\kappa}\left(\ell n\,\frac{\delta_5\,u_\tau}{\nu} + C\right)$$

$$\frac{\tau_w}{\rho\,U_M^2} = 0.123\;10^{-0.678\,H_5}\left(Re_{\theta_5}\right)^{-0.268}$$

$$H_5 = \frac{\delta_5^*}{\theta_5} \qquad Re_{\theta_5} = \frac{U_M\,\theta_5}{\nu}$$

The thicknesses of jet layer and wake layer are initially

$$b_j = \delta_{S1} \qquad b_w = \frac{\delta_F}{K_2} = 0.4\;\delta_F \tag{262}$$

where δ_{S1} and δ_F denote the boundary layer thicknesses at the lower- and upper-surface trailing edge of the upstream airfoil, respectively.

CONFLUENT BOUNDARY LAYER THICKNESS

The thickness δ_4 of the confluent boundary layer is obtained from

$$\delta_4 = \delta_5 + b_j + K_2\;b_w \qquad K_2 = 2.5 \tag{263}$$

where b_j and b_W are calculated from the empirical growth functions

$$\frac{d\,b_j}{dx} = 0.17\,\frac{U_M - U_w}{U_M + U_w} \tag{264}$$

$$\frac{d\,b_w}{dx} = 0.185\,\frac{U_e - U_w}{U_e + U_w} \tag{265}$$

and the initial values of equations (260) and (262). By definition, the wake thickness $b_W \equiv 0$ in main region II.

Displacement thickness and momentum thickness of the confluent boundary layer are calculated using

$$\begin{aligned} \delta^* &= \delta_5^* + \delta_j^* + \delta_w^* \\ \theta &= \theta_5 + \theta_j + \theta_w \end{aligned} \tag{266}$$

with

$$\delta_j^* = b_j \left[1 - \frac{U_M}{U_e} + \left(\frac{U_M}{U_e} - \frac{U_w}{U_e} \right) S_{M3} \right]$$

$$\theta_j = b_j \left[\frac{U_M}{U_e} \left(1 - \frac{U_M}{U_e} \right) - \left(1 - \frac{U_M}{U_e} \right) \left(\frac{U_M}{U_e} - \frac{U_w}{U_e} \right) S_{M3} + \frac{U_M}{U_e} \left(\frac{U_M}{U_e} - \frac{U_w}{U_e} \right) S_{M3} - \left(\frac{U_M}{U_e} - \frac{U_w}{U_e} \right)^2 S_{M5} \right]$$

$$\delta_w^* = b_w \left(1 - \frac{U_w}{U_e} \right) S_{M1}$$

$$\theta_w = b_w \left[\left(1 - \frac{U_w}{U_e} \right) S_{M1} - \left(1 - \frac{U_w}{U_e} \right)^2 S_{M2} \right]$$

and the constants

$$\begin{aligned} S_{M1} &= 1.178 \\ S_{M2} &= 0.786 \\ S_{M3} &= 0.5644 \\ S_{M5} &= 0.4331 \end{aligned}$$

SKIN FRICTION AND SEPARATION

Two definitions of the skin friction coefficient c_f are used

$$c_f = \frac{\tau_w}{\frac{\rho}{2} V_c^2} \tag{267}$$

$$\bar{c}_f = \frac{\tau_w}{\frac{\rho}{2} U_\infty^2} \tag{268}$$

The wall shear τ_w is computed from the friction velocity u_τ

$$\frac{\tau_w}{\rho} = u_\tau^2$$

Hence

$$c_f = \frac{2\,u_\tau^2}{V_c^2} \tag{269}$$

which is only printed, and

$$\bar{c}_f = 2\,u_\tau^2 \qquad \left(U_\infty = 1\right) \tag{270}$$

which is that skin friction coefficient used in the aerodynamic load computation.

Separation of the confluent boundary layer is assumed to take place if

$$c_f \leqslant 0.001 \tag{271}$$

is predicted.

SYMBOLS OF THE CONFLUENT BOUNDARY LAYER

The following list of symbols does not include the coding symbols of the modified method of Goradia.

Theory	Code	Definition
b_j	BJAVE	Thickness of the jet layer
b_W	BWAVE	Thickness of the wake layer
c_f	CFIP	Skin friction coefficient
c_P	CP	Pressure coefficient
$f(\eta)$		Jet layer velocity profile
$g(\eta)$		Wake layer velocity profile
H_5	HAVE	Wall layer shape factor, δ^*_5/θ_5
$\tilde{H}_5$	HVFAVE	Wall layer shape factor, δ^{**}_5/θ_5
h_{slot}	XH	Slot height at slot exit
n		Exponent of wall layer velocity profile
Re_{θ_5}	REAVE	Wall layer Reynolds number based on momentum thickness
S_{M1}	SM1	Integral, defined by equation (206)
S_{M2}	SM2	Integral, defined by equation (206)
S_{M3}	SM3	Integral, defined by equation (195)
S_{M4}	SM4	$1-S_{M3}$
S_{M5}	SM5	Integral, defined by equation (195)
t_{TE}	TETH	Trailing edge thickness of airfoil
u,v		Components of velocity in directions parallel and normal to the surface of the airfoil
U_e	UE	Velocity at the outer edge of the confluent boundary layer

Theory	Code	Definition
$\overline{U}_M$	UMAVE	Velocity at the outer edge of the wall layer, nondimensionalized by U_e
U_M		Velocity at the outer edge of the wall layer
$\overline{U}_W$	UWIAVE	Velocity at the outer edge of the jet layer, nondimensionalized by U_e
U_W		Velocity at the outer edge of the jet layer
x,y		Boundary layer coordinates, **x** parallel to the surface, y normal to it
x_0	XINI	**x**-location of the slot exit
$y_{1/2}$	Y2CAVE	Half-velocity point of the wake layer, where $u = 1/2 (U_W + U_e)$
δ_5	DLAVE	Wall layer thickness
δ_3	D3AVE	Outer edge of the jet layer
δ_4	D4AVE, D2AVE	Outer edge of the confluent boundary layer
δ_F	DELE	Boundary layer thickness at the upper-surface trailing edge of the upstream airfoil component
δ_{s1}	DELI	Boundary layer thickness at the lower-surface trailing edge of the upstream airfoil component
δ_{s2}	DELI2	Thickness of the boundary layer at the slot exit
δ^*	DLSTAV	Displacement thickness of the confluent boundary layer
δ^*_5	DSTRWL	Displacement thickness of the wall layer
δ^*_j	DSTAVE, DSTRJT	Displacement thickness of the jet layer
δ^*_W	DSTWAVE, DSTRWK	Displacement thickness of the wake layer
δ^{**}_5	D2SAVE	Energy dissipation thickness of the wall layer

Theory	Code	Definition
η		Nondimensional coordinate, defined by equations (189) and (201)
θ_5	THAVE	Wall layer momentum thickness
θ_{s2}	THETA2	Boundary layer momentum thickness at the slot exit
τ		Shear stress
$\tau_w/\rho U_M^2$	CF2BUM	Nondimensional wall shear stress
$\tau(\delta_3)/\rho U_M^2$	RTD3TW	Ratio of the shear stress at the outer edge of the jet layer and the wall shear stress
$\tau(\delta_5)/\rho U_M^2$	RTD5TW	Ratio of the shear stress at the outer edge of the wall layer and the wall shear stress
$(\tau_w-\tau(\delta_5))/\rho U_M^2$	TWMIT5	Difference between the wall shear stress and the shear stress at the outer edge of the wall layer
$\int_0^{\delta_5} \frac{\tau}{\rho U_M^2} \frac{\partial}{\partial y}\left(\frac{u}{U_M}\right) dy$	SHRINT	Wall layer shear integral, equation (181)

Subscripts

5	Wall layer parameters in main regions I and II
e	Outer edge of the confluent boundary layer
j	Jet layer
w	Wake layer

GLOBAL AERODYNAMIC PARAMETERS (BBD)

This section contains a description of the calculation of the aerodynamic forces and moments acting on multielement airfoils.

AERODYNAMIC COEFFICIENTS

LIFT AND MOMENT COEFFICIENTS

The lift coefficient c_ℓ of a multielement airfoil is calculated by integrating the pressure and friction forces. The calculations are performed in the global axis system. The forces and the moment acting on a multielement airfoil are

A	Component of the force in direction of the global X-axis, termed axial force
N	Component of the force in direction of the global Z-axis, termed normal force
$M_{0,0}$	Pitching moment about the origin of the global axis system, positive nose up.

Corresponding force and moment coefficients are defined by

$$c_a = \frac{A}{q_\infty c_{ref}} \qquad c_n = \frac{N}{q_\infty c_{ref}} \qquad c_{m_{o,o}} = \frac{M_{o,o}}{q_\infty c_{ref}^2} \tag{272}$$

where

$$q_\infty = \frac{1}{2} \rho_\infty U_\infty^2$$

is the dynamic pressure of the uniform freestream, and c_{ref} denotes the reference chord length of the multielement airfoil.

Both, the surface pressure p_s and the wall shear stress τ_W contribute to these forces and moment coefficients. Their contributions are calculated by discretizing the airfoil geometry in exactly the same way as in the Potential Flow calculation, i.e., by replacing the actual airfoil surface by a polygon. The corner points of the polygon (figure 36) are positioned on the airfoil surface and are identical with the so-called computational surface points defined in the geometry section. Writing these corner points in terms of the global airfoil coordinates (X_i,Z_i) the contributions of the surface pressure to c_a, c_n, and $c_{m_{0,0}}$ read

$$c_{a_P} = \frac{1}{c_{ref}} \sum_{m=1}^{N_c} \sum_{i=2}^{N_m} c_{P_c} \left(Z_i - Z_{i-1}\right) \tag{273}$$

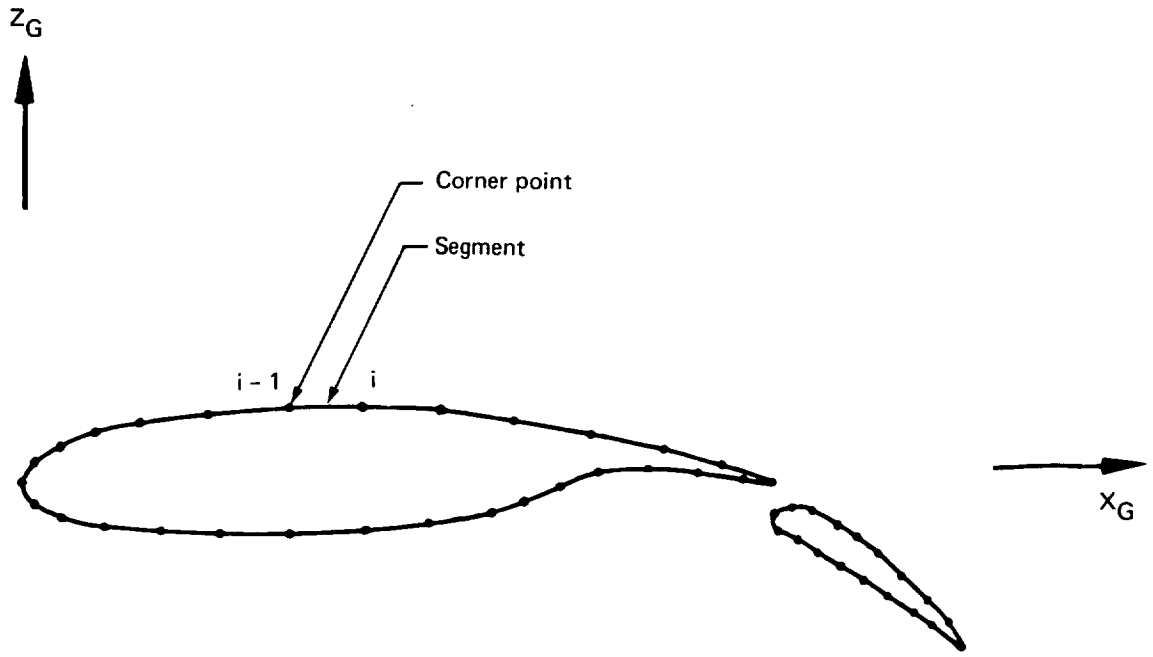

Figure 36. – Discretization of the Geometry

$$c_{n_P} = -\frac{1}{c_{ref}} \sum_{m=1}^{N_c} \sum_{i=2}^{N_m} c_{P_c} \left(X_i - X_{i-1}\right) \tag{274}$$

$$\left(c_{m_{O,O}}\right)_P = \frac{1}{\frac{2}{c_{ref}}} \sum_{m=1}^{N_c} \sum_{i=2}^{N_m} c_{Pc} \left[X_c \left(X_i - X_{i-1}\right) + Z_c \left(Z_i - Z_{i-1}\right)\right] \tag{275}$$

with c_{p_c} denoting the value of the surface pressure coefficient

$$c_P = \frac{p_s - p_\infty}{q_\infty} \tag{276}$$

at the midpoint of the i-th airfoil segment (X_c,Z_c). The coordinates of this point are given by

$$X_c = \frac{1}{2}\left(X_i + X_{i-1}\right) \qquad Z_c = \frac{1}{2}\left(Z_i + Z_{i-1}\right) \tag{277}$$

The symbols N_c and N_m are the total number of airfoil components and the number of surface points of the m-th airfoil component, respectively.

The contribution of the wall shear to c_a,c_n, and $c_{m_{0,0}}$ is

$$c_{a_F} = \frac{1}{c_{ref}} \sum_{m=1}^{N_c} \sum_{i=2}^{N_m} c_{f_c} \left(X_i - X_{i-1}\right) \tag{278}$$

$$c_{p_F} = \frac{1}{c_{ref}} \sum_{m=1}^{N_c} \sum_{i=2}^{N_m} c_{f_c} \left(Z_i - Z_{i-1}\right) \tag{279}$$

$$\left(c_{m_{o,o}}\right)_F = \frac{1}{2 c_{ref}} \sum_{m=1}^{N_c} \sum_{i=2}^{N_m} c_{f_c} \left[Z_c \left(X_i - X_{i-1}\right) - X_c \left(Z_i - Z_{i-1}\right)\right] \tag{280}$$

In these equations c_{f_c} is the value of the skin friction coefficient

$$c_f = \frac{\tau_w}{q_\infty} \tag{281}$$

at the midpoint of the i-th segment. Note, that for the purpose of computing the lift coefficient, the sign of c_f is reversed on the lower surface of each airfoil component.

$$c_{f_c} = -c_{f_c} \qquad \left(i \leqslant I_{stag}\right) \tag{282}$$

I_{stag} is the index of the stagnation point of the m-th component.

Axial-force, normal-force and pitching-moment coefficients are obtained from

$$c_a = c_{a_P} + c_{a_F} \qquad c_n = c_{n_P} + c_{n_F} \qquad c_{m_{o,o}} = \left(c_{m_{o,o}}\right)_P + \left(c_{m_{o,o}}\right)_F \tag{283}$$

The lift coefficient c_ℓ follows from

$$c_\ell = c_n \cos\alpha - c_a \sin\alpha \tag{284}$$

where α is the angle of attack.

DRAG COEFFICIENT

The drag coefficient of the airfoil is calculated using the Squire and Young formula (ref. 9). The drag coefficient c_{d_s} of each surface of each of the N_c airfoil components is obtained from

$$c_{d_s} = 2 \frac{\theta}{c_{ref}} \left(\frac{V_c}{U_\infty} \right)^{\frac{1}{2}(H + 5)} \tag{285}$$

where the boundary layer momentum thickness θ, the shape factor H, and the compressible potential flow velocity V_c are given by their values at the trailing edge point. In the case of a confluent boundary layer the chosen momentum thickness is that of the wall layer only, since θ of the outer wake portion of the confluent boundary layer is already represented by the upstream airfoil. The total profile drag of the high-lift airfoil c_d is the sum of the drag coefficients of the $2N_c$ surfaces.

OUTPUT OF COMPUTER PROGRAM

The output format of the NASA-Lockheed multielement airfoil code is described in the sequence in which it is printed. The definitions of the symbols of the output are contained in the table at the end of this section.

CASE INPUT

Table 4 shows an example of the format in which the user defined input data is printed. The sequence of the printed data agrees with the input format described in the section titled Processing of User Input. An exception is the printing of the airfoil surface points, which is done in the following sequence.

- First airfoil component, from the leading edge to the trailing edge
  - X - Coordinates of upper-surface points
  - Z - Coordinates of upper-surface points
  - X - Coordinates of lower-surface points
  - Z - Coordinates of lower-surface points

- Second airfoil component, from the leading edge to the trailing edge
  - X - Coordinates of upper surface points
    etc.

Note the leading edge point of each airfoil component appears twice.

GEOMETRY

Two different versions of the geometry of a multielement airfoil are printed out. They are

- Input surface points in user coordinates

- Computational surface points in global coordinates.

Tables 5 and 6 show examples of both types of the geometry printout. All surface point coordinates are multiplied by the factor S_F/c_{ref}. The symbols S_F and c_{ref} denote the scale factor and reference chord, respectively. Surface points of the other airfoil components are printed in the sequence defined by the user.

CASE OUTPUT

The computed results of each angle of attack-Mach number case are printed in the sequence described below. Note the term "iteration number" is used in the printout for a cycle of the iteration procedure. An iteration cycle is defined in the Iteration Procedure section.

Table 4. — Input Data

```
*****   CASE INPUT   *****

BOEING FOUR ELEMENT HIGH LIFT AIRFOIL
 NC =    4      NSP =  165

 I  NPP(I)   NPT
 1      1     47
    XP,ZP =  -.124500E-01  .100300E-01
                 XU =  -.828300E-01 -.822100E-01 -.807500E-01 -.788100E-01 -.764600E-01 -.737000E-01 -.705100E-01 -.669200E-01
                       -.629900E-01 -.586900E-01 -.540600E-01 -.491600E-01 -.441300E-01 -.390200E-01 -.338800E-01 -.287100E-01
                       -.234800E-01 -.181900E-01 -.128000E-01
                 ZU =  -.649200E-01 -.586700E-01 -.529600E-01 -.475600E-01 -.424200E-01 -.375200E-01 -.329000E-01 -.285300E-01
                       -.243800E-01 -.204700E-01 -.167600E-01 -.132200E-01 -.977000E-02 -.635000E-02 -.297000E-02  .390000E-03
                        .372000E-02  .702000E-02  .102500E-01
                 XL =  -.828300E-01 -.818700E-01 -.808000E-01 -.794300E-01 -.777100E-01 -.765500E-01 -.740800E-01 -.726700E-01
                       -.716600E-01 -.689500E-01 -.661500E-01 -.645300E-01 -.631300E-01 -.624500E-01 -.637600E-01 -.660300E-01
                       -.669900E-01 -.655200E-01 -.595300E-01 -.535400E-01 -.475600E-01 -.415700E-01 -.353100E-01 -.316600E-01
                       -.278200E-01 -.239800E-01 -.201400E-01 -.162900E-01 -.124500E-01
                 ZL =  -.649200E-01 -.721500E-01 -.751500E-01 -.776700E-01 -.800900E-01 -.814800E-01 -.836100E-01 -.845900E-01
                       -.851400E-01 -.862800E-01 -.860600E-01 -.854200E-01 -.839800E-01 -.807000E-01 -.769600E-01 -.722800E-01
                       -.682900E-01 -.625800E-01 -.531000E-01 -.436100E-01 -.341300E-01 -.246400E-01 -.153400E-01 -.110000E-01
                       -.680000E-02 -.259000E-02  .161000E-02  .582000E-02  .100300E-01
 2      3     73
    XP,ZP =  -.124500E-01  .100300E-01  .103970E+01 -.440300E-01  .109550E+01 -.756000E-01
                 XU =  -.400000E-03 -.340000E-03 -.150000E-03  .230000E-03  .840000E-03  .153000E-02  .374000E-02  .830000E-02
                        .129400E-01  .176500E-01  .223800E-01  .343400E-01  .463900E-01  .707000E-01  .951800E-01  .119790E+00
                        .144480E+00  .194080E+00  .243880E+00  .293800E+00  .343790E+00  .393850E+00  .443950E+00  .494100E+00
                        .544300E+00  .594540E+00  .644850E+00  .695230E+00  .745700E+00  .769310E+00  .796260E+00  .821600E+00
                        .846930E+00  .868100E+00  .888000E+00
                 ZU =   .810000E-03  .173000E-02  .284000E-02  .414000E-02  .566000E-02  .700000E-02  .103600E-01  .154600E-01
                        .195300E-01  .229900E-01  .260300E-01  .323400E-01  .374500E-01  .454400E-01  .514400E-01  .560300E-01
                        .595400E-01  .641700E-01  .665600E-01  .675100E-01  .675400E-01  .669000E-01  .657200E-01  .640200E-01
                        .617400E-01  .589100E-01  .553500E-01  .509600E-01  .455700E-01  .424000E-01  .390600E-01  .351300E-01
                        .313100E-01  .275100E-01  .241000E-01
                 XL =  -.400000E-03 -.380000E-03 -.290000E-03 -.800000E-04  .270000E-03  .830000E-03  .166000E-02  .252000E-02
                        .516000E-02  .103600E-01  .155000E-01  .206200E-01  .257300E-01  .384600E-01  .511600E-01  .765200E-01
                        .101850E+00  .127150E+00  .152430E+00  .202900E+00  .253260E+00  .303490E+00  .353600E+00  .403580E+00
                        .453450E+00  .503220E+00  .552930E+00  .602590E+00  .652230E+00  .701870E+00  .726590E+00  .750990E+00
                        .767480E+00  .783040E+00  .797500E+00  .822510E+00  .846550E+00  .867990E+00  .888070E+00
                 ZL =   .810000E-03  .130000E-03 -.510000E-03 -.127000E-02 -.206000E-02 -.289000E-02 -.376000E-02 -.448000E-02
                       -.612000E-02 -.833000E-02 -.999000E-02 -.114000E-01 -.126500E-01 -.153500E-01 -.176700E-01 -.218000E-01
                       -.256000E-01 -.291100E-01 -.323300E-01 -.377700E-01 -.418600E-01 -.445400E-01 -.458000E-01 -.456100E-01
                       -.440700E-01 -.414200E-01 -.379900E-01 -.340900E-01 -.299400E-01 -.257000E-01 -.224600E-01 -.155600E-01
                       -.809000E-02 -.700000E-03  .555000E-02  .150000E-01  .213300E-01  .239400E-01  .232700E-01
 3      1     43
    XP,ZP =  .103970E+01 -.440300E-01
                 XU =   .846690E+00  .847750E+00  .848560E+00  .850050E+00  .851450E+00  .854160E+00  .860690E+00  .867050E+00
                        .873300E+00  .879490E+00  .885620E+00  .891710E+00  .897750E+00  .909750E+00  .921620E+00  .933410E+00
                        .945110E+00  .956730E+00  .968260E+00  .979700E+00  .991060E+00  .100240E+01  .101373E+01  .102506E+01
                        .103970E+01
                 ZU =  -.233500E-01 -.199200E-01 -.183800E-01 -.162200E-01 -.147000E-01 -.124300E-01 -.852000E-02 -.592000E-02
                       -.409300E-02 -.277000E-02 -.185000E-02 -.127000E-02 -.980000E-03 -.117000E-02 -.221000E-02 -.392000E-02
                       -.624000E-02 -.919000E-02 -.128100E-01 -.171200E-01 -.219800E-01 -.270500E-01 -.321200E-01 -.372300E-01
                       -.440000E-01
                 XL =   .846690E+00  .845810E+00  .848180E+00  .850320E+00  .857320E+00  .869120E+00  .886830E+00  .904530E+00
                        .922130E+00  .951730E+00  .963530E+00  .975490E+00  .980960E+00  .985870E+00  .992410E+00  .100061E+01
                        .101278E+01  .102469E+01  .103964E+01
                 ZL =  -.233500E-01 -.269000E-01 -.301800E-01 -.321200E-01 -.336700E-01 -.352700E-01 -.376600E-01 -.400600E-01
                       -.432600E-01 -.464500E-01 -.480500E-01 -.485000E-01 -.471700E-01 -.457300E-01 -.433300E-01 -.403500E-01
                       -.392100E-01 -.400100E-01 -.444100E-01
 4      1     31
```

Table 4.| — (Concluded)

```
    XP,ZP =   .109550E+01 -.756000E-01
                  XU =   .998720E+00  .999630E+00  .100092E+01  .100210E+01  .100490E+01  .101022E+01  .101538E+01  .102039E+01
                         .103022E+01  .103983E+01  .104930E+01  .105868E+01  .106795E+01  .107714E+01  .108632E+01  .109091E+01
                         .109550E+01
                  ZU =  -.555800E-01 -.532600E-01 -.516100E-01 -.505700E-01 -.489100E-01 -.471700E-01 -.464400E-01 -.463600E-01
                        -.474500E-01 -.498700E-01 -.530900E-01 -.567800E-01 -.611300E-01 -.659400E-01 -.707500E-01 -.731700E-01
                        -.756000E-01
                  XL =   .998720E+00  .998790E+00  .999640E+00  .100035E+01  .100303E+01  .100789E+01  .101762E+01  .102735E+01
                         .103708E+01  .105653E+01  .106627E+01  .107599E+01  .108572E+01  .109059E+01  .109545E+01
                  ZL =  -.555800E-01 -.580700E-01 -.589300E-01 -.591400E-01 -.596200E-01 -.604800E-01 -.621900E-01 -.639000E-01
                        -.656200E-01 -.690400E-01 -.707500E-01 -.724600E-01 -.741700E-01 -.750300E-01 -.758900E-01

 IM =   2

  I    IC(I)    IPP(I)    ICR(I)    IPPR(I)      DELTA

  1        1         1         2          1     0.000000
  2        3         1         2          2     0.000000
  3        4         1         2          3     0.000000

  NA =   1      ALPHA =   .440000E+01

  NM =   1     FSMACH =   .160000E+00

 CREF =   .200000E+01   SF =   .200000E+01   TO =   .563000E+03   RN =   .100000E+01   PR =   .770000E+00   KF =   .100000E+01

  I                    LTRAN      XTRAN          ZTRAN

  1   UPPER SURFACE      0        0.             0.
      LOWER SURFACE      0        0.             0.
  2   UPPER SURFACE      0        0.             0.
      LOWER SURFACE      0        0.             0.
  3   UPPER SURFACE      0        0.             0.
      LOWER SURFACE      0        0.             0.
  4   UPPER SURFACE      0        0.             0.
      LOWER SURFACE      0        0.             0.
```

Table 5. — Input Geometry

BOEING FOUR ELEMENT HIGH LIFT AIRFOIL

COMPONENT NUMBER 2 USER COORDINATE SYSTEM

UPPER SURFACE		LOWER SURFACE	
X/CREF	Z/CREF	X/CREF	Z/CREF
-.000400	.000810	-.000400	.000810
-.000340	.001730	-.000380	.000130
-.000150	.002840	-.000290	-.000510
.000230	.004140	-.000080	-.001270
.000840	.005660	.000270	-.002060
.001530	.007000	.000830	-.002890
.003740	.010360	.001660	-.003760
.008300	.015460	.002520	-.004480
.012940	.019530	.005160	-.006120
.017650	.022990	.010360	-.008330
.022380	.026030	.015500	-.009990
.034340	.032340	.020620	-.011400
.046390	.037450	.025730	-.012650
.070700	.045440	.038450	-.015350
.095180	.051440	.051160	-.017670
.119790	.056030	.076520	-.021800
.144480	.059540	.101850	-.025600
.194080	.064170	.127150	-.029110
.243880	.066560	.152430	-.032330
.293800	.067510	.202900	-.037770
.343790	.067540	.253260	-.041860
.393850	.066900	.303490	-.044540
.443950	.065720	.353600	-.045800
.494100	.064020	.403580	-.045610
.544300	.061760	.453450	-.044070
.594540	.058910	.503220	-.041420
.644850	.055350	.552930	-.037990
.695230	.050960	.602590	-.034090
.745700	.045570	.652230	-.029940
.769310	.042400	.701870	-.025700
.796260	.039060	.726590	-.022460
.821600	.035130	.750990	-.015560
.846930	.031310	.767480	-.008090
.848100	.027510	.783040	-.000700
.888000	.024100	.797500	.005550
		.822510	.015000
		.846550	.021330
		.867990	.023940
		.888070	.023270

Table 6. — Computational Geometry

BOEING FOUR ELEMENT HIGH LIFT AIRFOIL

COMPONENT NUMBER 2 GLOBAL COORDINATE SYSTEM

UPPER SURFACE		LOWER SURFACE	
X/CREF	Z/CREF	X/CREF	Z/CREF
-.000400	.000810	-.000400	.000810
-.000340	.001730	-.000380	.000130
-.000150	.002840	-.000290	-.000510
.000230	.004140	-.000080	-.001270
.000840	.005660	.000270	-.002060
.001530	.007000	.000830	-.002890
.003740	.010360	.001660	-.003760
.008300	.015460	.002520	-.004480
.012940	.019530	.005160	-.006120
.017650	.022990	.010360	-.008330
.022380	.026030	.015500	-.009990
.034340	.032340	.020620	-.011400
.046390	.037450	.025730	-.012650
.070700	.045440	.038460	-.015350
.095180	.051440	.051160	-.017670
.119790	.056030	.076520	-.021800
.144480	.059540	.101850	-.025600
.194080	.064170	.127150	-.029110
.243880	.066560	.152430	-.032330
.293800	.067510	.202900	-.037770
.343790	.067540	.253260	-.041860
.393850	.066900	.303490	-.044540
.443950	.065720	.353600	-.045800
.494100	.064020	.403580	-.045610
.544300	.061760	.453450	-.044070
.594540	.058910	.503220	-.041420
.644850	.055350	.552930	-.037990
.695230	.050960	.602590	-.034090
.745700	.045570	.652230	-.029940
.769310	.042400	.701870	-.025700
.796260	.039060	.726590	-.022460
.821600	.035130	.750990	-.015560
.846930	.031310	.767480	-.008090
.868100	.027510	.783040	-.000700
.888000	.024100	.797500	.005550
		.822510	.015000
		.846550	.021330
		.867990	.023940
		.888070	.023270

DETAILED OUTPUT FOR ITERATION NUMBER 0

The computed potential flow and viscous flow parameters are printed in the following sequence. Each boundary layer and wake layer summary includes a column with the corresponding potential flow pressures.

- First Airfoil Component
  - Upper Surface

    Laminar boundary layer summary
    Turbulent boundary layer summary
  - Lower Surface

    Laminar boundary layer summary
    Turbulent boundary layer summary
- Second Airfoil Component
  - Upper Surface

    Laminar boundary layer summary
    Turbulent boundary layer summary
  - Lower Surface

    Laminar boundary layer summary
    etc.
- First Airfoil Component

  Wake layer summary
- Second Airfoil Component

  Confluent boundary layer summary
  Wake layer summary
  etc.

Tables 7, 8, 9, and 10 show examples of the three boundary layer and wake layer summaries. Obviously, the ordinary turbulent boundary layer results are only printed if transition from laminar to turbulent flow has occured. The user is reminded the Nash and Hicks method and the modified confluent boundary layer method are not used in this iteration cycle. Therefore, only the results of the Truckenbrodt method for ordinary turbulent boundary layers and the results of the Goradia method for confluent boundary layers are printed.

Table 7. — Laminar Boundary Layer Summary

LAMINAR BOUNDARY LAYER SUMMARY

BOEING FOUR ELEMENT HIGH LIFT AIRFOIL

UPPER SURFACE
COMPONENT NUMBER 1
ITERATION NUMBER 4

STAGNATION TEMPERATURE	= 563.00	DEGREES RANKINE	,	STAGNATION PRESSURE	= 2090.764	LB/SQ FT	
FREESTREAM MACH NUMBER	= .16000		,	AIRFOIL CHORD	= .224	FT	
REYNOLDS NUMBER PER FOOT	= 1.000000	MILLION	,	PRANDTL NUMBER	= .7700		
HEAT TRANSFER FACTOR K	= 1.0000		,	SEPARATION CORRELATION NO.	= .069627		
SPEED OF SOUND	= 1163.128	FT/SEC	,	KINEMATIC VISCOSITY	= .00018398	SQ FT/SEC	
ANGLE OF ATTACK	= 4.4000	DEGREES	,				
STAGNATION AT X/C	= -.08205615		,	STAGNATION AT Z/C	= -.07074806		

X/C	S/C	M	DM/D(S/C)	H	THETA/C	DELS/C	DELTA/C	CF	CP
-.082830	.005879	.063516	9.276265	2.504334	.000030	.000076	.000259	.032267	.84628
-.082210	.012160	.111530	5.573848	2.473757	.000032	.000080	.000281	.015109	.51451
-.080750	.018054	.132928	3.938691	2.480866	.000039	.000097	.000340	.010604	.30930
-.078810	.023791	.157249	4.143128	2.493124	.000040	.000100	.000345	.009097	.03393
-.076460	.029443	.180133	3.613974	2.489544	.000041	.000101	.000351	.007575	-.26531
-.073700	.035067	.198023	2.792066	2.483018	.000043	.000107	.000371	.006251	-.52584
-.070510	.040681	.211518	1.819403	2.469465	.000046	.000114	.000401	.005052	-.73751
-.066920	.046337	.218479	1.053332	2.456779	.000051	.000126	.000449	.004078	-.85171
-.062990	.052052	.223474	.410707	2.438246	.000057	.000138	.000498	.003224	-.93574
-.058690	.057864	.223123	-.079973	2.415469	.000065	.000156	.000572	.002406	-.92978
-.054060	.063797	.222530	-.093589	2.413190	.000072	.000174	.000639	.002126	-.91973
-.049160	.069842	.222003	-.520877	2.375178	.000079	.000187	.000714	.001227	-.91082

SCRIT/C = .06305975 RECRIT = 189.59 STRAN/C = .07417284 RTRAN = 228.97 THETA1/C = .00008695

CN LAMINAR SEPARATION HAS OCCURRED AT X/C = -.045593 S/C = .074173

SHORT BUBBLE TRANSITION REYNOLDS NO. = 228.967111

Table 8. — Turbulent Boundary Layer Summary

TURBULENT BOUNDARY LAYER SUMMARY

BOEING FOUR ELEMENT HIGH LIFT AIRFOIL

UPPER SURFACE
COMPONENT NUMBER 2
ITERATION NUMBER 4

STAGNATION TEMPERATURE	=	563.00	DEGREES RANKINE	STAGNATION PRESSURE	=	2090.764	LB/SQ FT
FREESTREAM MACH NUMBER	=	.16000	,	AIRFOIL CHORD	=	1.777	FT
REYNOLDS NUMBER PER FOOT	=	1.000000	MILLION ,	PRANDTL NUMBER	=	.7700	
HEAT TRANSFER FACTOR K	=	1.0000	,	TRANSITION POINT, S/C	=	.10443	
(INITIAL MOMENTUM THICKNESS)/C	=	.00012	,	INIT. INCOMPR. FORM FACTOR	=	1.37177	
ANGLE OF ATTACK	=	4.4000	DEGREES				

X/C	S/C	M	DM/(S/C)	H	THETA/C	DELS/C	DELTA/C	CF	CP
.067716	.104428	.289662	-.450712	1.371766	.000116	.000158			
.070700	.107538	.288310	-.418710	1.394880	.000125	.000175	.001060	.005454	-2.179141
.095180	.132742	.281025	-.278505	1.553996	.000197	.000306	.001413	.003792	-2.025716
.119790	.157777	.274314	-.281124	1.633172	.000270	.000440	.001832	.003100	-1.887386
.144480	.182715	.266979	-.288955	1.557254	.000348	.000542	.002485	.003282	-1.739487
.194080	.232531	.253101	-.240086	1.614289	.000517	.000835	.003555	.002736	-1.469323
.243880	.282388	.243052	-.180049	1.454198	.000686	.000998	.005393	.003290	-1.281664
.293800	.332317	.235138	-.122665	1.404155	.000855	.001201	.007145	.003382	-1.138682
.343790	.382307	.230800	-.080979	1.382707	.000998	.001379	.008588	.003372	-1.062108
.393850	.432371	.227037	-.078217	1.370828	.001139	.001561	.009983	.003329	-.996736
.443950	.482485	.222964	-.070781	1.362649	.001292	.001761	.011471	.003275	-.927081
.494100	.532664	.219939	-.055082	1.354862	.001434	.001943	.012891	.003235	-.876099
.544300	.582915	.217433	-.047187	1.348227	.001570	.002117	.014276	.003199	-.834330
.594540	.633235	.215194	-.041505	1.342513	.001705	.002289	.015654	.003166	-.797396
.644850	.683671	.213251	-.042131	1.338354	.001836	.002457	.016984	.003131	-.765632
.695230	.734242	.210937	-.025443	1.332374	.001981	.002639	.018521	.003106	-.728141
.745700	.784999	.210681	-.081927	1.333604	.002071	.002762	.019318	.003064	-.724007
.769310	.808821	.207870	-.099618	1.337565	.002194	.002935	.020324	.003009	-.679018
.796260	.835977	.205734	-.085958	1.340638	.002307	.003093	.021251	.002962	-.645207
.821600	.861620	.203353	-.056181	1.340571	.002430	.003257	.022384	.002930	-.607898
.846930	.887237	.202852	-.149426	1.349057	.002488	.003357	.022589	.002875	-.600103
.868100	.908745	.197293	-.530181	1.405552	.002738	.003848	.022824	.002585	-.514757
.888000	.928935	.181439	-1.040283	1.509119	.003548	.005354	.026388	.002096	-.283551

Table 9. — Confluent Boundary Layer Summary

CONFLUENT BOUNDARY LAYER SUMMARY

BOEING FOUR ELEMENT HIGH LIFT AIRFOIL

UPPER SURFACE
COMPONENT NUMBER 2
ITERATION NUMBER 4

STAGNATION TEMPERATURE	=	563.00	DEGREES RANKINE	,	STAGNATION PRESSURE	=	2090.764 LB/SQ FT
FREESTREAM MACH NUMBER	=	.16000		,	SLOT HEIGHT, H/C	=	.02516
REYNOLDS NUMBER PER FOOT	=	1.000000	MILLION	,	SLOT EXIT, X/C	=	.89013
ANGLE OF ATTACK	=	4.4000	DEGREES	,	SPEED OF SOUND	=	1163.128 FT/SEC

X/C	S/C	M	DM/D(S/C)	H	THETA/C	DELS/C	DELTA/C	CF	CP
MAIN REGION-I									
.343790	.382307	.230800	-.080979	1.499092	.000923	.002712	.025668	.002895	-1.062108
.393850	.432371	.227037	-.078217	1.539700	.000953	.002884	.028341	.002733	-.996736
.443950	.482485	.222964	-.070781	1.552576	.001035	.003100	.030786	.002652	-.927081
.494100	.532664	.219939	-.055082	1.556221	.001146	.003281	.033177	.002588	-.876099
.544300	.582915	.217433	-.047187	1.556421	.001274	.003434	.035459	.002529	-.834330
.594540	.633235	.215194	-.041505	1.560460	.001438	.003603	.037873	.002441	-.797396
.644850	.683671	.213251	-.042131	1.567641	.001641	.003799	.040492	.002331	-.765632
.695230	.734242	.210937	-.025443	1.585505	.001899	.004092	.043502	.002179	-.728141
.745700	.784999	.210681	-.081927	1.589672	.002129	.004285	.046148	.002090	-.724007
.769310	.808821	.207870	-.099618	1.622781	.002296	.004615	.047922	.001950	-.679018
.796260	.835977	.205734	-.085958	1.670188	.002527	.005085	.050342	.001767	-.645207
.821600	.861620	.203353	-.056181	1.713457	.002714	.005506	.052344	.001623	-.607898
.846930	.887237	.202852	-.149426	1.730647	.002832	.005721	.053685	.001561	-.600103
.868100	.908745	.197293	-.530181	1.746572	.003154	.006398	.056939	.001491	-.514757
.888000	.928935	.181439	-1.040283	1.746572	.004547	.009179	.070447	.001379	-.283551

X---------WALL LAYER---------XX----CORE LAYER----XX-----JET LAYER----XX---------WAKE LAYER---------X

X/C	DELTA1	N	UL/UE	DELTA2	UC/UE	DELTA3	UW/UE	Y1C	DELTA4	UE/UF
.3438	.008940	4.0073	.9693			.016120	.8560	.019940	.025668	.2290
.3939	.009229	3.7058	.9326			.016901	.8775	.021477	.028341	.2253
.4440	.010008	3.6194	.9072			.017874	.8884	.023039	.030786	.2213
.4941	.011063	3.5957	.8904			.018960	.8996	.024647	.033177	.2183
.5443	.012273	3.5944	.8810			.020081	.9103	.026232	.035459	.2159
.5945	.013827	3.5685	.8792			.021468	.9205	.028030	.037873	.2137
.6449	.015757	3.5234	.8850			.023189	.9308	.030110	.040492	.2117
.6952	.018206	3.4159	.8960			.025423	.9401	.032655	.043502	.2095
.7457	.020385	3.3917	.9125			.027408	.9505	.034904	.046148	.2092
.7693	.021978	3.2114	.9146			.028918	.9510	.036519	.047922	.2064
.7963	.024145	2.9842	.9210			.031026	.9516	.038753	.050342	.2043
.8216	.025945	2.8033	.9240			.032739	.9518	.040581	.052344	.2020
.8469	.027059	2.7373	.9287			.033793	.9536	.041750	.053685	.2015
.8681	.030119	2.6789	.9269			.036807	.9490	.044859	.056939	.1960
.8880	.043339	2.6789	.9327			.050016	.9222	.058188	.070447	.1804

Table 10. — Wake Summary

WAKE LAYER SUMMARY

BOEING FOUR ELEMENT HIGH LIFT AIRFOIL

COMPONENT NUMBER 2
ITERATION NUMBER 4

STAGNATION TEMPERATURE = 563.00 DEGREES RANKINE , STAGNATION PRESSURE = 2090.764 LB/SQ FT
FREESTREAM MACH NUMBER = .16000 , REYNOLDS NUMBER PER FOOT = 1.000000 MILLION
ANGLE OF ATTACK = 4.4000 DEGREES

X/C	S/C	M	DM/D(S/C)	H	THETA/C	DELS/C	DELUP/C	DELLW/C	CP
.888035	0.000000	.159328	6.592259	1.475693	.003646	.005381	.028335	.002086	.00834
.889887	.001888	.171774	3.860881	1.255387	.002230	.002799	.023256	.002047	-.15154
.897059	.009061	.199468	.762314	1.200737	.001888	.002267	.022732	.002395	-.54790
.910992	.023034	.210121	.301159	1.178113	.001776	.002093	.023103	.002711	-.71500
.924431	.036558	.214193	.084104	1.166198	.001749	.002039	.023814	.003008	-.78100
.937567	.049834	.215310	-.067877	1.159969	.001771	.002055	.024756	.003302	-.79930
.950583	.063077	.214411	-.202785	1.158209	.001843	.002135	.025947	.003610	-.78456
.963605	.076429	.211703	-.320737	1.160390	.001966	.002281	.027408	.003942	-.74051
.976551	.089918	.207377	-.410066	1.166074	.002141	.002496	.029128	.004301	-.67119
.989420	.103402	.201848	-.451740	1.174048	.002352	.002761	.030998	.004672	-.58452
1.001848	.116516	.195923	-.442472	1.182622	.002576	.003047	.032882	.005040	-.49408
1.013854	.129146	.190335	-.397796	1.190779	.002801	.003335	.034734	.005400	-.41106
1.025645	.141600	.185381	-.367617	1.198949	.003033	.003637	.036615	.005765	-.33935

LOAD SUMMARIES FOR ITERATION NUMBERS 0 TO 3

Overall lift, drag, and moment coefficients as well as axial and normal force coefficients are printed out in a load summary. The various coefficients are defined in the section titled Global Aerodynamic Parameters. A sample output is shown in table 11.

DETAILED OUTPUT FOR ITERATION NUMBER 4

This output type is similar to the detailed printout of the results of iteration number 0. The difference is a summary of the ordinary turbulent boundary layer results of the Nash and Hicks method which follows the printed results of the Truckenbrodt method. An example of the turbulent boundary layer summary of the Nash and Hicks method is given by table 12. Results of the modified confluent boundary layer method are contained in table 13.

LOAD SUMMARY FOR ITERATION 4

The format of this summary is identical to the one of the load summaries of previous iteration numbers.

SUMMARY OF SURFACE DISTRIBUTIONS OF FLOW PARAMETERS

A table summarizing final values of surface distributions of the most important potential flow and viscous flow parameters is printed at the end of each data case. An example is shown in table 14.

Table 11. — Load Summary

LOADS SUMMARY SHEET

BOEING FOUR ELEMENT HIGH LIFT AIRFOIL

FREESTREAM MACH NUMBER	= .16000 ,	ANGLE OF ATTACK	= 4.40000	DEGREES	
REYNOLDS NUMBER PER FOOT	= 1.00000 MILLION ,	REFERENCE CHORD	= 2.00000	FEET	

ITERATION NUMBER	TOTAL LIFT COEFFICIENT	TOTAL DRAG COEFFICIENT	TOTAL MOMENT ABOUT (0,0)	AXIAL FORCE COEFFICIENT	NORMAL FORCE COEFFICIENT
0	1.687664	.018793	-.703936	-.120315	1.683395
1	1.643357	.019746	-.689085	-.111176	1.639660
2	1.642396	.019753	-.689407	-.110331	1.638761
3	1.642792	.019763	-.689646	-.110531	1.639143

Table 12. — Turbulent Boundary Layer Summary of Nash and Hicks Method

TURBULENT BOUNDARY LAYER SUMMARY (NASH-HICKS METHOD)

BOEING FOUR ELEMENT HIGH LIFT AIRFOIL

UPPER SURFACE
COMPONENT NUMBER 2
ITERATION NUMBER 4

STAGNATION TEMPERATURE	= 563.00	DEGREES RANKINE	STAGNATION PRESSURE	= 2090.764	LB/SQ FT
FREESTREAM MACH NUMBER	= .16000		AIRFOIL CHORD	= 1.777	FT
REYNOLDS NUMBER PER FOOT	= 1.000000	MILLION	PRANDTL NUMBER	= .7700	
HEAT TRANSFER FACTOR K	= 1.0000		TRANSITION POINT, S/C	= .10443	
(INITIAL MOMENTUM THICKNESS)/C	= .00012		INIT. INCOMPR. FORM FACTOR	= 1.57637	
ANGLE OF ATTACK	= 4.4000	DEGREES			

X/C	S/C	M	DU/DS	H	THETA/C	DELS/C	DELTA/C	CF	CP	CD-SY
.06772	.10443	.28966		1.57637	.00012					
.07070	.10754	.28831	-1.27918	1.57246	.00012	.00020	.00095	.00448	-2.17914	
.09518	.13274	.28102	-.85234	1.52595	.00019	.00030	.00152	.00402	-2.02572	
.11979	.15778	.27431	-.86139	1.50394	.00026	.00039	.00207	.00370	-1.88739	
.14448	.18271	.26698	-.88633	1.49424	.00033	.00050	.00264	.00343	-1.73949	
.19408	.23253	.25310	-.73782	1.48310	.00048	.00072	.00382	.00304	-1.46932	
.24388	.28239	.24305	-.55421	1.47185	.00064	.00094	.00504	.00283	-1.28166	
.29380	.33232	.23514	-.37797	1.45775	.00078	.00114	.00625	.00272	-1.13868	
.34379	.38231	.23080	-.24973	1.44164	.00091	.00131	.00740	.00269	-1.06211	
.39385	.43237	.22704	-.24135	1.42939	.00103	.00148	.00859	.00265	-.99674	
.44395	.48248	.22296	-.21850	1.42258	.00116	.00165	.00963	.00259	-.92708	
.49410	.53266	.21994	-.17011	1.41640	.00128	.00182	.01071	.00255	-.87610	
.54430	.58291	.21743	-.14578	1.41003	.00140	.00198	.01176	.00252	-.83433	
.59454	.63324	.21519	-.12826	1.40424	.00151	.00213	.01280	.00249	-.79740	
.64485	.68367	.21325	-.13023	1.40004	.00163	.00228	.01383	.00246	-.76563	
.69523	.73424	.21094	-.07866	1.39424	.00173	.00242	.01483	.00245	-.72814	
.74570	.78500	.21068	-.25337	1.39575	.00187	.00261	.01591	.00239	-.72401	
.76931	.80882	.20787	-.30812	1.40182	.00197	.00276	.01652	.00232	-.67902	
.79626	.83598	.20573	-.26596	1.40946	.00208	.00294	.01724	.00224	-.64521	
.82160	.86162	.20335	-.17386	1.41062	.00216	.00305	.01782	.00221	-.60790	
.84693	.88724	.20285	-.46263	1.41181	.00224	.00316	.01842	.00218	-.60010	
.86810	.90874	.19729	-1.64304	1.44987	.00253	.00366	.01962	.00192	-.51476	
.88800	.92893	.18144	-3.22528	1.59013	.00331	.00527	.02250	.00123	-.28355	

Table 13. — Confluent Boundary Layer Summary, Modified Method of Goradia

CONFLUENT BOUNDARY LAYER SUMMARY, MODIFIED METHOD OF GORADIA

BOEING FOUR ELEMENT HIGH LIFT AIRFOIL

UPPER SURFACE
COMPONENT NUMBER 2
ITERATION NUMBER 4

STAGNATION TEMPERATURE	= 563.00	DEGREES RANKINE	,	STAGNATION PRESSURE	= 2090.764	LB/SQ FT
FREESTREAM MACH NUMBER	= .16000		,	SLOT HEIGHT, H/C	= .02516	
REYNOLDS NUMBER PER FOOT	= 1.000000	MILLION	,	SLOT EXIT, X/C	= .89013	
ANGLE OF ATTACK	= 4.4000	DEGREES	,	SPEED OF SOUND	= 1163.128	FT/SEC

X/C	S/C	M	DM/D(S/C)	H	THETA/C	DELS/C	DELTA/C	CF	CP
MAIN REGION-1									
.343790	.382307	.230800	-.086786	1.434997	.000927	.001331	.024215	.002990	-1.062108
.393850	.432371	.227037	-.075165	1.448316	.001006	.001456	.026777	.002721	-.996736
.443950	.482485	.222964	-.081273	1.457881	.001121	.001634	.029247	.002489	-.927081
.494100	.532664	.219939	-.060276	1.456783	.001235	.001799	.031529	.002346	-.876099
.544300	.582915	.217433	-.049882	1.454630	.001363	.001983	.033704	.002231	-.834330
.594540	.633235	.215194	-.044488	1.453556	.001507	.002191	.035808	.002134	-.797396
.644850	.683671	.213251	-.038515	1.453087	.001663	.002417	.037856	.002054	-.765632
.695230	.734242	.210937	-.045756	1.460291	.001855	.002709	.039941	.001958	-.728141
.745700	.784999	.210681	-.005055	1.446332	.001975	.002857	.041746	.001973	-.724007
.769310	.808821	.207870	-.118005	1.477693	.002175	.003213	.043003	.001817	-.679018
.796260	.835977	.205734	-.078656	1.498086	.002343	.003510	.044263	.001719	-.645207
.821600	.861620	.203353	-.092854	1.525475	.002529	.003859	.045535	.001605	-.607898
.846930	.887237	.202852	-.019547	1.521190	.002601	.003957	.046424	.001610	-.600103
.868100	.908745	.197293	-.258476	1.629271	.003032	.004940	.048429	.001268	-.514757

Table 14. — Summary of Surface Distributions of Flow Parameters

BOEING FOUR ELEMENT HIGH LIFT AIRFOIL

COMPONENT NUMBER 4

X/C	Z/C	S/C	V/VO	CP	CF	DELTA/C	DELS/C	H
1.09545	-.07589	0.00000	-.77932	.39676	.00283	.00247	.00047	1.47367
1.09059	-.07503	.00494	-.79440	.37284	.00305	.00227	.00043	1.46276
1.08572	-.07417	.00989	-.80326	.35857	.00324	.00213	.00039	1.45015
1.07599	-.07246	.01976	-.80412	.35717	.00335	.00194	.00035	1.44736
1.06627	-.07075	.02963	-.80056	.36294	.00324	.00170	.00033	1.47977
1.05653	-.06904	.03952	-.79606	.37018	.00253	.00135	.00033	1.64868
1.03708	-.06562	.05927	-.78065	.39467	.00259	.00107	.00026	1.65313
1.02735	-.06390	.06915	-.77480	.40384	.00265	.00091	.00022	1.65624
1.01762	-.06219	.07903	-.77285	.40688	.00284	.00073	.00018	1.64868
1.00789	-.06048	.08891	-.77724	.40002	.00304	.00052	.00013	1.66934
1.00303	-.05962	.09384	-.82466	.32344	.00319	.00032	.00009	1.77648
1.00035	-.05914	.09656	-1.02262	-.04635	.01023	.00008	.00005	1.47346
.99964	-.05893	.09730	-1.02905	-.05974	.02094	.00006	.00003	2.43989
.99879	-.05807	.09851	-.73746	.46072	.02024	.00006	.00004	2.51148
.99872	-.05558	.10100	.00646	1.00637	.00016	.00007	.00004	2.50138
.99963	-.05326	.10350	.41168	.83678	.00781	.00009	.00005	2.50452
1.00092	-.05161	.10559	.61113	.63210	.00956	.00009	.00005	2.47118
1.00210	-.05057	.10715	.70822	.50328	.00935	.00011	.00006	2.45766
1.00490	-.04891	.11042	.78698	.38468	.00721	.00014	.00008	2.44486
1.01022	-.04717	.11602	.87279	.24098	.00646	.00018	.00010	2.45493
1.01536	-.04644	.12121	.94439	.10946	.00633	.00020	.00011	2.45918
1.02039	-.04636	.12624	.99658	.00692	.00606	.00022	.00013	2.46000
1.03022	-.04745	.13613	1.08284	-.17500	.00549	.00025	.00014	2.45127
1.03983	-.04987	.14604	1.11562	-.24820	.00400	.00030	.00017	2.42074
1.04930	-.05309	.15604	1.10863	-.23240	.00256	.00037	.00020	2.38981
1.05868	-.05678	.16612	1.09407	-.19982	.00076	.00045	.00023	1.39270
1.06795	-.06113	.17636	1.04493	-.09314	.00531	.00100	.00021	1.54090
1.07714	-.06594	.18673	.97601	.04800	.00437	.00146	.00030	1.52714
1.08632	-.07075	.19710	.89707	.19756	.00225	.00181	.00051	1.79535
1.09091	-.07317	.20229	.83267	.31005	.00116	.00221	.00078	2.09057
1.09550	-.07560	.20748	.74490	.44962	.00087	.00318	.00112	2.09057

NORMAL END

SYMBOLS OF PRINTED OUTPUT

Output	Theory	Definition
ALPHA		Angle of attack in degrees
	c_a	Axial force coefficient
	c_d	Drag coefficient
CF	c_f	Skin friction coefficient, note warning immediately following this list of symbols
	c_m	Pitching-moment coefficient
	c_n	Normal-force coefficient
CP	c_p	Surface-pressure coefficient
CREF	c_{ref}	Reference length
DELTA	Δ	Angle of rotation between the coordinate system of an airfoil component and the reference coordinate system in degrees
DELTA/C	δ/c_{ref}	Nondimensional boundary-layer thickness
DELTA1	δ_5	Outer edge of the wall layer
DELTA3	δ_3	Outer edge of the jet layer
DELTA4	δ_4/c_{ref}	Nondimensional value of the confluent boundary layer thickness
DELS/C	δ^*/c_{ref}	Nondimensional boundary layer displacement thickness
DM/(S/C)	$\frac{\partial M_e}{\partial (s/c_{ref})}$	Derivative of local Mach number With respect to arc length
DU/DS	$\frac{\partial (U_e/U_\infty)}{\partial (s/c_{ref})}$	Derivative of the surface velocity with respect to arc length
FSMACH	M_∞	Freestream Mach number
H	H	Shape factor; in the confluent boundary layer summary, H is the shape factor of the wall layer
IC		Indices of components in the order that their data is stored

Output	Theory	Definition
ICR		Index of reference component for each component
IM		Index of main component
IPP		Index of pivot point used in placing each component
IPPR		Index of pivot point on reference component used in placing each component
KF	k	Heat transfer factor
LTRAN		Transition option: =0 free transition; =1 fixed transition
M	M_e	Local Mach number
N	n	Exponent of power-law velocity profile (reciprocal value)
NA		Number of angles of attack
NC	N_C	Number of airfoil components
NM		Number of Mach numbers
NPP		Number of pivot points for each component
NPT		Number of input points for each component
NSP		Total number of computational surface points
PR	Pr	Prandtl number
RECRIT	$Re_{\theta inst}$	Momentum thickness Reynolds number at the point of instability
RTRAN	$Re_{\theta tran}$	Momentum thickness Reynolds number at transition
RN	$Re_{ft}*10^{-6}$	Reynolds number per foot in millions
SF		Scale factor of conversion of input geometry to feet
S/C	s/c_{ref}	Nondimensional arc length
SCRIT/C	$(s/c_{ref})_{inst}$	Location of the point of instability
STRAN/C	$(s/c_{ref})_{tran}$	Transition location

Output	Theory	Definition
THETA/C	θ/c_{ref}	Nondimensional momentum thickness; in a confluent boundary layer summary, this is the value of the wall layer only
THETAI/C	θ_I/c_{ref}	Initial value of θ/c_{ref} of the turbulent boundary layer calculation
TO	T_0	Freestream stagnation temperature in °R
UE/UF	U_e/U_∞	Ratio of the velocity at the outer edge of the confluent boundary layer and the freestream velocity
UL/UE	U_m/U_e	Ratio of the velocity at the outer edge of the wall layer and the velocity at the outer edge of the confluent boundary layer
UW/UE	U_W/U_e	Ratio of the velocity at the outer edge of the jet layer and the velocity at the outer edge of the confluent boundary layer
V/VO	V_c/U_∞	Ratio of compressible surface velocity and freestream velocity
X/C,Z/C X/CREF, Z/CREF	X_G/c_{ref} Z_G/c_{ref}	Nondimensional coordinates of the global axis system
X(M.S.),	X_pS_F/c_{ref}	Pivot point coordinates in the global axis system scaled by S_F/c_{ref}
Z(M.S.)	Z_pS_F/c_{ref}	
	$(X_p)_IS_F/c_{ref}$ $(Z_p)_IS_F/c_{ref}$	Pivot point coordinates in input coordinates of an individual airfoil component scaled by S_F/c_{ref}
XTRAN, ZTRAN	$(X_I,Z_I)_{tran}$	Location of the transition point in input coordinates
XL,ZL		Lower-surface point coordinates in input axis system
XU,ZU	$(X_I,Z_I)u$	Upper-surface point coordinates in input axis system
Y1C	$Y_{1/2}/c_{ref}$	Half velocity point of the wake layer

Note: Two different definitions of the skin friction coefficients CF are used. In all boundary layer summaries, the skin friction is referred to the local dynamic pressure. In the summary of the surface distributions of flow parameters, CF is based on the freestream value of the dynamic pressure.

COMPUTED RESULTS

This section of the document summarizes evaluation results of the new version of the computer program. Most details of this study are described in a supplemental document (ref. 6). Figure 37 shows the geometry of the analyzed airfoil configurations. Corresponding airfoil parameters are also in reference 6, such as gap, overlap, and flap settings; and the investigated flight conditions including Reynolds number, Mach number, and angle of attack range.

In the following test-theory comparison, three versions of the NASA/Lockheed multielement program are referred to:

VERSION A

This is the baseline version of the computer program, made operational for negative overlap of neighboring airfoil components. The base line version was available from the NASA in June 1976.

VERSION B

This version is described in reference 5. It differs from version A in these areas:

- Ordinary turbulent boundary layer flow is calculated using the method of Nash and Hicks.
- Profile drag is predicted by the Squire and Young formula.

VERSION C

This is the version described in this document.

TEST-THEORY COMPARISONS

BASIC GA(W)-1 AIRFOIL

The basic GA(W)-1 airfoil was chosen to test the program capability in predicting performance characteristics of single airfoils. Figures 38 and 39 contain theoretical lift, pitching moment, and drag curves and their comparison with the experimental data of McGhee and Beasley (ref. 23). Both, version A and the new program version C predict identical lift and moment curves, which in turn agree with measured GA(W)-1 data up to the onset of trailing edge stall at about 8 degrees angle of attack.

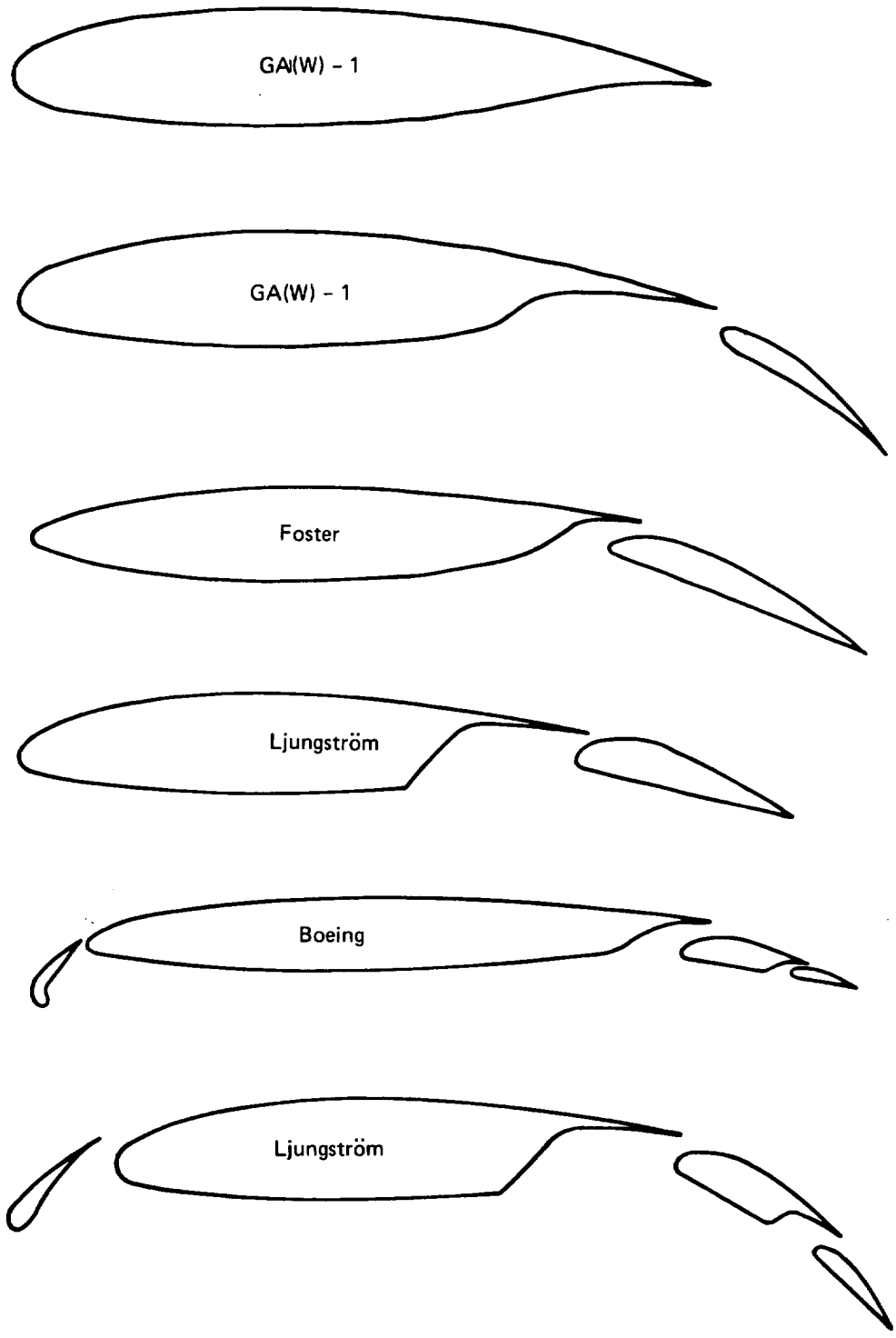

Figure 37. – Analyzed Airfoil Configurations

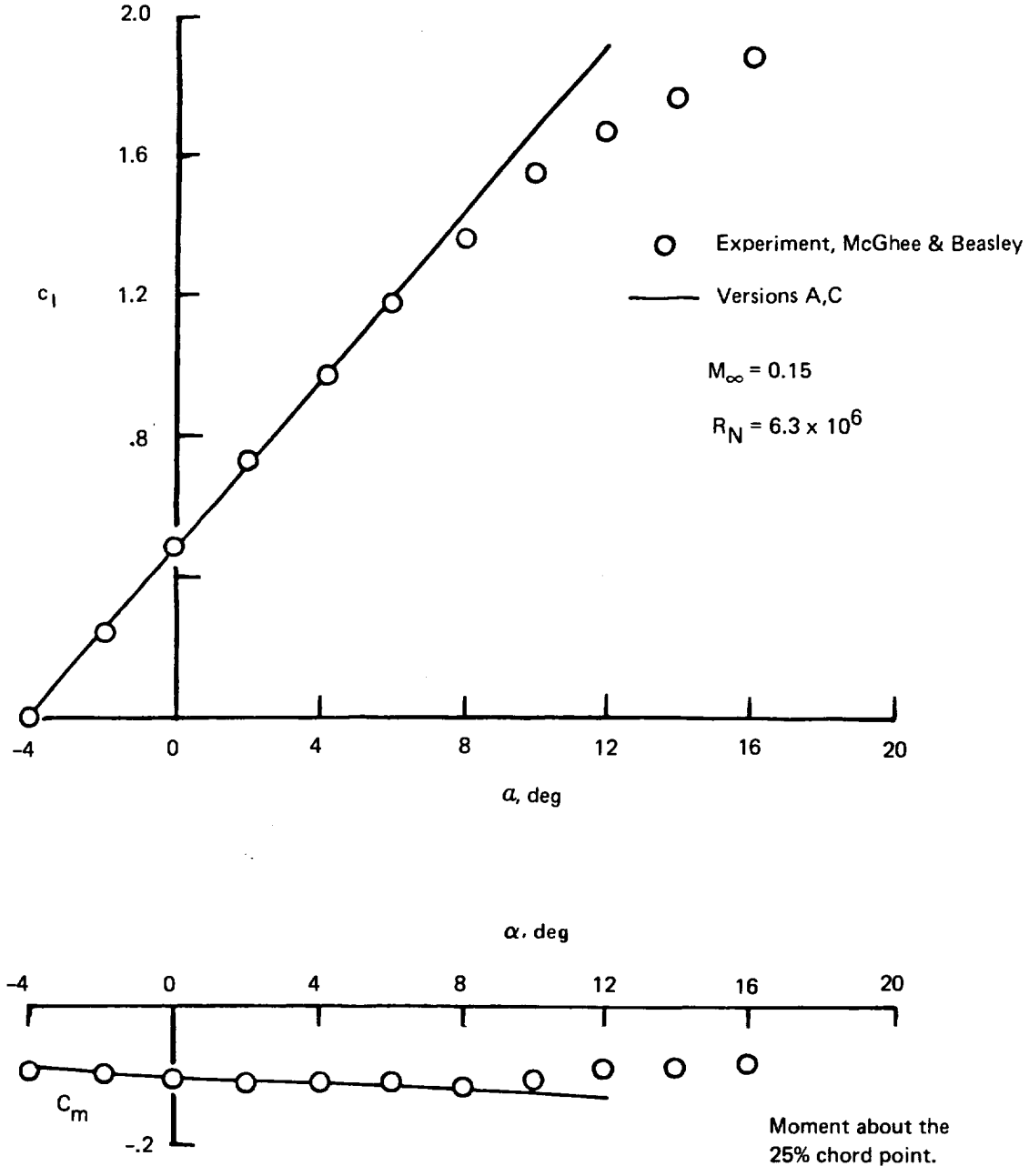

Figure 38. — Lift and Pitching Moment of GA(W)-1 Single Airfoil

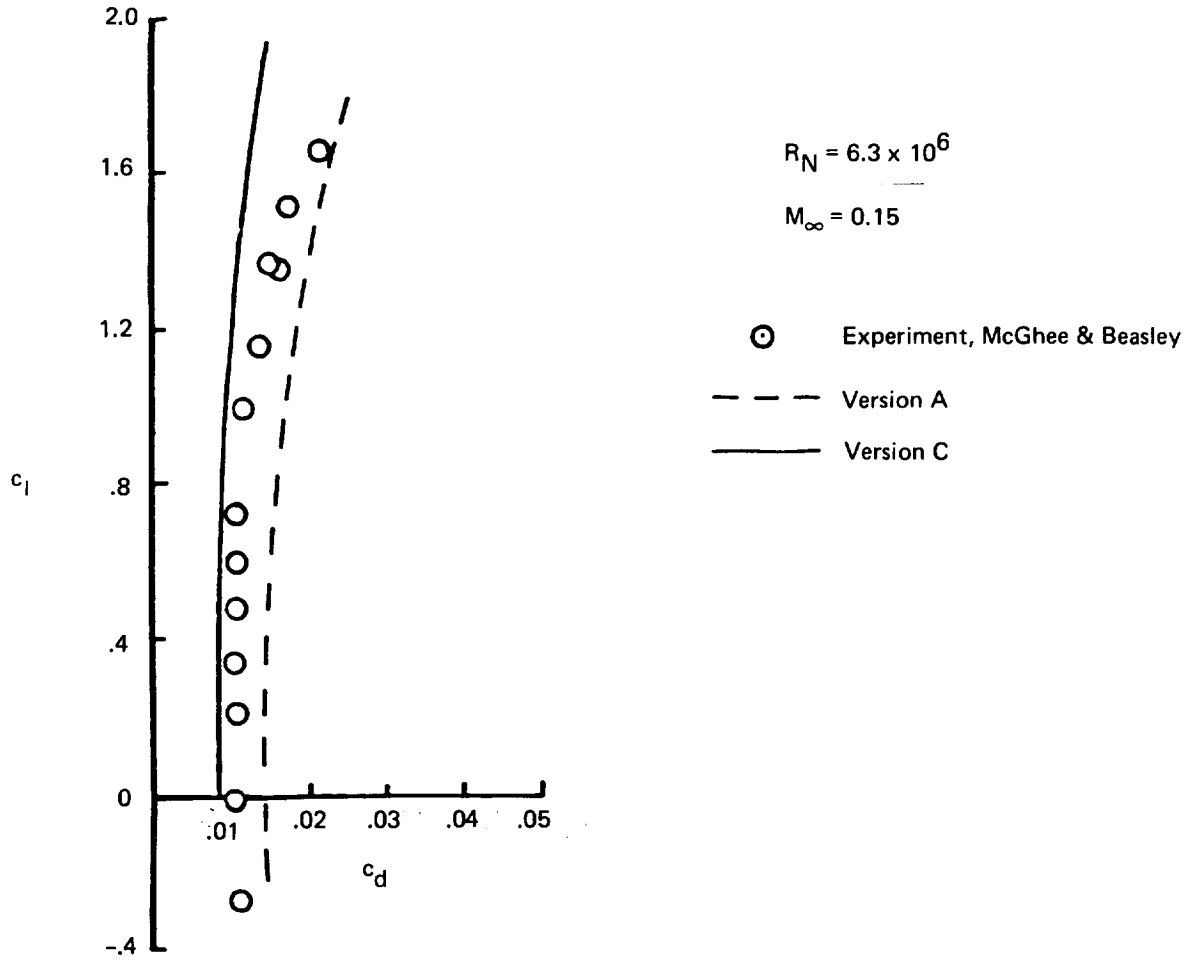

Figure 39. — Drag Polar of GA(W)-1 Single Airfoil

Differences between drag polars are observed in Fig. 39. Version A, utilizing an integration of surface pressure and skin friction in the prediction of profile drag, gives the highest drag coefficients. Version C, applying the Squire and Young formula, offers drag values that are lower than the corresponding experimental drag coefficients. The lack of agreement of the three drag polars emphasizes the fact that even for single airfoils at low speed the problem of obtaining theoretically accurate drag data is not yet solved.

GA(W)-1 WITH 30% CHORD FLAP

The GA(W)-1 airfoil with a single 30% chord trailing edge flap served as the principal test case for this type of general aviation high-lift airfoil. The experimental data were measured by Wentz, Seetharam, and Fiscko (ref. 24 and 25). The data include global airfoil parameters as well as detailed surface pressures and boundary-layer characteristics.

Lift- and pitching-moment characteristics of this airfoil with a flap deflection of 10 degrees are shown in figure 40. The computed data of version C agree with the experimental results in the pre-stall angle of attack range, whereas, version B slightly mispredicts lift and moment curves.

Differences between theoretical predictions and experimental data were noted at higher flap angles, but are not shown in this document. Details of these results and a discussion of possible reasons for the observed discrepancies are given in reference 6.

BOEING HIGH-LIFT AIRFOIL

The Boeing four-element high-lift airfoil, (fig. 37), was used as the main test case for multiple airfoils. It consists of a wing section with a leading-edge flap and a double-slotted trailing edge flap. Global airfoil parameters and detailed distributions of surface pressures and boundary layer data are available for comparisons.

The lift and drag curves of this airfoil at a Reynolds number of two million, based on the wing reference chord, are given in figures 41 and 42. The experimental lift coefficients are balance data whereas the profile drag is obtained from wake rake measurements.

All attempts failed using program version A to obtain a converged solution for this airfoil. Program version B arrived at converged solutions between 8 and 20 degrees angle of attack, but underpredicted the lift by a considerable amount, see fig. 41. The prediction of the lift coefficient is greatly improved by version C, but the reader should note that the potential flow solution already provides a very good approximation to the lift curve. The theoretical values of the profile drag of version C, shown in figure 42, are relatively close to the measured profile drag. In judging the quality of the agreement of the two types of drag curves, one should consider the problems of two-dimensional high-lift testing and the uncertainties in applying the Squire and Young formula to theoretical drag predictions.

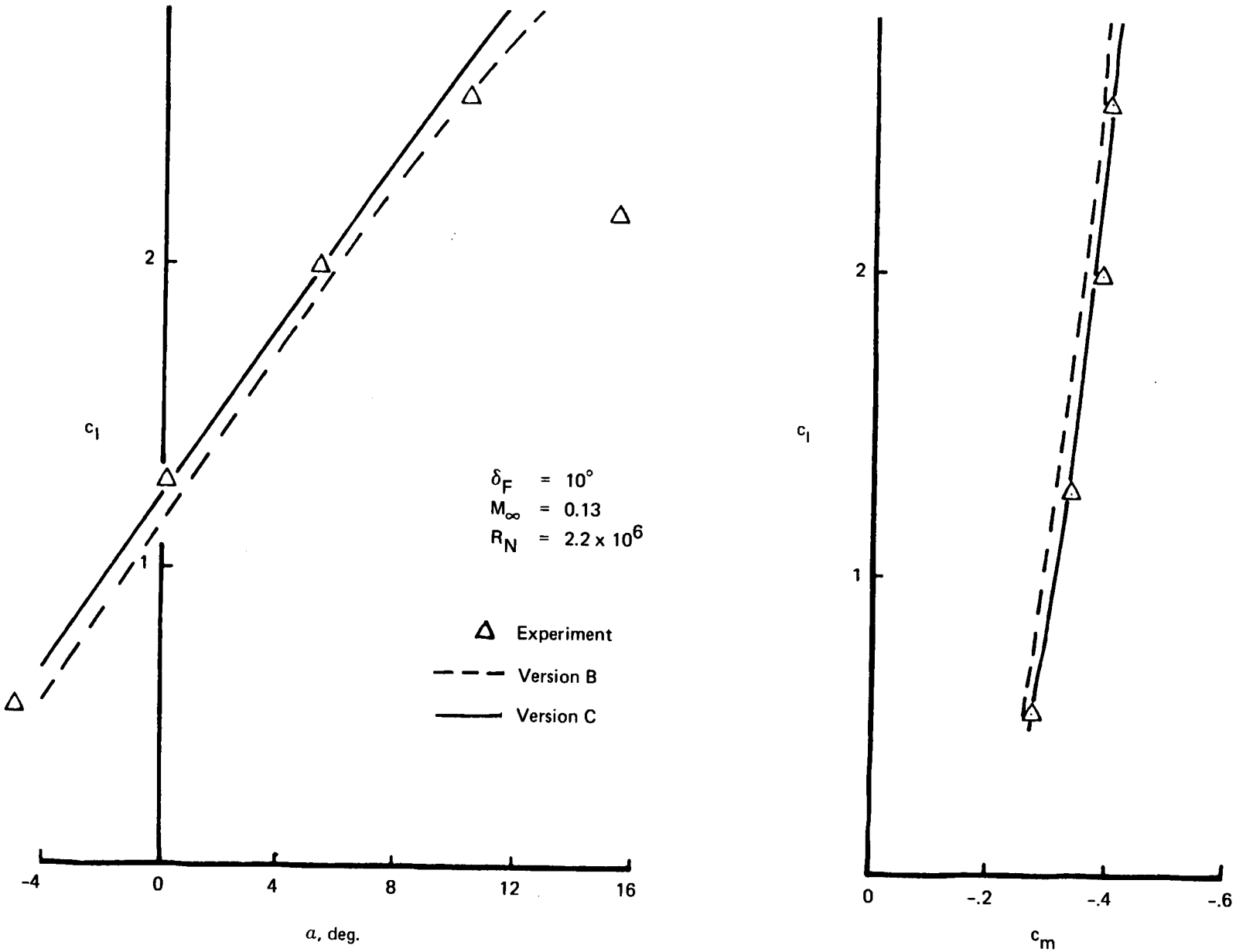

Figure 40. — Lift and Pitching Moment Characteristics of GA(W)-1 With 30% Chord Flap

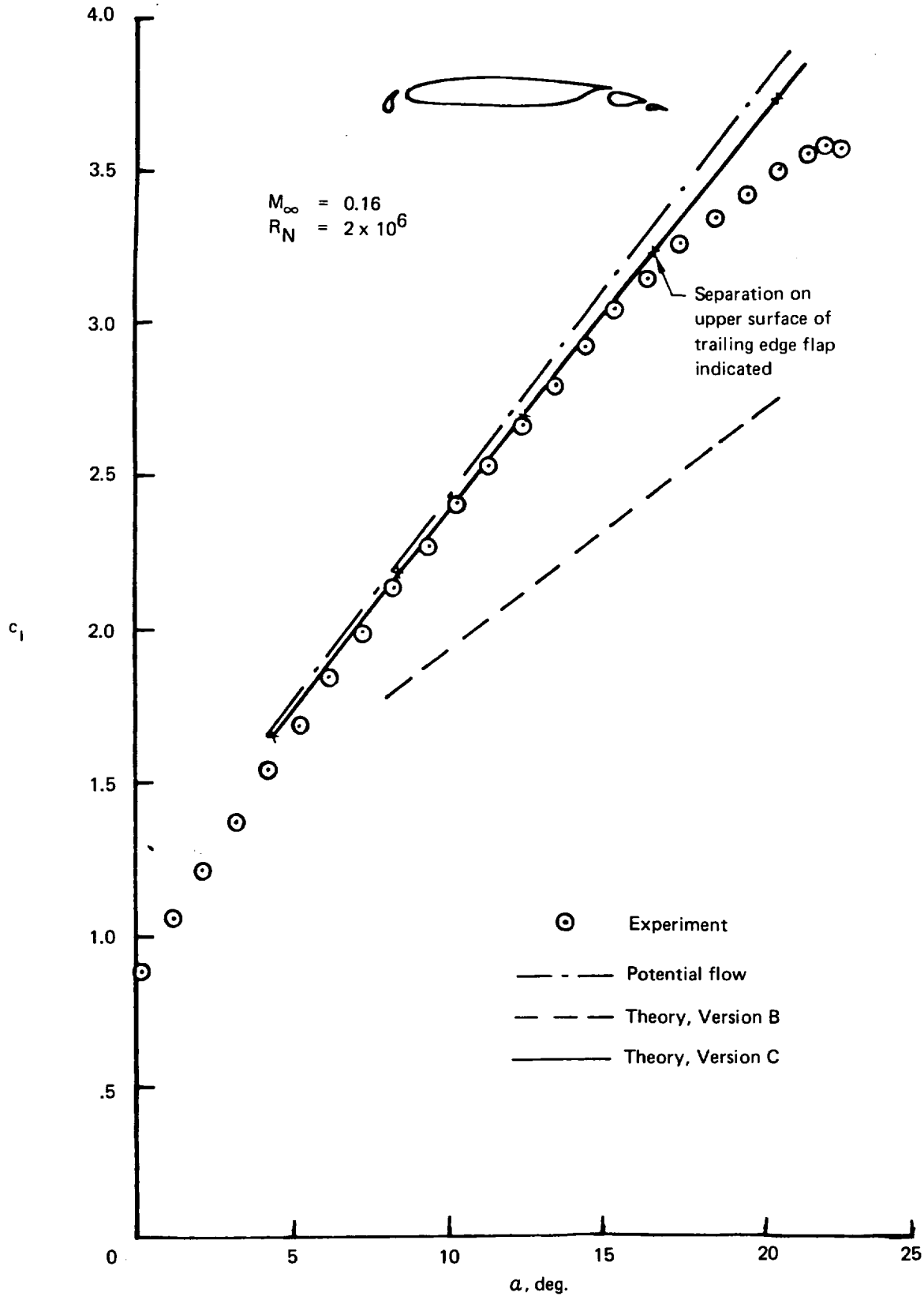

Figure 41. — Lift Curve of Boeing Four-Element Airfoil

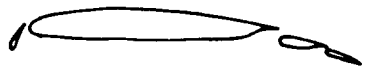

$M_\infty = 0.16$
$R_N = 2 \times 10^6$

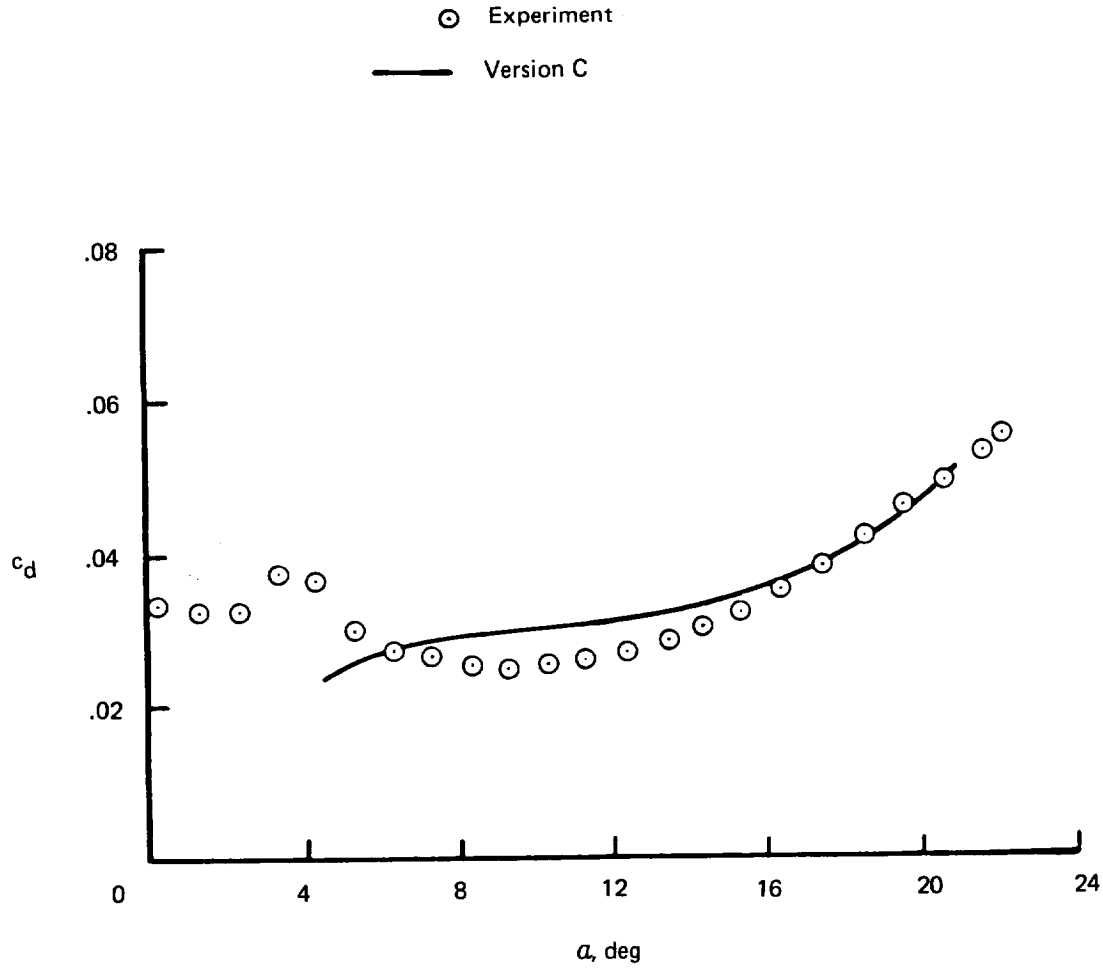

Figure 42. – Drag of Boeing Four-Element Airfoil

The pitching-moment characteristics of version C are compared with experimental data in figure 43. The discrepancy of the two curves at higher lift values is due to trailing-edge stall which is not modeled by the program.

Figure 44 demonstrates the excellent convergence characteristics of the new program version C.

Figures 45 and 46 contain comparisons of theoretical and experimental surface pressures at 8.4^{0} angle of attack. These figures confirm the earlier findings, that version C indeed provides the best theoretical results. Differences between the theory of version C and experiment, however, are noted in the cove region of the main flap demonstrating the need for a model of the recirculating flow in the cove.

Figure 47 shows boundary layer velocity profiles on the upper surface of the main component at several chordwise stations. The experimental velocity profiles reveal that very little confluence of slat wake and wing boundary layer has taken place and that an initially existing weak confluent boundary layer above the wing has degenerated early into an ordinary turbulent boundary layer. This feature of the flow field is very well simulated by version C.

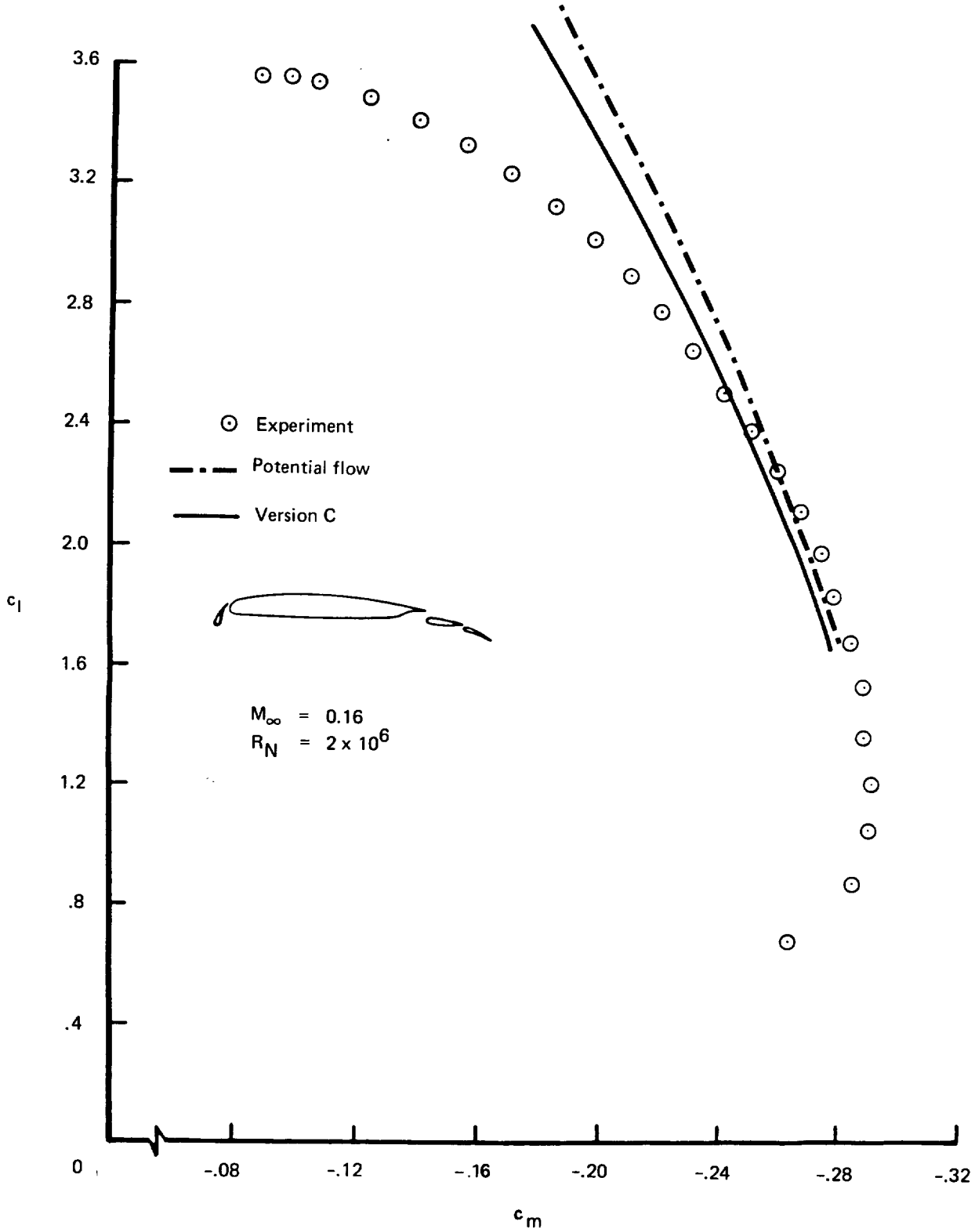

Figure 43. — Pitching Moment Characteristics of Boeing Four-Element Airfoil

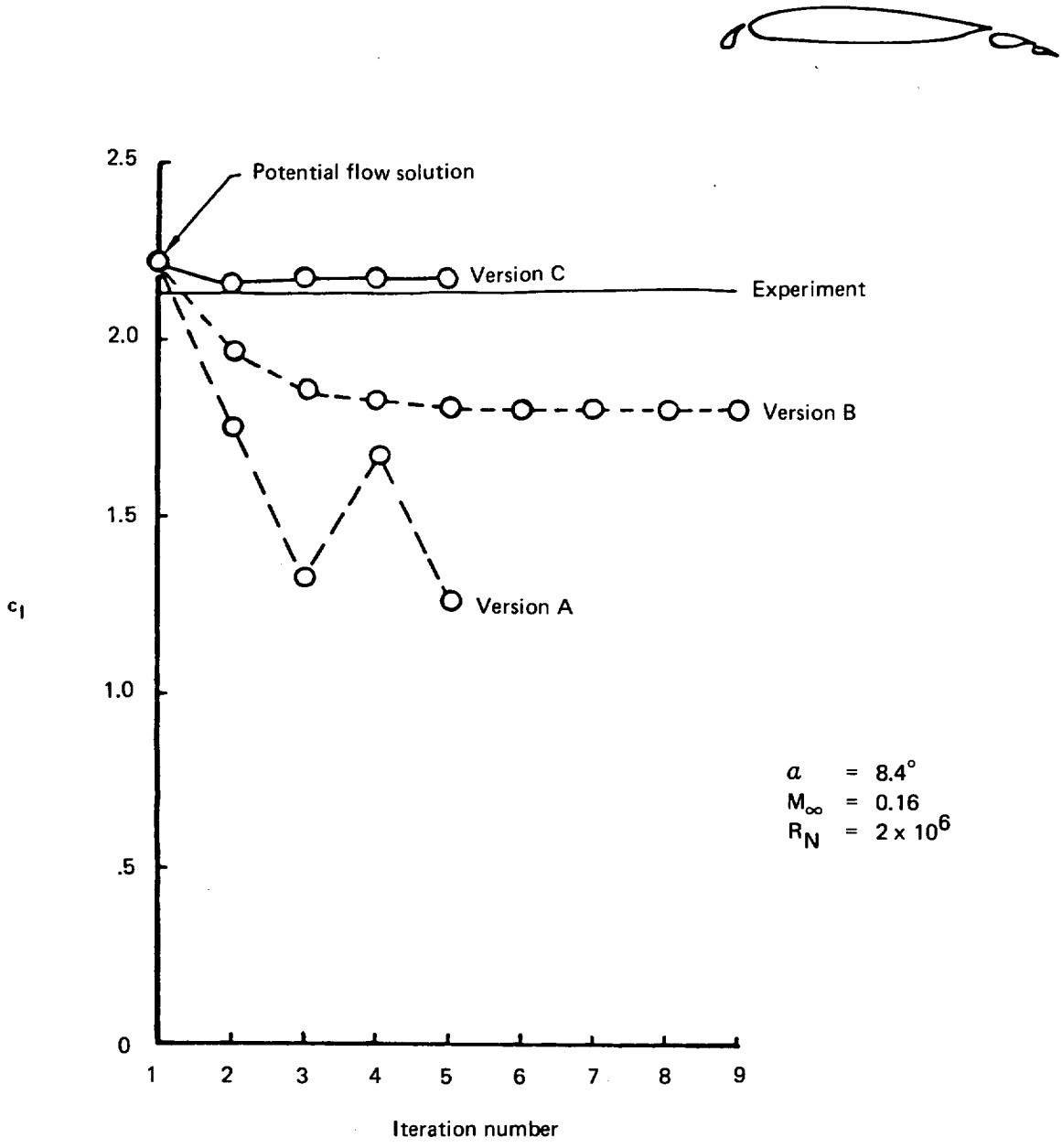

Figure 44. — Convergence Characteristics of Program Versions for Boeing Four-Element Airfoil

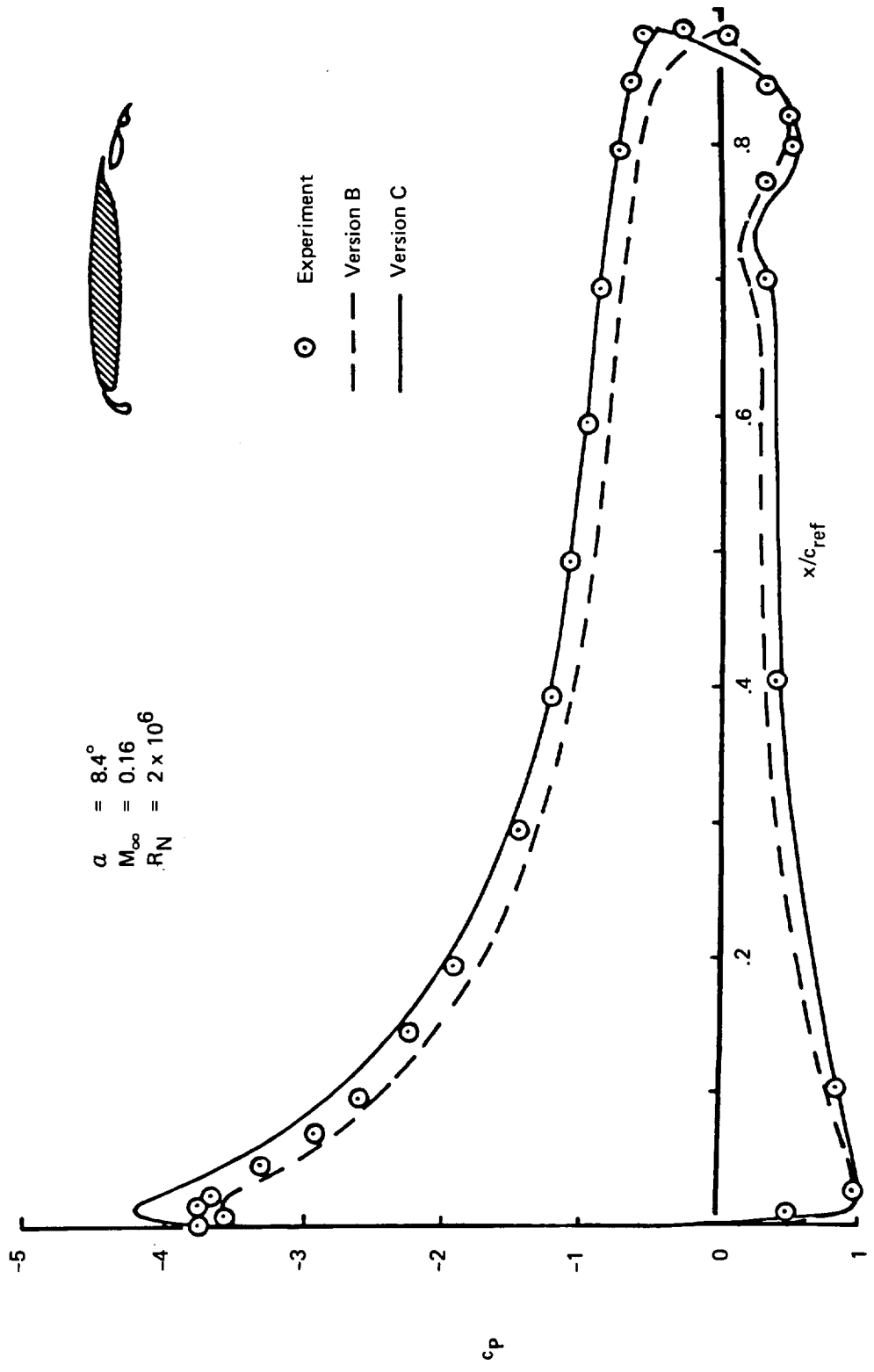

Figure 45. — Wing Surface Pressures of Boeing Four-Element Airfoil

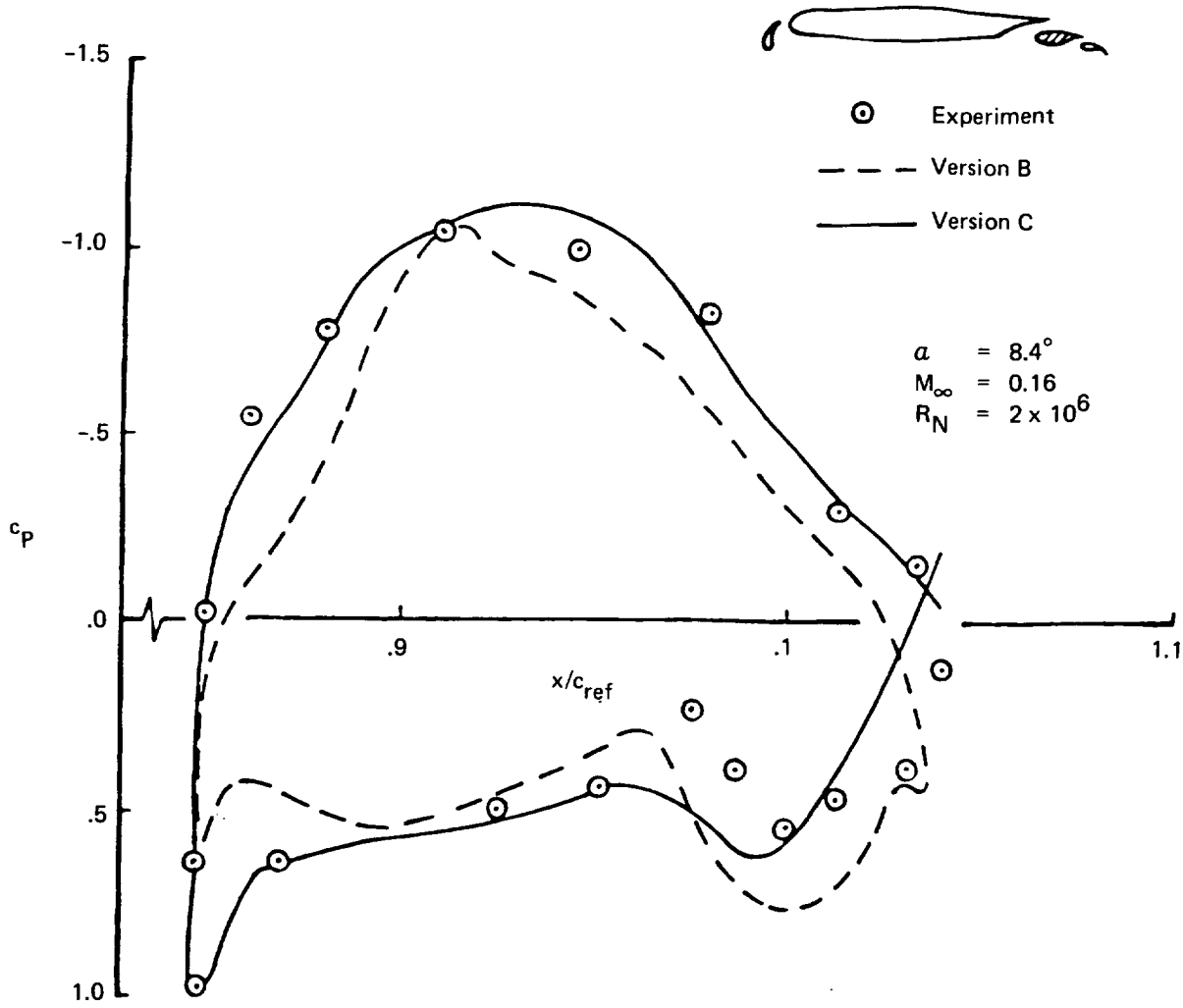

Figure 46. — Main Flap Surface Pressures of Boeing Four-Element Airfoil

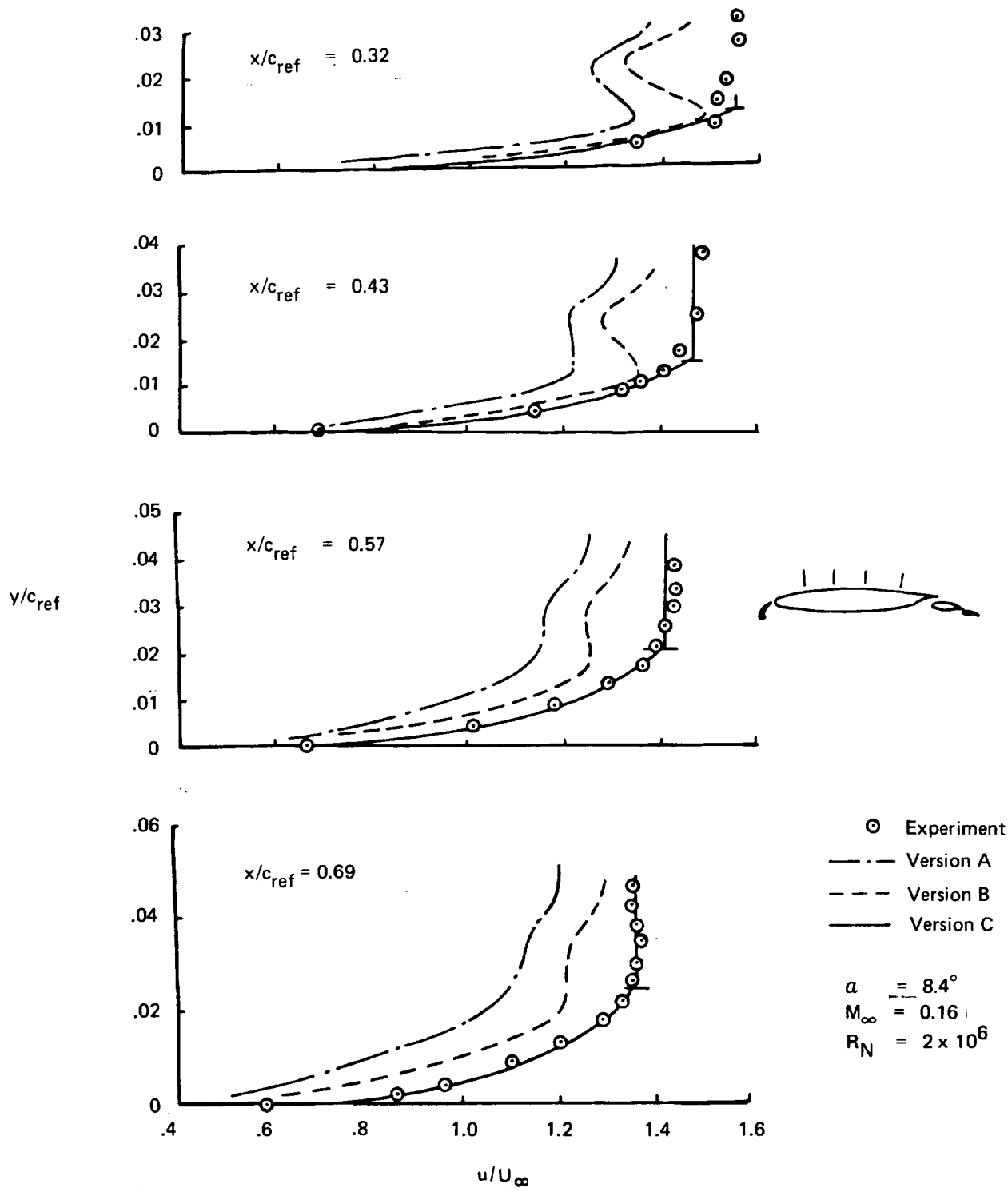

Figure 47. — Boundary Layer Profiles on Upper Wing Surface of Boeing Four-Element Airfoil

CONCLUSIONS

The aerodynamic model of the NASA-Lockheed multielement airfoil program has been extensively modified and most of the computer code has been rewritten using a structured approach to computer software design. The new version of the computer program has been documented in great detail and has been evaluated by comparing its theoretical predictions with recent experimental data of high-lift airfoils. Based on a relatively short evaluation phase of two months, the following conclusions about the reliability and quality of the program predictions are drawn.

- The reliability of the program executions has been greatly improved. All test cases run have produced converged solutions within a few iteration cycles. This improvement is a consequence of the application of the structured approach to computer programming where much attention was paid to the functional decomposition of the aerodynamic model, its numerical implementation, and the data flow within the code.

- The accuracy of the program predictions has been improved. This is due to several major modifications of the aerodynamic model - above all, due to the different representation of the viscous flow displacement effects and the improved model of the potential core region.

- The computed results are consistent with the basic assumptions of the aerodynamic model. Best results are obtained in cases where most of the flow is attached to the airfoil's surface, but the quality of the predictions gradually deteriorates with increasing trailing edge stall and cove separation.

- The usefulness of the confluent boundary layer method of Goradia and its modification utilizing Coles' velocity profile for the purpose of predicting the onset of confluent boundary layer separation has not yet been tested. Optimized configurations were chosen for most of the program evaluation with little confluence of wakes and boundary layers.

- The performance of the program needs to be tested for configurations at off optimum shape design.

- The evaluation of the computer program was hampered by the shortage of reliable experimental high-lift data. Additional wind tunnel testing of some of the more important high-lift airfoil configurations would increase the confidence in their performance predictions.

- Much additional theoretical work on two-dimensional high-lift airfoils needs to be done. A solution of the following two problems would immediately widen the range of applicability of the program.

The first one concerns a practical model of cove separation, which should be part of every computational method, in the high-lift area. A simple model of the recirculating flow in the cove region would improve the prediction of local effects such as pressures in the cove region; but, more important, might provide better initial values for the computations in the potential core region and the subsequent confluent boundary layer calculation.

The second problem is that of predicting the profile drag of multielement airfoils. The validity of the Squire and Young formula for the drag predictions of this type of airfoil, which replaced the pressure and skin friction integration of the earlier versions of the program, is questionable. Improvements in the drag prediction could be made by a better flow model of the wake behind a high-lift airfoil. This, in turn, requires improvements in the simulation of near wakes and confluent boundary layers.

Boeing Commercial Airplane Company
P.O. Box 3707
Seattle, Washington 98124
December 1977

REFERENCES

1. Stevens, W. A.; Goradia, S. H.; and Braden, J. A.: *Mathematical Model for Two-Dimensional Multi-Component Airfoils in Viscous Flow*. NASA CR-1843, July 1971.

2. Goradia, S. H.: "Confluent Boundary Layer Flow Development With Arbitrary Pressure Distribution." Ph.D Thesis, Georgia Institute of Technology, August 1971.

3. Morgan, H. L., Jr.: "A Computer Program for the Analysis of Multi-Element Airfoils in Two-Dimensional Subsonic, Viscous Flow." Aerodynamic Analyses Requiring Advanced Computers, Conference, Langley Research Center in Hampton, Virginia, March 1975.

4. Smetana, F. O.; Summey, D. C.; Smith, N. S.; and Carden, R. K.: *Light Aircraft Lift, and Drag, and Moment Prediction – A Review and Analysis*. NASA CR-2523, May 1975.

5. Brune. G. W.; Hahn, M.; Mark, J. L.; and Manke, J. W.: *Modification and Clarification of the NASA/Lockheed Multi-Element Airfoil Computer Program*. Boeing Document, D6-45072, February 1977.

6. Brune, G. W.; and Manke, J. W.: *A Critical Evaluation of the Predictions of the NASA/Lockheed Multi-Element Airfoil Computer Program*. NASA CR-145322 March 1978.

7. Green, J. E.; Weeks, D. J.; and Brooman, J. W. F.: *Prediction of Turbulent Boundary Layers and Wakes in Compressible Flow by a Lag-Entrainment Method*. RAE TR 72231, January 1973.

8. Coles, D. E.: "The Law of the Wake in the Turbulent Boundary Layer." *J. of Fluid Mech.*, Vol. 1, pp. 191-226, 1956.

9. Squire, H. B.; and Young, B. A.: *The Calculation of the Profile Drag of Airfoils*. RAE-Report R.&M. no. 1838, November 1937.

10. Nash, J. F.; and Hicks, S. G.,: An Integral Method Including the Effects of Upstream History on the Turbulent Shear Stress." Computation of Turbulent Boundary Layers – 1968, AFOSR-IFP-Stanford Conference, August 1968.

11. Oeller, H. J., "Die inkompressible Potentialströmung in der ebenen Gitterstufe (Incompressible Potential Flow in Two-Dimensional Cascades)." *Wissenschaftliche Gesellschaft für Luft-und Raumfahrt E. V.*, pp. 349-353, Jahrbuch 1962. (In German, not translated.)

12. Shapiro, A. H.: *The Dynamics and Thermodynamics of Compressible Fluid Flow* Vol. 1 The Ronald Press Company, New York, N. Y., 1953.

13. Cohen, C. B.: and Reshotko, E.: *The Compressible Laminar Boundary Layer With Heat Transfer and Arbitrary Pressure Gradient.* NACA 1294, 1956.

14. Pohlhausen, K., "Zur näherungsweisen Integration der Differentialgleichung der laminaren Reibungsschicht (On the Approximate Integration of the Differential Equations of Laminar Boundary Layers)." *ZAMM1, 252-268, 1921. (In German, Not Translated.)*

15. Cohen, C. B.; and Reshotko, E.: *Similar Solutions for the Compressible Laminar Boundary Layer With Heat Transfer and Pressure Gradient.* NACA 1293, 1956.

16. Schlichting, H.: *Boundary Layer Theory.* Sixth ed. McGraw-Hill, New York, 1968.

17. Granville, P. S.: *The Calculation of Viscous Drag of Bodies of Revolution*, Navy Department. The David Taylor Model Basin, Report no. 849, 1953.

18. Goradia, S. H.; and Lyman, V.: "Laminar Stall Prediction and Estimation of $C_{\ell_{max}}$." *Journal of Aircraft*, vol. 11, no. 9, September 1974.

19. Truckenbrodt, E.: "Ein Quadraturverfahren zur Berechnung der laminaren and turbulenten Reibungsschicht bei ebener und rotationssymmetrischer Strömung." *Ing. Arch.*, vol. 20, pp 221-228, 1952. (NASA TM 1379, 1955.)

20. Kline, S. J.; et al.: "Proceedings: Computation of Turbulent Boundary Layers – 1968." AFOSR-IFP-Stanford Conference, Stanford University, August 18-25, 1968.

21. Broyden, C. G.: "Quasi-Newton or Modification Methods." Numerical Solution of Nonlinear Algebraic Systems." G. D. Bryne and C. A. Hill, eds., Academic Press, 1973.

22. Goradia, S. H.; and Colwell, G. T.: "Parametric Study of a Two-Dimensional Turbulent Wall Jet in a Moving Stream With Arbitrary Pressure Gradient." *AIAA Journal,* vol. 9, no. 11, 1971.

23. McGhee, R. J.; and Beasley, W. D.; *Low Speed Aerodynamic Characteristics of a 17-Percent Thick Airfoil Section Designed For General Aviation Applications.* NASA TN D-7428, 1973.

24. Wentz, W. H., Jr.; and Seetharam, H. C.; *Development of a Fowler Flap System For a High Performance General Aviation Airfoil.* NASA CR-2443, December 1974.

25. Wentz, W. H., Jr.; Seetharam, H. C.; and Friscko, K. A.: *Force and Pressure Tests of the GA(W)-1 Airfoil With a 20% Aileron and Pressure Tests With a 30% Fowler Flap.* NASA CR-2833, June 1977.